CRANFIELD UNIVERSITY

YUN CHENG

PRELIMINARY FUSELAGE STRUCTURAL CONFIGURATION OF A FLYING-WING TYPE AIRLINER

SCHOOL OF ENGINEERING
MSc THESIS

MSc BY RESEARCH
Academic Year: 2011 - 2012

Supervisor: Dr. Rui Pires
January 2012

CRANFIELD UNIVERSITY

SCHOOL OF ENGINEERING

MSc BY RESEARCH

Academic Year 2011 - 2012

YUN CHENG

PRELIMINARY FUSELAGE STRUCTURAL CONFIGURATION OF A FLYING-WING TYPE AIRLINER

Supervisor: Dr. Rui Pires
January 2012

This thesis is submitted in partial fulfilment of the requirements for the degree of Master of Science

THESIS “HEALTH” WARNING

This thesis has been assessed as of satisfactory standard for the award of a Master of Science by research degree. Readers must be aware that the work contained is not necessarily 100% correct, and caution should be exercised if the thesis or the data it contains is being used for the future work. If in doubt, please refer to the supervisor named in the thesis, or Department of Aerospace Technology.

ABSTRACT

The flying-wing is a type of configuration which is a tailless airplane accommodating all of its parts within the outline of a single airfoil. Theoretically, it has the most aerodynamic efficiency. The fuel consumption can be more efficient than the existed conventional airliner. It seems that this configuration can achieve the above mentioned requirements.

According to these outstanding advantages, many aircraft companies did a great deal of projects on the flying-wing concept. However, the application was only for sport and military use; for airliner, none of them entered production.

FW-11 is a flying-wing configuration airliner which is a design cooperation between Cranfield University and Aviation Industry Corporation of China (AVIC). Aiming the spatial economic and environmental needs, this 200-seat airliner would attract attention from airline companies for cost saving and environmental protection.

Before start, this program is designated for a new generation commercial aircraft to compete with the existing same capability airliner, such as Airbus A320 and Boeing 767. As the first team of this program, the aim is to finish the conceptual design and prepare the relevant document for next two teams that will perform preliminary and detail design.

As a member of FW-11 program and as part of the GDP, the author has been through the four conceptual design stages: engine manufacturers, aircraft family issues, structure design and the establishment of 3-D CAD model.

The aim of IRP study is to focus on the initial fuselage design.

Keywords:

Preliminary design, Flying-wing, multi-bubble, structure initial design, AVIC program.

ACKNOWLEDGEMENTS

I would like to show my great gratitude to my supervisor Dr. Rui Pires. With his advices and inspirations, I got so many benefits to help me finish my whole year study and research. And also, even my English study and daily life would be embarrassed without his support.

I also give my sincere thanks to China Scholarship council and AVIC, they gave me this chance to study abroad, and provided the full scholarship to me.

TABLE OF CONTENTS

LIST OF FIGURES

LIST OF TABLES

LIST OF EQUATIONS

LIST OF ABBREVIATIONS

CU	Cranfield University
MTOW	Maximum Take-Off Weight
FE	Finite Elements
FEA	Finite Elements Analysis
AVIC	Aviation Industry Corporation of China
CU	Cranfield University
IRP	Individual Research Program
GDP	Group Design Project
FW	Flying-wing
BWB	Blended-wing body

1 INTRODUCTION

1.1 Background

There are so many airliner configurations, and all of them were attempt to be superior to others in terms of speed, range or capacity etc. For two airliners which have the same design condition, the critical advantages is the optimal balance between the cost and the structure feasibility, this is the first design constraint.

Second, with the raising public awareness for environment sustainable development, the solution for pollutions, such as carbon emission and noise, is expected by more and more governments, airline companies and individuals.

The flying-wing is a type of configuration which is a tailless airplane accommodating all of its parts within the outline of a single airfoil. Theoretically, it has the most aerodynamic efficiency. The fuel consumption can be more efficient than the existed conventional airliner. It seems that this configuration can achieve the above mentioned requirements.

According to these outstanding advantages, many aircraft companies did a great deal of projects on the flying-wing concept. However, the application was only for sport and military use; for airliner, none of them entered production.

Boeing Company already designed a BWB configuration airliner, the code is X-48b which based on the X-48 of McDonnell Douglas Company. During the research period, they found that passengers did not feel comfortable in the cabin without windows.

According to that, it seems the flying-wing concept can only be adopted in the design of UAV and tanker, but the design work always compromise for some adverse conditions. There still will be enough passengers who want to buy some more economic tickets.

1.2 Aim and Objectives

This research focuses on the initial design for the fuselage structure of a 200-seats flying wing aircraft. Based on the conceptual design, the challenges of fuselage structure are discussed to meet feasible solutions. Attention will be then paid to finding viable structure solutions to solve the challenges such as cabin pressurization, landing gear bay. Research on composite materials will also be performed to investigate its applicability to this aircraft concept.

1.3 Methodology

These methodologies will be used in the whole research:

- Literature review;
- GDP conceptual design and CAD model;
- Identification of fuselage design challenges;
- Research viable solutions for challenges;
- Structure investigation of solutions.

2 LITERATURE REVIEW

2.1 Introduction

Unlike the conventional aircraft, the flying-wing concept is so unique and outstanding that is has already been researched through a whole century. Because of its superior aerodynamic and structural benefits, many countries and companies did a great deal of research on it. However, none of them such as B-2 bomber have been used for civil transport. Until now, numerous prototypes were produced to test and verify the application of flying-wing theory, and there are many flying-wing configuration aircraft in active service, and the outlook shows more and more aircraft design research have already been or will be considered to involve in this concept. Recently, a program named X-48B, which try to use the flying-wing theory to design a new generation airliner, has already been launched by Boeing Company.

The demerits of this configuration are mainly on the control and stability from a view point of technology. With the development of the technique, there problems can be solved by technological advances in terms of materials, flight computer-aided control systems, structures, propulsion systems and aerodynamics.

Comparing with conventional airliner, the length of fuselage for flying –wing configuration is dramatically less. The structure weight of outer wing can be reduced. It means for the same wing span, the weight penalty for the flying-wing is less than the conventional one. In other word, the lift-to-drag ratio can be increased by adopting the FW configuration.

However, there are many challenges for flying-wing. At the beginning, it is thought that this configuration can have enough capability to carry more passengers, and also have enough room for more fuel tanks. Nonetheless, from the view point of passengers, a wide, non-widows, box-like cabin seems be lack of attractively by comparing the conventional circle cylinder fuselage. The emergency exit is also a challenge for the fuselage design. Passengers can

only escape from the leading edge, trailing edge, even the top surface of fuselage. For designers, the decoration and the arrangement for passenger cabin should be considered carefully.

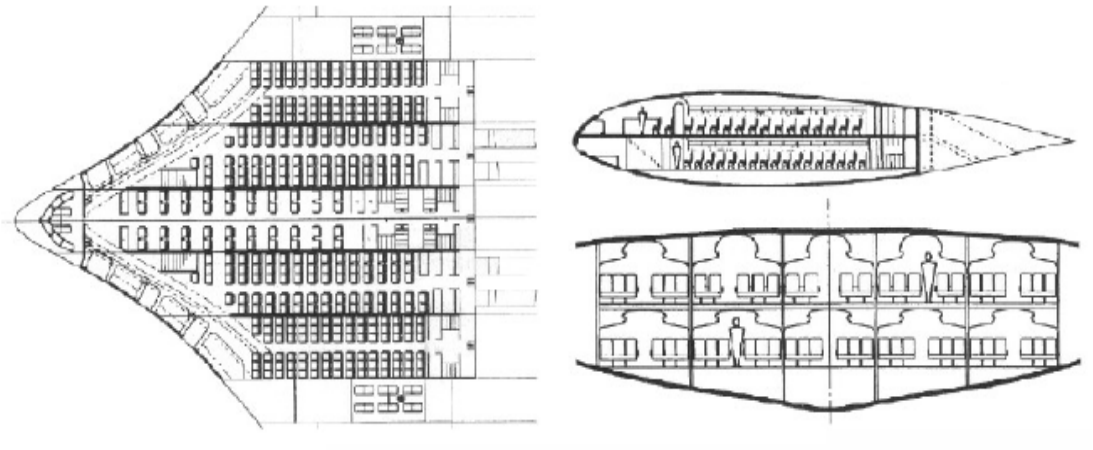

Figure 2.1Blended Wing Body passenger cabin configuration [1]

2.2 Flying-wing configuration aircraft

2.2.1 Northrop N-1M

Northrop N-1M is a flying-wing configuration developed in 1939 and 1940 by Northrop Corporation in the United States. It is considered an “aerodynamically clean design” type which means all of the structures for drag increase such as fuselage, vertical and horizontal stabilisers and protruding engine support are cancelled. This aircraft is the first flying-wing type in U.S.A., and the archetype of XB-35 and YB-49 bomber.

In July 1940, the first boomerang-shaped flying scale mock-up was emerged. The size of this model is 38 feet a wingspan, 17 feet length and 5 feet height.

Figure 2.2 N-1M in National Air and Space Museum [2]

The control surface in this aircraft is not the same as the conventional aircraft: the elevator and aileron was replaced by elevons to control pitch and roll on the trailing edge of the wing, and the rudder was replaced by a split flap device to control yaw on the wing tips.

The first test of N-1M is on 3th July, 1940 at Baker Dry Lake, California, however, it is failed. The report said that this aircraft cannot fly when the height is more than 5 feet off the ground, and the attack angle should be maintain a exact angle to sustain the flight.

The disadvantages of N-1M are the condition of overweight and chronically underpowered. But it is a successful forerunner for the flying-wing concept. Basing on it, the long range XB-35 and YB-49 was developed.

2.2.2 Armstrong Whitworth A.W.52 [3]

Armstrong Whitworth A.W.52 is another type of flying-wing aircraft developed in Britain at the end of World War II. It is proposed to have a huge wing so that the head-room can be arranged in there. At the first stage, a wooden glider A.W.52G was made for testing, and made its first testing in March 1943.

The A.W.52 was designed to support by four or six turbojet engine, and the landing gear can be retractable. The trailing edge was designed to be straight in

the centre section, the vertical stabiliser was arranged at wingtips which have the rudders on it. Elevons were used for controlling roll and pitch at the wing. The attack angle is higher than the conventional aircraft so that the take-off and landing distance is longer.

To maintain the laminar flow over the wing, the wing surface should be smooth enough. So the approach for wing manufacturing is to separate the whole wing to two parts: upper and lower. The skin was assembled before stringers and ribs to keep surface smooth as much as possible. When each part was finished, the two halves were joined together. The engine was arranged near the centreline of the wing to reduce the interference to the upper wing surface.

The first test of A.W.52 powered by Rolls-Royce Nene engines is on 13 November 1947. The results showed the performance is not as same as expected: The laminar flow control is not satisfied.

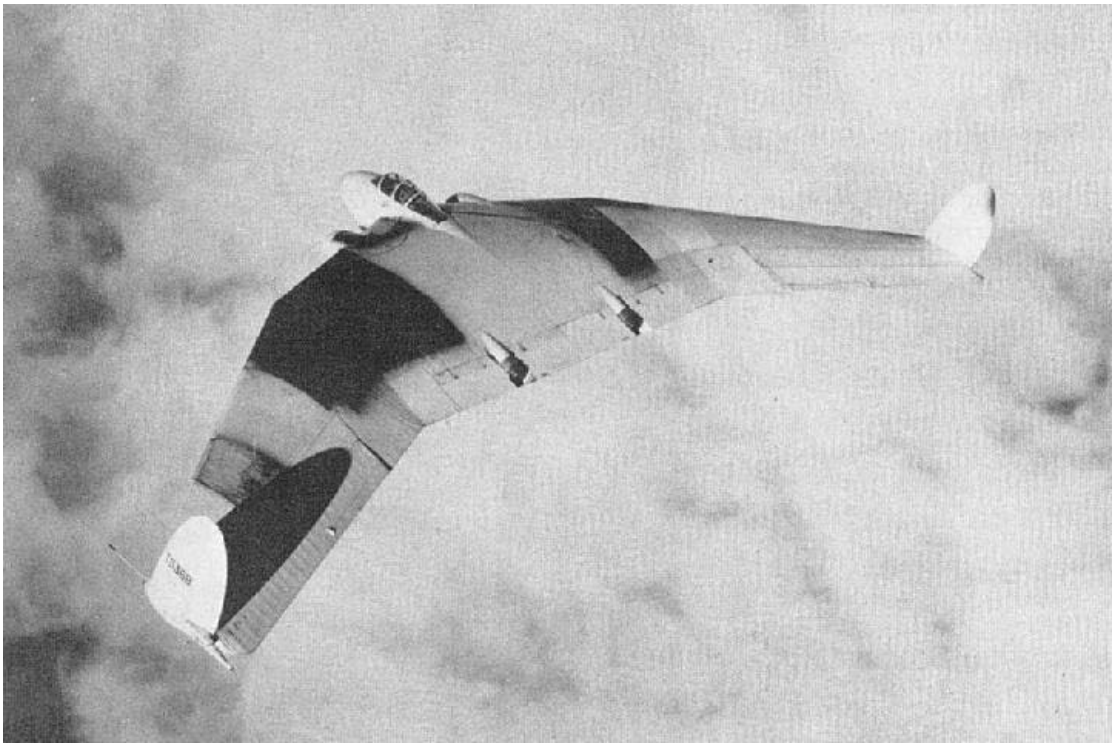

Figure 2.3 2.2.2 Armstrong Whitworth A.W.52 [3]

2.2.3 Northrop YB-49 [4]

Northrop YB-49 is a flying-wing configuration and jet-powered aircraft. this heavy bomber aircraft was Based on the technique accumulated from N-1M to YB-35, developed by Northrop Corporation in U.S.A after Second World War.

The first testing of Northrop YB-49 is on 21th October, 1947. The results showed the performance of this jet-powered aircraft was superior than XB-35 powered by piston –engine.

The second prototype crashed because of the structural failure on 5th June, 1948. The outer wings was separated from the centre section, five crews were killed by this accident. The reason of lost was the post-stall high speed dive from its flying-wing design.

The Bombing target tests showed the defect as described: "extremely unstable and very difficult to fly on a bombing mission ... because of the continual yawing and the pitching which was evident upon application of the rudders, undoubtedly due to the control arrangements or elevons peculiar to the YB-49."

Figure 2.4 Northrop YB-49 [5]

2.3 Blended wing body configuration aircraft

Blended Wing Body (BWB) is a branch of the flying-wing concept. This type of aircraft has an extraordinary fuselage which can generate most of the lift force. The connection between the wing and the fuselage is blended smoothly, and the shape of the fuselage is as same as airfoil shape of the wing.

A research reviewed that BWB could produce more 50% lift-to-drag ratio than the conventional aircraft. One of the advantages of the Blended Wing Body is the high efficiency lift contributed by wings and fuselage. This feature can lead to save more fuel conception and life cycle.

2.3.1 Boeing X-48B

X-48B is a miniature of a Blended Wing Body Type airliner developed by Boeing Phantom Works and Cranfield Aerospace. The size of X-48B is 6.4 m wingspan, 178 kg weighs. The main materials it used is composite material.

The first fly test is on 20 July, 2007. The whole flight continued about half hour and reached an altitude of 2286m. The initial testing was finished on 19 March, 2010. This successful testing showed the problems such as the low-speed flight-control characteristics have initially solved.

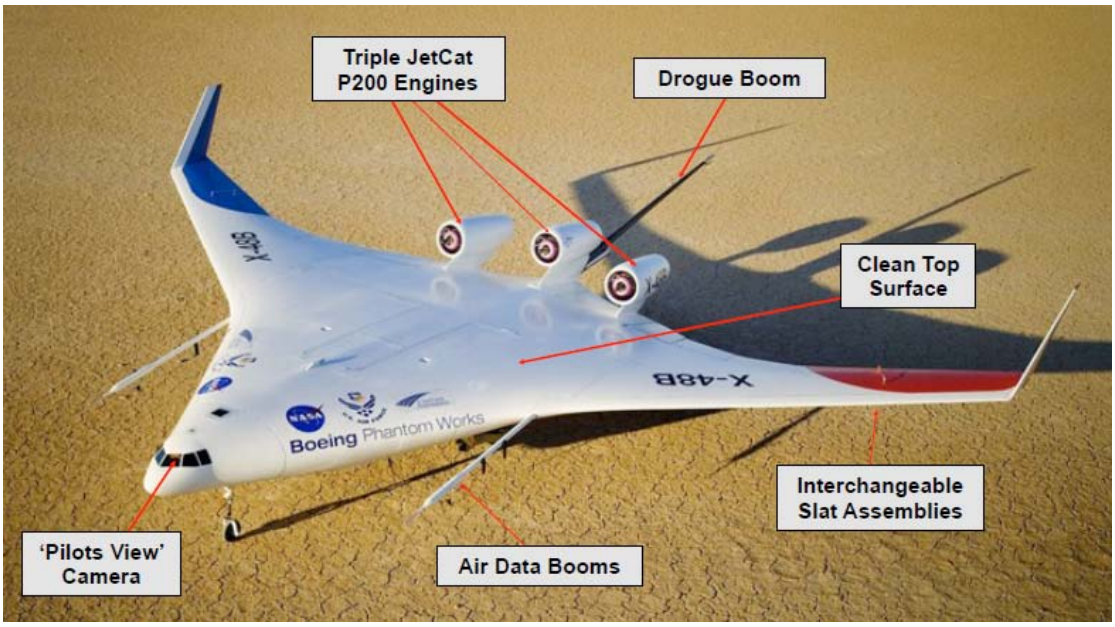

Figure 2.5 Boeing X-48B Blended Wing Body configuration airliner [6]

Table 2.1 shows the basic properties of the mentioned aircraft.

Table 2.1 Basic properties of N-1M, A.W. 52, YB - 49 AND X 48B

	Northrop N-1M	**A.W.52**	**Northrop YB-49**	**Boeing X48B**
Wingspan(m)	11.6	27.4	52.4	6.22
Length(m)	5.2	11.4	16.0	
Height(m)	1.5	4.4	6.2	
Empty weight(kg)	1814kg	8919kg	40116kg	227kg
Top speed(km/h)	322	805	793	219
Engine mounted	2 Franklin 6AC264F2	2 Rolls-Royce Nene centrifugal-flow turbojet	8 Allison/General Electric J35-A-5 turbojet	3 JetCat p200 turbojet

2.4 Conventional airliner fuselage design

2.4.1 Introduction

For conventional semi-monocoque fuselage of airliner, as shown in figure 2.6, can be divided for four parts: forward section, mid section, aft section and after body.

In this configuration, the skin carries the shear from external transverse and torsion forces and internal cabin pressure. The auxiliary structures for skin are the stringers and frames. Stringers just sustain the axial loads from bending moment in the ideal condition. The function of frames is the shape containing of the fuselage and the length reduction of stringers. Reinforced frames

(bulkheads) can distribute the concentrated forces from the heavy load such as wings and landing gear.

The principle of the fuselage design for 200-seats airliner should obey Certification Specifications for Large Aeroplanes CS-25.

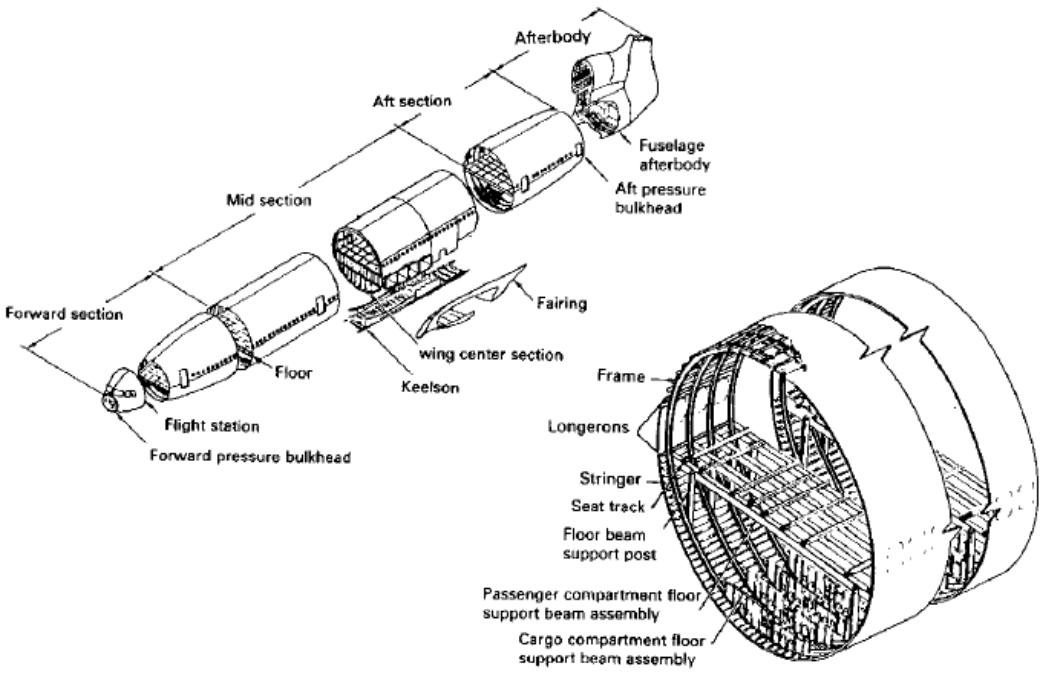

Figure 2.6 Conventional fuselage structure [7]

2.4.2 Methodology

2.4.2.1 Baseline

The design methodology for fuselage listed below：

- Using the approach of durability and damage tolerance design principle
- Adopting the material which has better combination properties and choosing the proper heat treated condition.
- Controlling the stress and stress concentration of components and avoiding structure fatigue.

- Rational structure for maintenance and producing process

2.4.2.2 Skin thickness initial sizing by using Denis Howe's methods [8]

In the design phase, the thickness of skin should be calculated at first, the following equations suggested by Denis Howe are the initial design approach to estimate the skin thickness.

From his suggestion, the condition of pressurized skin should be considered at first. When the pressure is higher than nearly 0.3 bar (4.4 lb/in^2), the fuselage cross section should be circle or made up of circular arcs. And for the cross section where the curvature changes, some support ties should be arranged to avoid the bending loads. the thickness of inner skin for pressurization is given by:

$$\boldsymbol{t_p = \frac{\Delta P \cdot R}{\sigma_p}} \qquad \textbf{(2-1)}$$

Where

Δp is the maximum working differential pressure

R is the local radius of the shell

σ_p is the allowable tensile working stress, the value 100MN/$\mathrm{m}^2$for all materials in $\pm$45℃ condition was adopted in this thesis.

The torsion shear can be considered to the fin root bending moment. The thickness of inner skin for torsion shear is given by:

$$\boldsymbol{t_q = \frac{T}{2A\sigma_S}} \qquad \textbf{(2-2)}$$

Where:

T is the applied ultimate torque.

A is the enclosed area of the fuselage cross section

σ_s is the allowable shear stress, assumed at 50% of ultimate tensile stress.

It is completed to calculate the skin allowable thickness for bending stress.

The thickness of equation skin thickness is given by:

$$\mathbf{t_e = \frac{M}{\sigma_a A}} \tag{2-3}$$

Where:

M is the applied ultimate bending moment.

σ_a is the allowable bending stress.

A is the area enclosed by the fuselage cross section.

t_e is the equvalent skin thickness.

The empirical equation for estimate the skin thickness is the contribution percent to the effective thickness. This effective thickness provided by stringers is almost between 50 and 100 percent of the skin contributes from experience. Under the worst condition, the skin thickness is given by:

$$t_b = 0.65 t_e \tag{2-4}$$

Under the ultimate bending, if the compression members have enough support to avoid the local and overall buckling, then the allowable bending stress can be assumed to equal to 0.2 percent proof stress; if the compression members are a widely reinforced plate, then the allowable bending stress can be assumed to the lesser of 0.2 percent proof stress or σ_b, The equation of σ_b is given by:

$$\sigma_b = F_B \cdot \bar{A} \cdot \sqrt{\frac{M}{A \cdot L}} \tag{2-5}$$

Where

F_B is according to the form of construction, the value can be checked in table 2.2.

$\bar{A}$ is the function of the material

M is the ultimate bending moment

A is the area enclosed by the fuselage cross section.

L is the frame pitch

Table 2.2 The value of buckling efficient factors [8]

Construction (see **Fig.** 13.4)	F_B
Zed stringer	
Built-up	**0.96**
Machined	**1.02**
Blade stringer	**0.81**
Top hat stringer	**0.96**
Trapezoidal corrugated, semi-sandwich	**0.83**
Triangular corrugated, semi-sandwich	**0.85**
Truss core sandwich	**0.78**

The value of allowable bending stress is given by:

$$\boldsymbol{\sigma_a = \min(\sigma_{0.2}, \sigma_b)} \quad \textbf{(2-6)}$$

The final thickness of skin which takes the pressure loads, torsion shear and overall bending moment is the greatest value of t_p from Eqn. (2-1), t_p from Eqn. 2-2 and t_b from Eqn. (2-4).

2.4.2.3 Stringer initial sizing by using Denis Howe's methods

The method to estimate the initial size of stringer section in Denis Howe's book is:

- The pitch of stringers is between 1.5 and 5 times the stringer height, it is suggested that in the initial design phase, this value can be assumed 3.5;
- The width of stringer flanges can be estimated 40% of the stringer height;
- The thickness of stringer can be as same as the skin.

- The width of flange is normally 16 times than its thickness.

Figure 2.7 shows the initial sizing of Zed shape stringer.

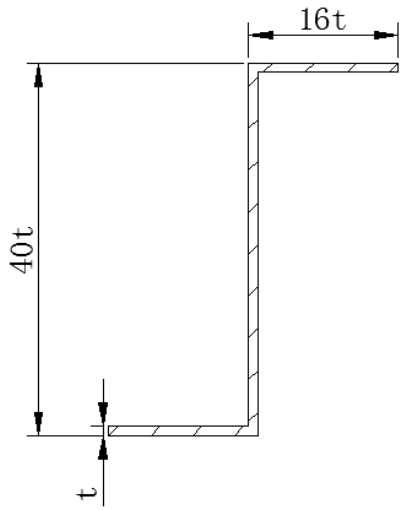

Figure 2.7 The initial sizing of Zed shape stringer

The stringer has many types of shape to select, each of them have their advantages and disadvantages, figure 2.8 shows four types of typical stringer cross section.

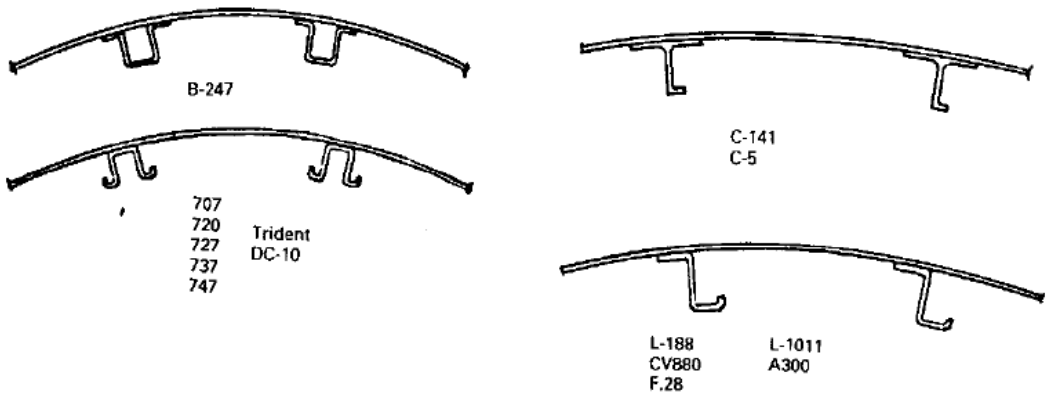

Figure 2.8 Typical stringer cross section [7]

2.4.2.4 Frame initial sizing by using Denis Howe's methods

The frame pitch for pressurization skin is normally 0.5 meter in the conventional airliner from suggestion.

The rules for estimating the size of frames are:

- The width of frame normally 3-5% of the fuselage width, although it is constrained internal layout;
- For shell support frames, the thickness is usually similar with the skin thickness;
- The width of frame flanges can be estimated 40% of the frame height.

Figure 2.9 shows the relationship between thickness and the others.

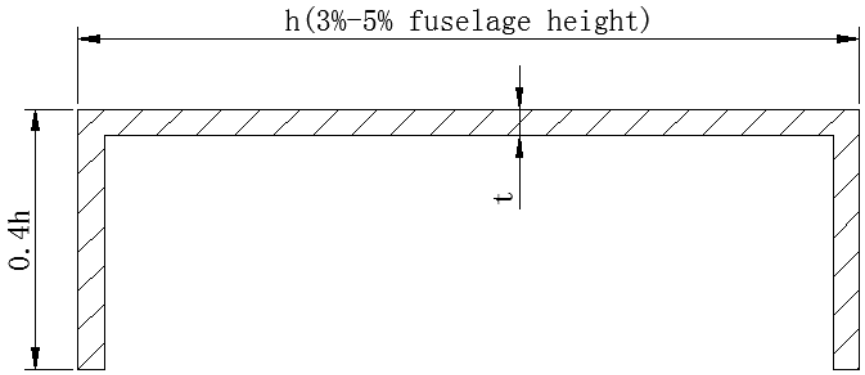

Figure 2.9 The initial sizing of C shape frame

2.4.2.5 Pressurization bulkheads initial sizing by using Denis Howe's methods

There are two types of pressure bulkheads: flat and domed, as shown in figure 2.10. The flat bulkhead resists the bending load and tension; the domed just resists the membrane tensile in ideal condition.

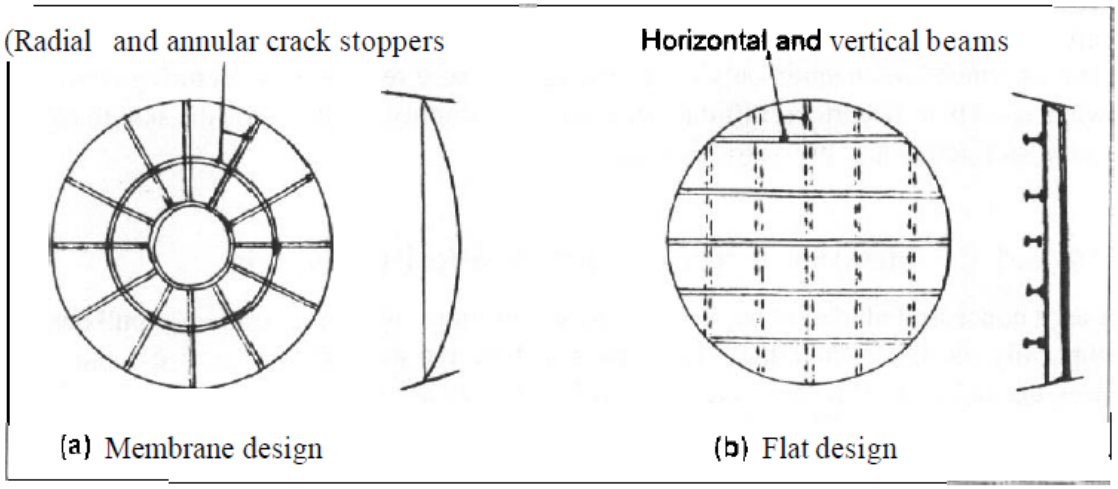

Figure 2.10 flat and domed pressure bulkheads [8]

a. Domed pressure bulkheads

This type of bulkheads can be calculated by using the same method as the pressurized skin. In Denis Howe's book, the tensile stress caused by the pressure in the hemi-sphere shell can be treated in the same way as the longitudinal stress in the cylinder skin which comprises nearly half of the value of the tensile in the skin.

$$t_p = \frac{\Delta P \cdot R}{2\sigma_p} \quad \textbf{(2-7)}$$

Where

Δp is the maximum working differential pressure

R is the local radius of the hemi-sphere shell

σ_p is the allowable tensile working stress

b. flat pressure bulkheads

For the isotropic material, the thickness of the flat bulkhead is given by:

$$t_p = \left[\frac{0.71\Delta P a^2\{n^3/n^3 + 1.5\}}{\sigma_a}\right]^{1/2} \quad \textbf{(2-8)}$$

Where

σ_a is the allowable stress, in the absence of other information this may be taken to the same as σ_p

Δp is the maximum working differential pressure

a is the length of the shortest side

n is the ratio of the longer to shorter side

In the condition which has two rows of fasteners at each panel edge, then the formula is given by:

$$\boldsymbol{t_p = \left[\frac{0.5\Delta P a^2\{n^4/n^4 + 0.6\}}{\sigma_a}\right]^{1/2}} \quad \textbf{(2-9)}$$

2.5 Different structures for pressurization cabin of flying-wing aircraft

There are mainly three types of configurations for the flying-wing (or BWB), multi-bubble, integrated skin & shell and the Y braced box configuration. Comparing to the conventional structure, the weight penalty of them can extremely increase by the auxiliary load-taking structure, this issue should be considered and the cabin layout is subjected to some compromise. For passengers, it would be crowded and there will hardly have any window.

2.5.1 Multi-bubble configuration

Figure 2.11 shows a typical multi-bubble type. Using the conventional airliner cabin as a precursor reference, the target of this configuration is for the balance of the tension induced by the internal cabin pressure, and the outer-ribbed shell only resists the external resultant compressive loads.

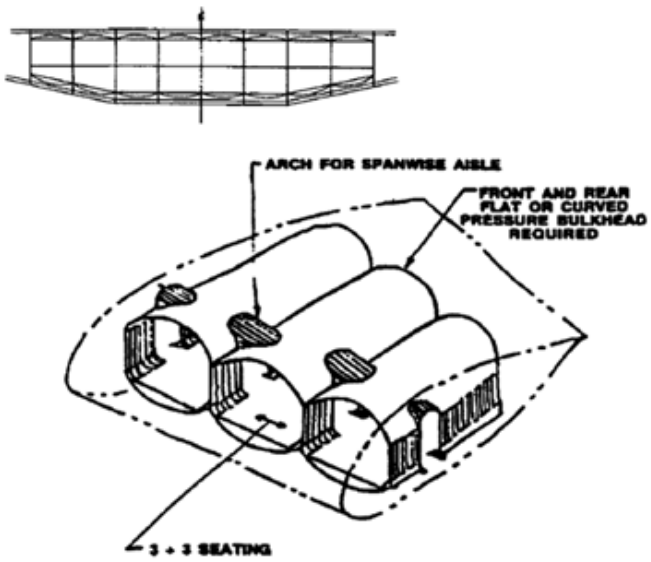

Figure 2.11 Multi-bubble configuration [9]

2.5.2 Integrated skin & shell concept

Being distinct from the semi-monocoque fuselage, this configuration mainly use the thick sandwich panel (figure 2.12) to be the wing surface, and take the loads form pressurization, wing bending and exterior aerodynamic loads.

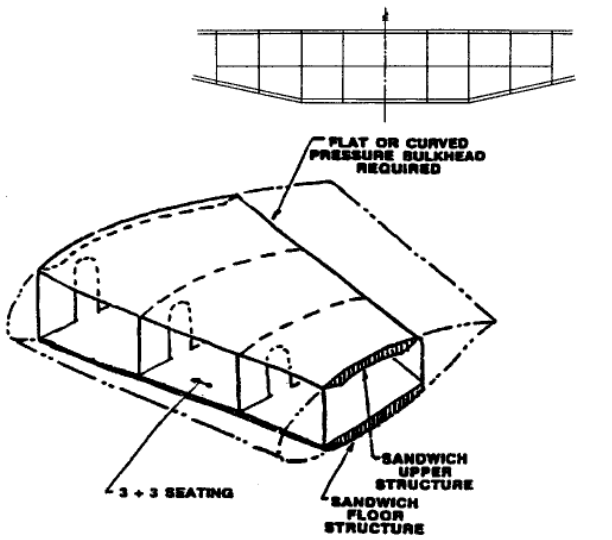

Figure 2.12 Integrated skin & shell concept [9]

2.5.3 Y braced box

If the fuselage of the flying-wing (or BWB) is considered to have just one layer of lamina skin, according the wing surface, the cabin structure shall be like separated boxes. In this Y braced box configuration (figure 2.13), the bending form the joint of the roof and cabin walls can be reduced.

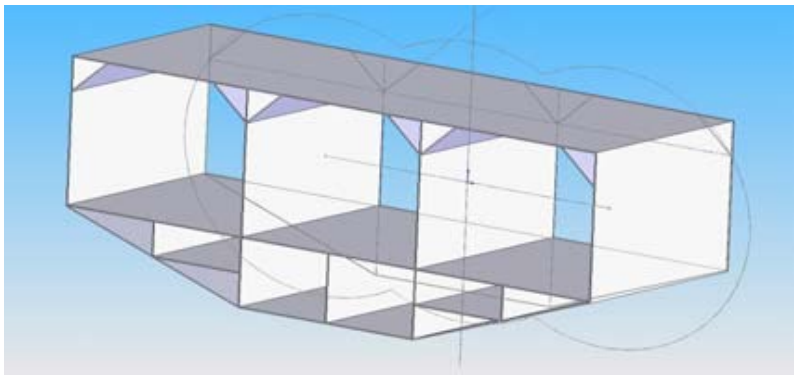

Figure 2.13 Y braced box [10]

2.5.4 Conclusion

All of these three types seem that they have something in common. If the inner lamina of the sandwich panel is designed to the arch laminar, the integrated

skin & shell shape looks like the multi-bubble, and the differences to Y braced box is not obvious. In the stage of research, the author should choose the reasonable configuration and do some initial design to minimize the weight penalty.

2.6 Composite materials

2.6.1 The advantages and disadvantages of composite material [11]

With the development of the material technology, composite material already plays an important role in airframe structure. The extreme weight reduction is the first best thing for the structure, theoretically, 42 percent of weight can be reduced by using the carbon fibre structure to change the conventional aluminium alloy. However, from the author's experience, 5 percent weight reduction is a successful composite optimized aircraft structure by using the proven technique. For aircraft, it is the most efficient way to reduce the weight. Comparing with the alloy materials, the advantages of the composite materials mainly are:

Easier to manufacturing and assemble;

Many composites, like stringers, frames and skin, can be designed to a stiffened panel. Alloy material stiffened panel is already used in air manufacturing successfully, but the disadvantages still cannot be ignored. The residual stress by machining should be considered in the stage of design, and the flexibility of the shape should be restricted. As far as these concerned by the composite materials, the process of production is moulding and solidification. By using this method, the residual stress can be reduced. Also, in manufacturing stage, the assembly of these composite can save a great number of man-hour.

Higher in terms of cost effective;

The benefit from gross weight reduction by using composite material is far more than alloys although the price is still more expensive. Obviously, as the author written above, the fuel consumption and the cost of manufacturing can be reduced remarkably. Additional, the technique of aircraft maintenance for

composite materials is mainly by using the method of bonding repair instead of riveting, welding and bolting etc. The merits of it are not only reliable, but also uncomplicated and economic. As the first production composite material airliner, Boeing claimed the 787 would be near to 20 percent more fuel-efficient than the 767, with approximately eight percent of the efficiency gain from the increased use of lighter-weight composite materials. And the mean time between maintenance can be extended to 1000 hours from the 500 hours of Boeing 767, and the maintenance costs can be reduced to 32 percent of Boeing 777.

Higher in terms of strength-to-weight ratio and stiffness-to-weight ratio, it can reduce the weight penalty;

Higher in terms of fatigue resisting capability;

In materials science, fatigue is the progressive and localized structural damage that occurs when a material is subjected to cyclic loading. The capability of materials for resisting the fatigue loading is often referred to as anti-fatigue property. Unlike metal alloy, the cracks of composite material have no sudden change, so there is enough interval to maintain and remedy, although the demerit is it does not always show the visible fatigue cracks.

Higher in terms of reliability and vibration reduction.

There are many fibres in resin matrix of composite material, once the structure is overloading, the component would not crack in a short term. The damping between fibres and matrix is so high that it can lead to a reduction of the vibration.

However, there still are several disadvantages vs. metals:

- Material is expensive
- Lack of established design allowable
- Corrosion problems can result from improper coupling with metals, especially when carbon or graphite is used (sealing is essential)
- Degradation of structural properties under temperature extremes and wet conditions

- Poor energy absorption and impact damage
- May require lightning strike protection
- Expensive and complicated inspection methods
- Reliable detection of substandard bonds is difficult
- Defects can be known to exist but precise location cannot be determined
- Barely Visible Impact Damage is hardly to inspect

2.6.2 Brief introduction for some types of composite material

2.6.2.1 CFRP

Carbon-fibre-reinforced polymer, reinforced by carbon and glass fibers, is a new type polymer which has a high ratio of strength to weight and a long service lifetime. This material has already been used for the fuselage of Boeing 787 Dreamliner and Airbus A350 XWB.

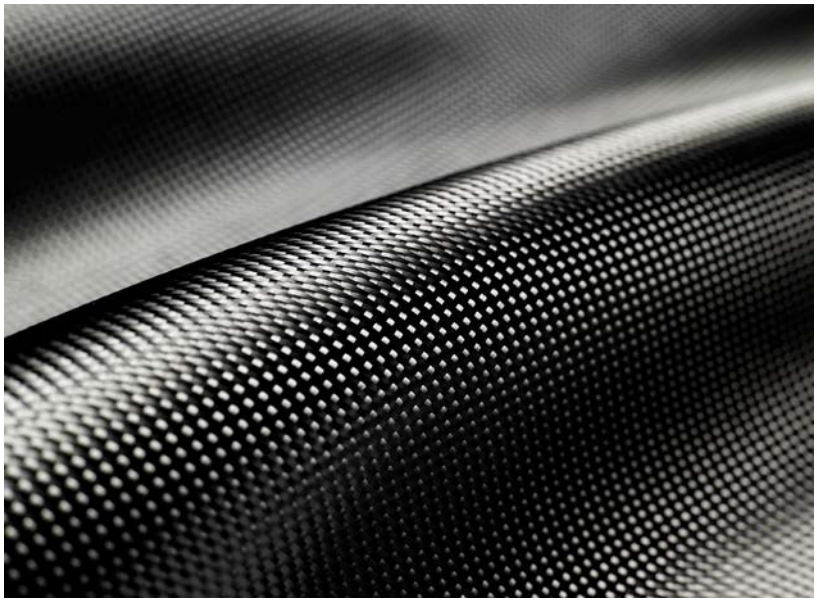

Figure 2.14 Carbon-fibre-reinforced polymer [12]

2.6.2.2 Sandwich structured composite

Two typical composite material of type are honeycomb core and syntactic core. Attached by two layers of skin and a thick core, the properties of it are the considerably higher shear stiffness to weight ratio from the core and the high bending stiffness to weight ratio from the panel.

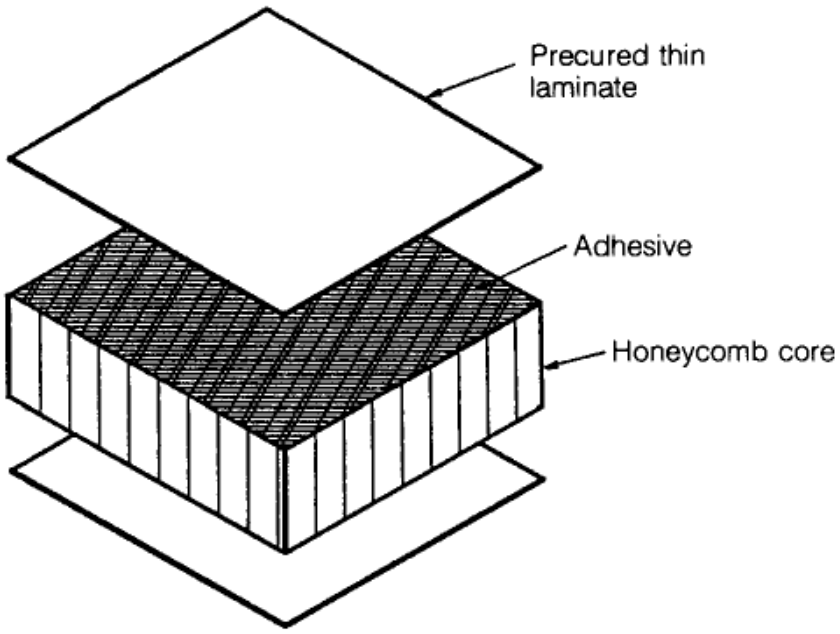

Figure 2.15 Typical Honeycomb sandwich construction [11]

2.6.2.3 GLARE

Figure 2.16 shows “GLARE”-Glass Laminate Aluminium Reinforced Epoxy, a new type of composite material made by Cytec Engineered Materials, is consisted of several layers of metal and prepreg (shows figure 3.4) and already be used in Airbus A380 horizontal and vertical stabilizers successfully.

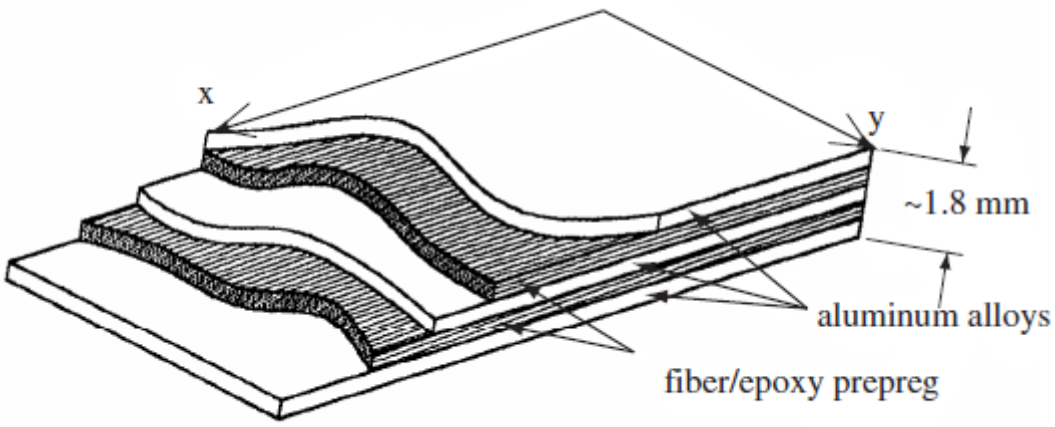

Figure 2.16 GLARE lamina [13]

2.6.3 Composite materials in modern airliners

2.6.3.1 Boeing 787 Dreamliner

The Boeing 787 Dreamliner is a successful airliner which uses 80% composite materials by volume and 50% by weight developed by Boeing Commercial Airplanes. This long range, middle size, wide body airplane have 210 to 290 seats which is quite near FW-11. Benefit from the efficiency of weight reduction of composite materials, 20% fuel was reduced comparing the similarly-sized Boeing 767. Figure 2.17 shows the parts which are manufactured by different materials.

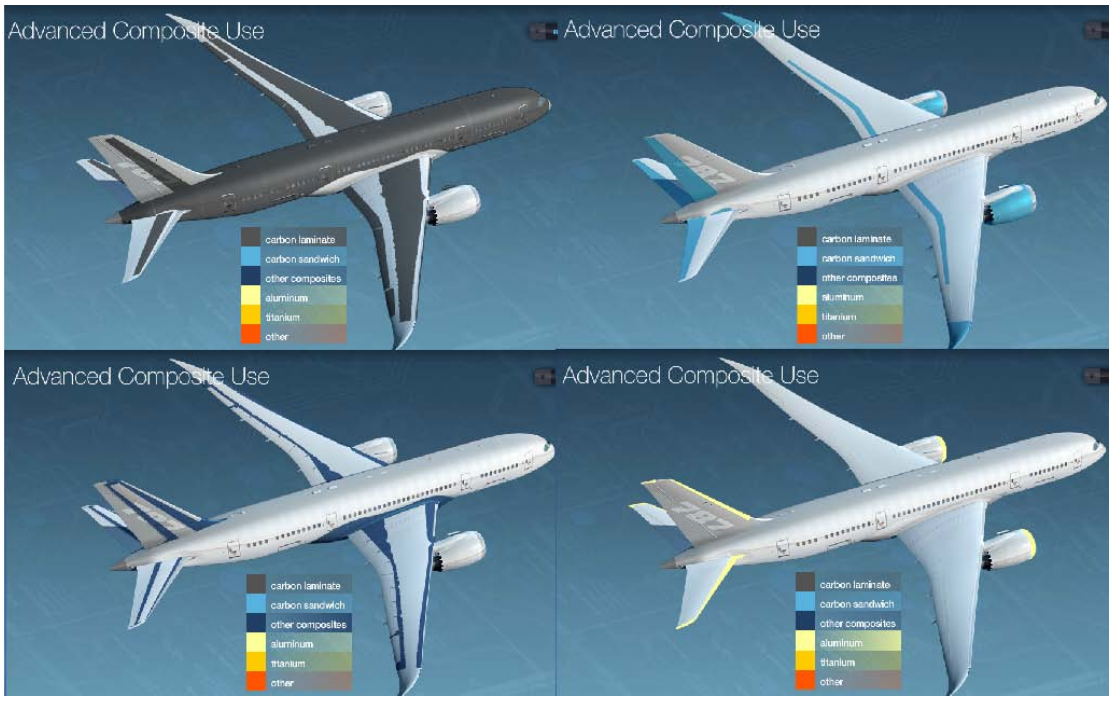

Figure 2.17 The advanced materials used in Boeing 787 Dreamliner: carbon fibre (top left), carbon sandwich (top right), other composite materials (bottom left), aluminium alloys (bottom right). [14]

The primary structure of B787 is mainly used the Torayca 3900-series highly toughened carbon fibre-reinforced epoxy prepreg supplied by Toray Industries (Tokyo, Japan). This trademarked series composite materials are made with intermediate modulus T800S fibre and used to make the vertical tail, the horizontal stabilizer, the unpressurized aft fuselage skins and stringers, the

centre fuselage, mid-fuselage, aft wheel well bulkhead, forward fuselage section, The centre wing box, the fixed trailing edge, the wing tips, fabricate cargo and access doors, etc.

Another prepreg in use is HexMC produced by Hexcel (Dublin, Calif.). This type of composite material is mainly used to produce the 787's larger window frames. Because of the lower density property, the weight reduction is almost 50 percent from aluminium alloy. It is also used for other structure components: including highly loaded gussets, pressure pans, clips, brackets and other small components.

Another extraordinary advance is the fuselage barrel which is made for a one-piece structure as shown in figure 2.18. This technique can eliminate the longitudinal connection between skin shells to reduce the weight from fasteners and auxiliary structure components, and the drag from aerodynamics.

Figure 2.18 Boeing 787 one-piece fuselage barre [15]

2.6.3.2 Airbus A350 XWB

Airbus A350 extra wide body (XWB) is a potential competitor to Boeing 787 Dreamliner, developed by Airbus Corp. it is claimed that the 52 percent of airframe is made of reinforced plastic composite, more than 50 percent of Boeing 787.It is the first airplane Airbus attempted to design the composite fuselage which is a tendency for the aircraft structure and adopted by Boeing 787 firstly. Airbus pronounced this type of airliner can save 25 percent step-change in fuel efficiency compared to its current long-range competitor. [16]

The design philosophy of Airbus is a conservative approach. The technology Boeing used to produce the one-piece fuselage barrel is not appreciated. They believe it is simple to control the weight through the method of optimizing the thickness of skin panel instead of the traditional placing skin shells over frames as shown in figure 2.19. However, the composite material adoption in A350 XWB is still a tactic revolution.

Figure 2.19 Airbus A350 XWB forward fuselage section [17]

The other part of A350 XWB is also replaced by composite materials: the rear fuselage section is made of a type of integrated carbon fibre as same as the horizontal stabilizer and fin/rudder assembly.

The wing of A350 XWB is designed to be composed of carbon fibre stringers and skins which is provided by Harbin Aircraft Group in China and manufactured by EADS in Broughton UK as shown in figure 2.20. It is also a first composite materials wing of Airbus.

Figure 2.20 A350 XWB Left Hand upper wing cover is being lifted into the first Main Assembly jig (Jig C) at the A350 North Factory in Broughton, UK. (22 November 2011) [17]

3 FLYING-WING FUSELAGE PRELIMINARY DESIGN

3.1 Introduction

3.1.1 Three versions of pressurization cabin

In the group design project, the author took part in the structure layout group to establish the baseline of the fuselage structure by using the data given by the other groups such as the outline of fuselage from aerodynamic group, cabin configuration and seat arrangement from cabin layout group and landing gear position from CG group.

At the first stage, the main assignment for structure lay out group is to define the base configuration type of the whole fuselage before the other components arrangement.

According to the theory of different types of the pressurization, three of the team members were in charge of building the 3D models based on the airfoil outline. Three versions of fuselage configuration were established for structure effective comparison. The plan is to find out the best solution for the cabin configuration.

Version 1

The author was in charge of the conventional type of multi-bubble, as shown in figure 3.1.

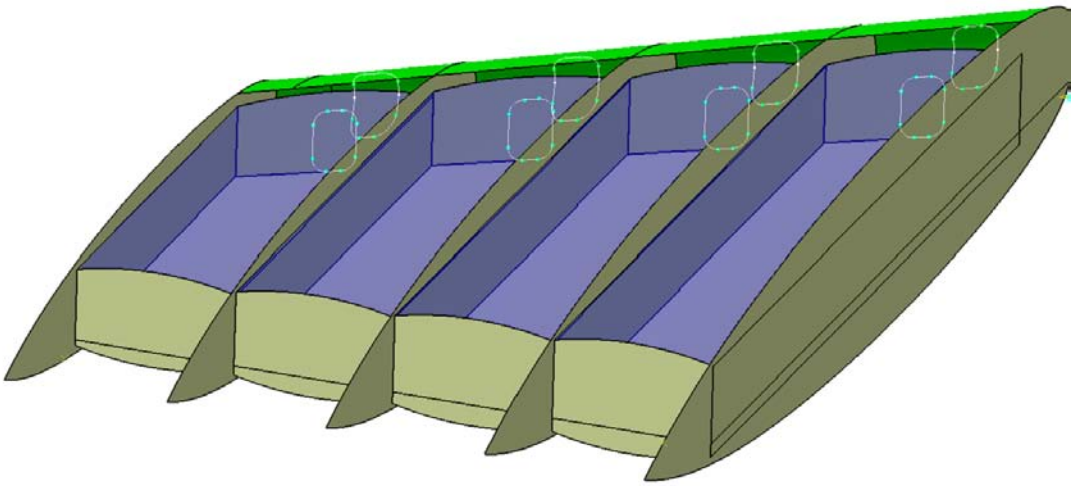

Figure 3.1 Multi-bubble cabin structure

Version 2

The model given by figure 3.2 was built by Pang Huahua, who was responsible for the columned multi-bubble configuration.

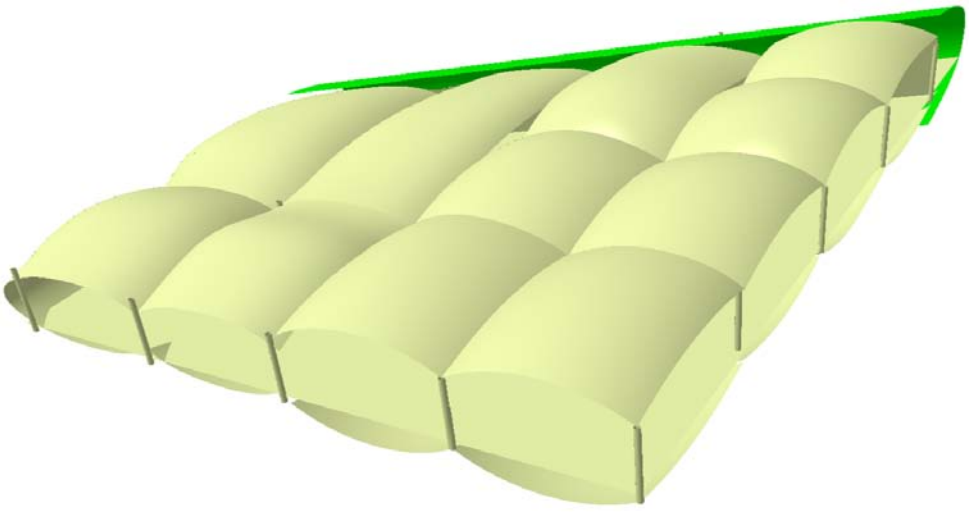

Figure 3.2 Columns support multi-bubble cabin structure

The main difference between version 1 and version 2 is the shape of pressurization skin and its auxiliary support beams. Version 1 merely uses ribs to be the support columns, but the struts can be simplified the ribs as shown in version 2.

Version 3

This type of fuselage designed by Xu rongxin was based on the theory of ribbed/ honeycomb panel configuration shown in figure 3.3.

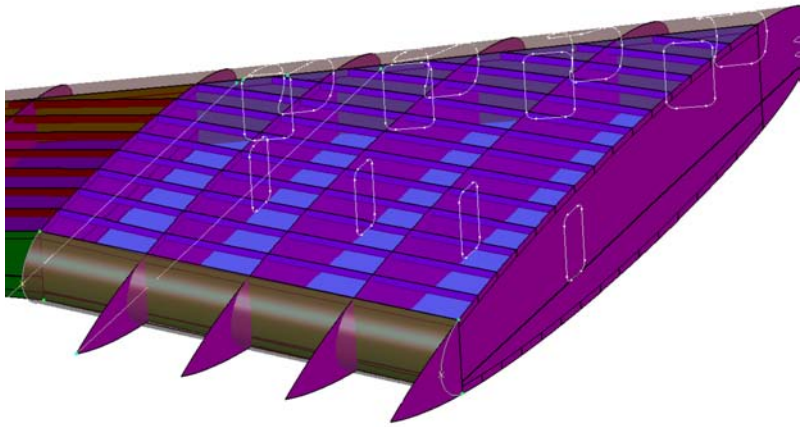

Figure 3.3 Ribbed panel structure

One thing should be noticed that there is a arched pressurization shell in the location of rear spar, which was considered to be a flat pressure bulkhead in version 1 and 2. And the advantages of this configuration are one layer of skin and the room efficiency in wing box.

3.1.2 Comparison in structural effective

For being lack of data, the main comparison between these three versions of fuselage was focused on the structural effective.

Figure 3.4 shows the multi-bubble theory. For the ordinary multi-bubble of version 1, the merit is mainly that this configuration can reduce the bending caused by the pressure in inner skin layer, so the thickness of the skin can be reduced to minimize the weight. However, it also can bring a contradiction between the weight and the space in the FW-11 flying-wing configuration.

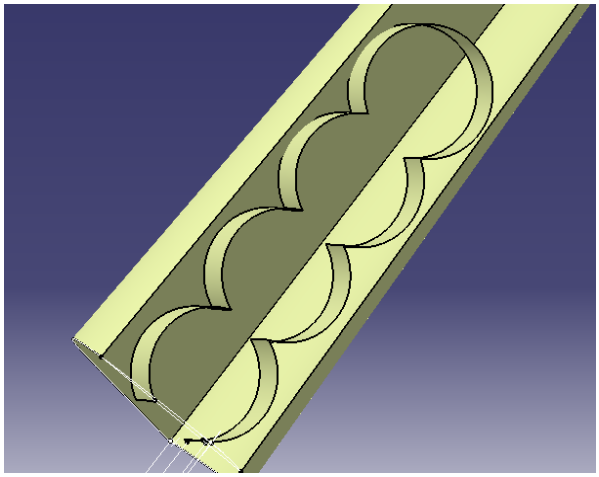

Figure 3.4 Room wasted condition of multi-bubble structure

For the columned multi-bubble configuration, the main embarrassments are this shape of the pressurization skin can bring much weight penalty and waste more room than the conventional multi-bubble configuration, although the sphere shape skin can extremely avoid the bending. From the manufacturing view point, this layout may increase the difficulty from and skin forging and assembling.

Unlike the multi-bubble configuration, the ribbed/ honeycomb panel configuration which has just one layer of skin can use the room effectively. But for nearly flat pressurization skin, the way to reduce bending is to thicken the skin and reduce the area of skin shell which needs the strong supported stringers in the mean time. Obviously, this solution can bring a great deal of weight penalty from the shell and the support structure.

3.1.3 Final configuration establishing in GDP

After comparison this three versions, the group thought all of these three types were not suitable for the FW-11. The other neglected theory Y braced box was researched again for the structural effective advantages. The configuration is applied in figure 3.5.

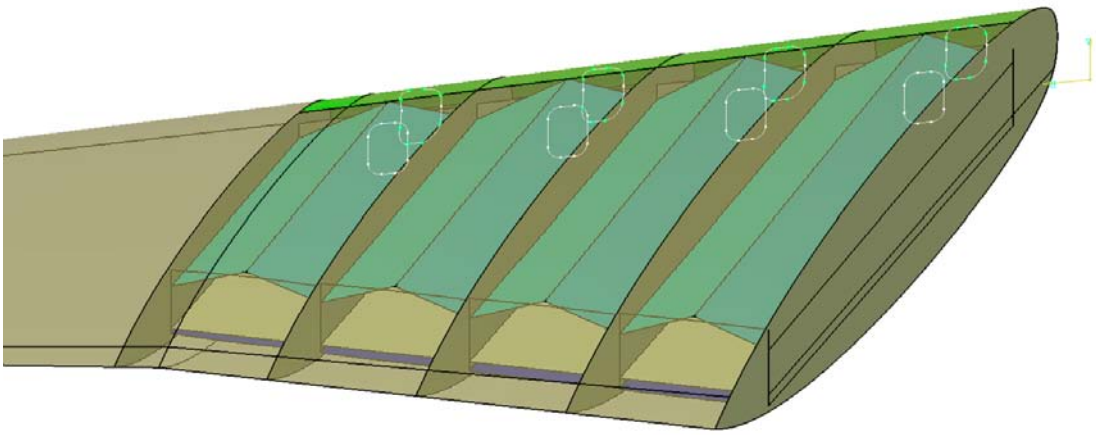

Figure 3.5 Y braced box structure

In this configuration, the braces just resist tension and small bending form pressure, which is critical for the thickness of pressure skin. The braces can be optimized to an arch shape as shown in figure 3.6. Apparently, vaulted shell seems similar to the compromised multi-bubble configuration the author did before, and the advantages which also have the similarity is the pressure can be changed to the membrane tensile instead of the bending. It seems that this type is very suitable for the FW-11, but there are still some demerits, such as the weight of additional fasteners, hard for routine maintenance and the inner layer has to resist external resultant loads.

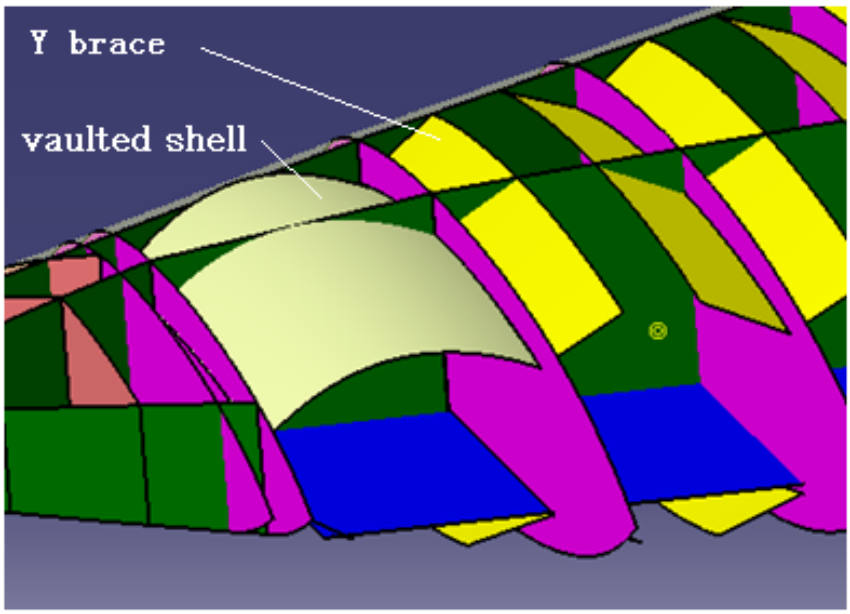

Figure 3.6 Y braced box optimized structure

The connection between the braced and the skin may use the method shown in figure 3.7 by using the Y braced integrate with the external skin. A little advance can be made by split the skin up: Flat/Vaulted Honeycomb Core connected with outer skin and inner vaulted shell. Apparently, it will bring some trouble for assembling.

There are still some demerits, such as the weight of additional fasteners, hard for routine maintenance and the inner layer has to resist external resultant loads.

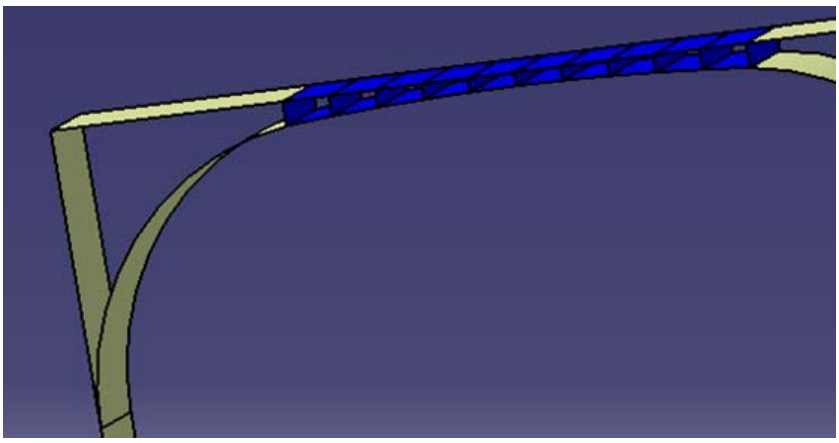

Figure 3.7 Y braced with ribbed panel

For fail-safe design, once the inner skin failed, the way to keep pressure should be considered. One solution is all of the ribs between cabins of passenger can be designed to airtight seal bulkheads. Once the inner skin in a cabin failed, passengers can evacuate to the others through doors. Another solution is that all of skins should be made sure they can both resist the pressure loads. Both of these solutions can bring a great deal of weight penalty.

If decided using the way of two layers of sealed skin, evidently, the weight penalty from outer skin is far more than the inner skin. One solution is keeping both room (separated by interior and exterior skin) pressurization, the pressure between inner and outer skin is lower than the passengers' cabin. Then the inner skin can be designed thinner for balancing the weight penalty.

3.2 Configuration selection

There is no further work for comparison in the group design project, so the pressure cabin configuration still needs to be analysed.

Generally speaking, for the conventional airplane, the critical factor for the skin thickness is the pressure differential. According to this, the research about cabin should focus on the stress concentration caused by pressure. The methodology to prove the structural effective in this thesis is the finite element analysis adopted by the author.

3.2.1 Pressure differential

The pressure loads for inner skin can be calculated in this phase. For FW-11, the maximum operating altitude is 13700m, and the cabin pressure is equal to value of 2483m. According to the data of standard atmosphere [18] and CS-25 [19], the pressure of 13700m altitude is 14785Pa, and the cabin pressure must be more that 75266Pa (the pressure at 2483m altitude). If select 2 Δp as the ultimate load, the value of Δp (the maximum relief valve setting) is complied in table 3.1:

Table 3.1 Y braced with ribbed panel

Δp	**1.33 Δp**	**2 Δp**
60481Pa	80439Pa	120962Pa

3.2.2 Model building

The main purpose of the models is to compare the different type of fuselage by using Finite element analysis, and discuss the advantages and challenges of them. When a more proper model structure is established, the following research will focus on the structure arrangement based on it.

From Denis Howe's suggestion, the frame pitch in the initial design phase can be estimated among 500mm [8]. Although the inner skin in FW-11 is considered to mainly resist the pressure load, the pitch can be wider, the model for FE analysis still select the 500mm length skin between two frames for initial estimation.

Figure 3.8 shows the location of the model for the whole plane.

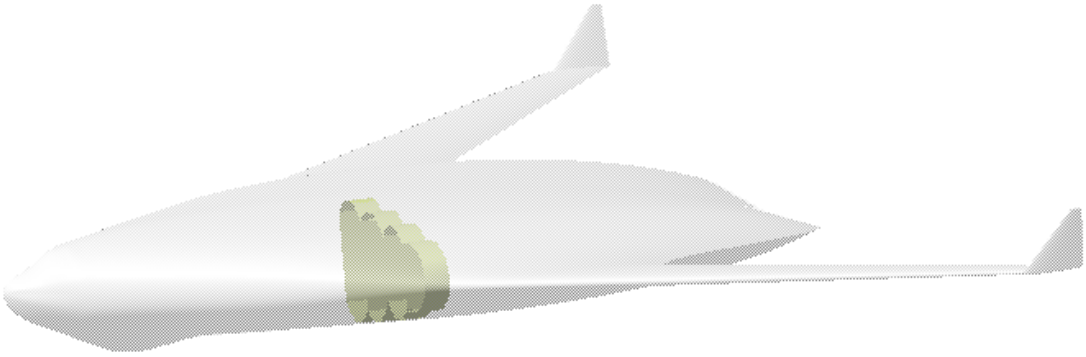

Figure 3.8 The sample location in fuselage

The cross-section of the FW-11 fuselage in the latitude direction is shown in figure 3.9. For evaluating these models, the condition of the three version should keep the same height.

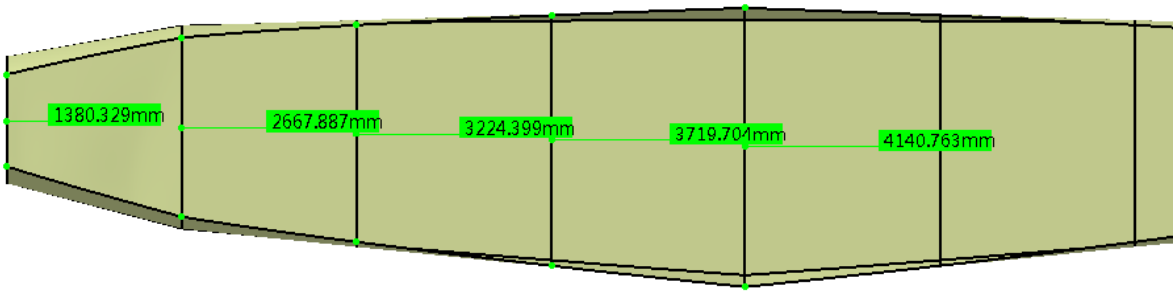

Figure 3.9 The height of FW-11 fuselage rib

Version 1

The first model is based on the Y braced box theory established in GDP.

The skin can be considered flat for between frames, the method to arrange the braces is shown in figure3.10.

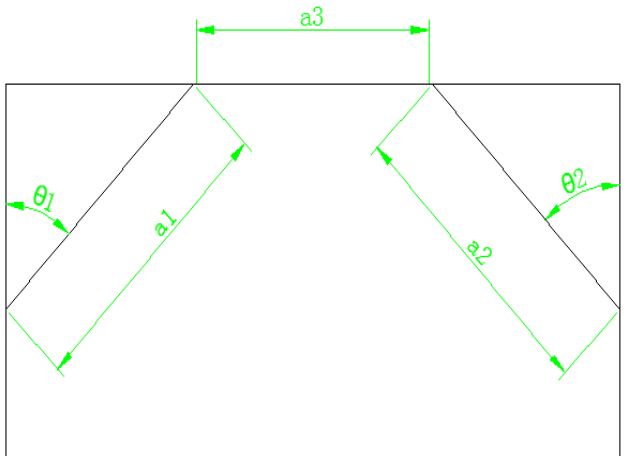

Figure 3.10 Simplified structure size of Y braced box cabin

The uniform pressure in skin and braces can be transformed to point forces. A good solution is the width of braces and skin should be same, so that the thickness of them can be equal to resist the pressure, namely:

$$a_1 = a_2 = a_3$$

The sizing of $\theta_1 \text{and} \theta_2$ can use the stress analysis as shown in figure 3.11.

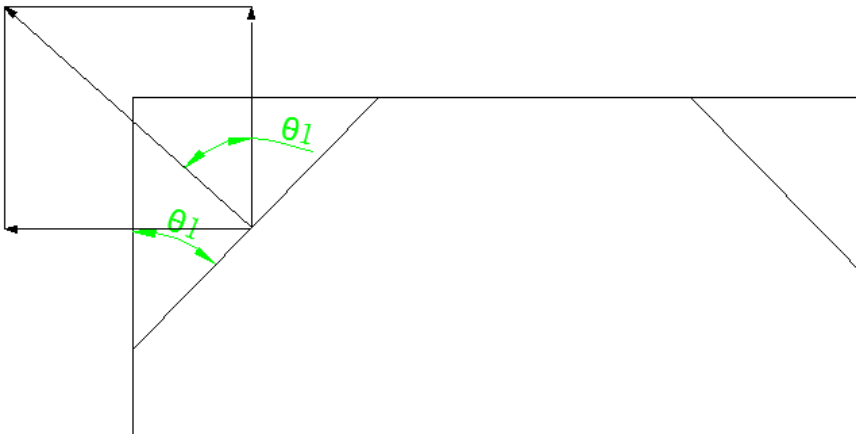

Figure 3.11 Pressure stress components on brace

The pressure stress on a braced can be break into vertical stress component and horizontal stress component, the latter can interfere the junction of skin and ribs. The stress concentration can be avoided if the stress/ strain in each end of the braced are equal. If the angle between skin and rib is α, then the value θ is given by:

$$\theta = \frac{180 - \alpha}{2} \quad \textbf{(3-1)}$$

The width of skin is given by:

$$a = L/(1 + \frac{1}{2\sin\theta} + \frac{1}{2\cos\theta}) \quad \textbf{(3-2)}$$

By using this method, the model is shown in figure3.12:

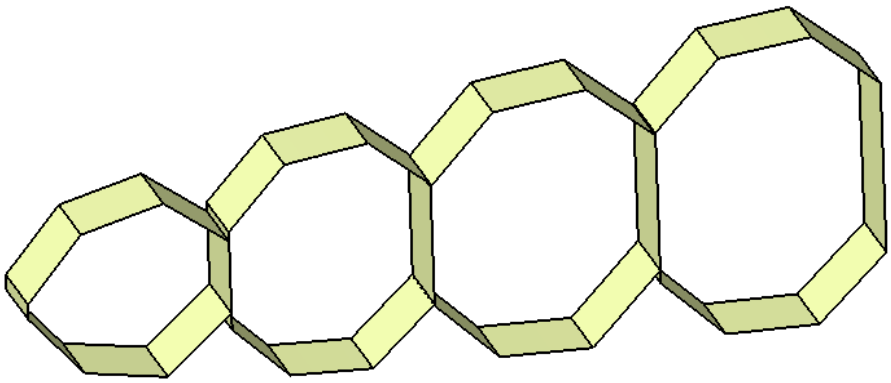

Figure 3.12 Y braced box fuselage model

Version 2

If use the arched braces to replace the flat braces, then the model can be built as shown in figure 3.13. The dimension size of version 2 is the same as version one.

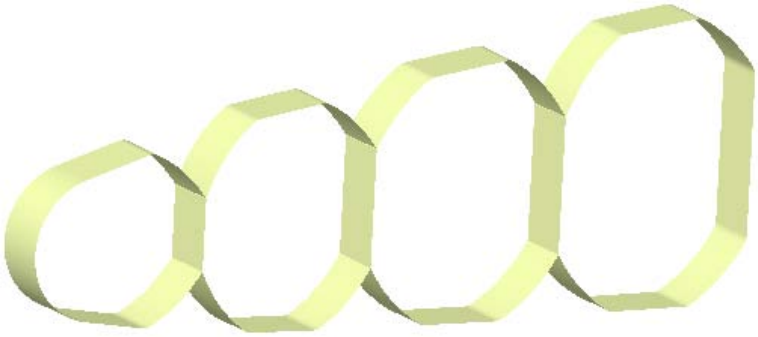

Figure 3.13 Arched braced box fuselage model

Version 3

The third model is decided to use the multi-bubble configuration. The method to calculate the radius of the shell is applied in appendix A. the model is applied in figure 3.14.

Figure 3.14 Multi-bubble fuselage model

3.2.3 Finite element analysis

The software to do the FE analysis is Patran & Nastran [20]. The purpose is to check the tensor concentration under the ultimate pressure which is 120962Pa.

3.2.3.1 Finite element analysis model rules

The model principle is:

- The loads in consideration is only the uniform pressure 60562Pa, the value is from the pressure differential when the airliner in 13700 meters level. This analysis focus on the skin tensile from pressure, so the other loads is not necessary.
- The vertical beams and floor beams is simplified to a shell by being lack of exact data so that the model can easy to built.
- The model just pick a section of the whole model, the reason is the shape of the cabins is symmetrical in the longitude direction. And the width of the model is 500mm.
- There is no support component in the skin shell. The main purpose of the FE analysis is to try to find out the stress concentration area in the skin, and use the results to the guide line for the stringer pitch definition. The thickness of skin means equivalent thickness.
- The ribbed/ honeycomb panel configuration is not reality for the airliner due to the large pressurization cabin, so the analysis is not necessary.

3.2.3.2 Geometrical models build up

a. Models

The models have already been built in CATIA, as shown in section 2.2. The data was imported to Patran, and the model units is 1000mm.

b. Material selection

The materials in this analysis are aluminium alloys. To distinguish the properties of three fuselage version, the material should be as same as the others. Table 3.2 shows the materials used in three models.

Table 3.2 Material selection in models

Type	Y-brace	Arched-Brace	Outer skin	Arched shell	bulkhead	Beam sheel
Y-braced box	Al 2090-T83		Al 2090-T83		Al 2090-T83	Al 2199
Arched braced box		Al 2090-T83	Al 2090-T83		Al 2090-T83	Al 2199
Multi-bubble				Al 2090-T83		Al 2199

The material property is shown in table 3.3.

Table 3.3 Material properties [21]

Matrerial	Elastic Modulus (MPa)	Poisson Ratio	Density (kg/mm^3)
Al 2090-T83	79000	0.30	2.58×10^{-6}
Al 2199	77200	0.33	2.64×10^{-6}

c. Mesh

The average mesh length in three models is 50mm. This accuracy is proper in the initial estimation phase for time saving. Because all the elements in the model are surfaces, all the meshes are quadrangle elements.

d. Boundary condition

The surface edges are constrained in all directions and rotations as shown the red lines which represent the frames in figure 3.15. In these models, the edges represent the frames in the fuselage, for the reason of simpler method before the initial design of frames. The reason for the boundary constraining is to assume the frames is rigid, and then the tension on skin surface caused by the pressure can be as same as the real theoretical condition.

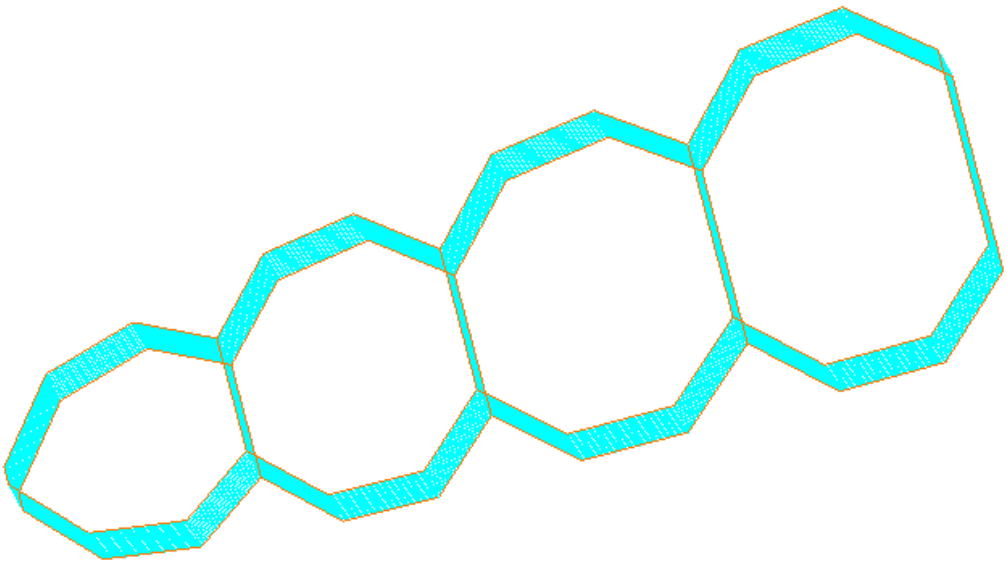

Figure 3.15 Constrained boundaries

e. Loads

The only loads took into account is the uniform pressure. All the loads are on the interior surface of cabins. Figure 3.16 shows the loads on the interior surface in the multi- bubble shape.

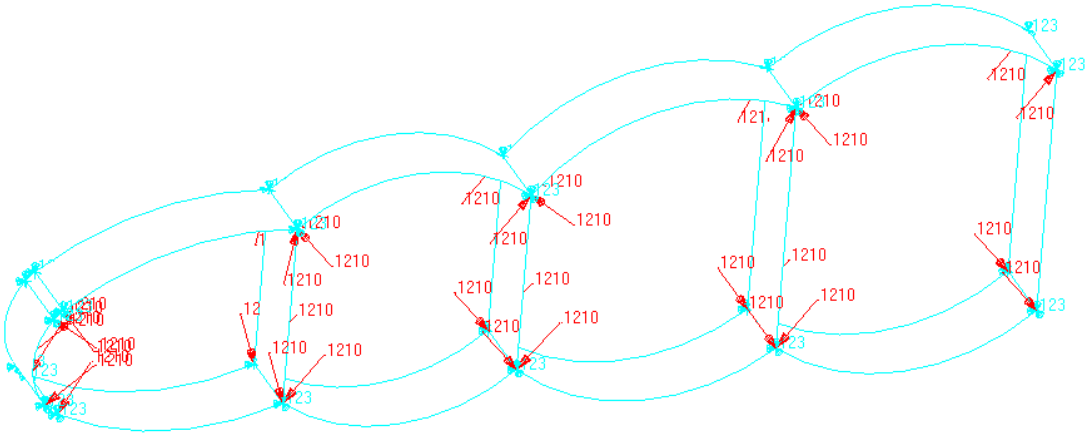

Figure 3.16 Pressure loads on panels

f. Results

Version 1

The result for the Y-braced box is shown in figure 3.17.

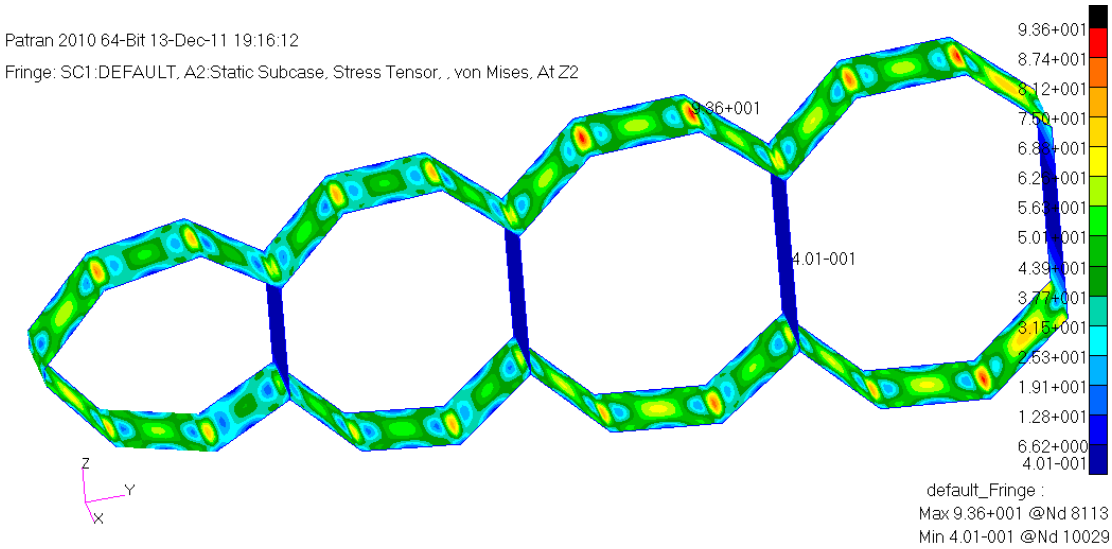

Figure 3.17 Y braced box model FEA results (1000mm)

As except, the flat skin can cause stress concentration. This configuration can equally distribute the tensile loads to the braces and skin, but to the single skin/braced panel, the bending caused by the pressure is not desirable. The main stress concentrations happened in the junction between braces and skin, braces and beam shell.

Table 3.4 shows the adjusted thickness of every part.

Table 3.4 Skin thickness of Y braced box model components

Part	Braces	skin	bulkhead	Beam shell
Average Thickness	20 mm	20 mm	15 mm	2 mm

The mass estimation can use Patran to calculate, the total mass of version 1 is 1.16×10^3kg.

Version 2

If replace the braces and the bulkhead to the arch shape, then the result of FE analysis is shown in figure 3.18.

The calculation about radius of the braces and arched bulkheads can check Appendix A.

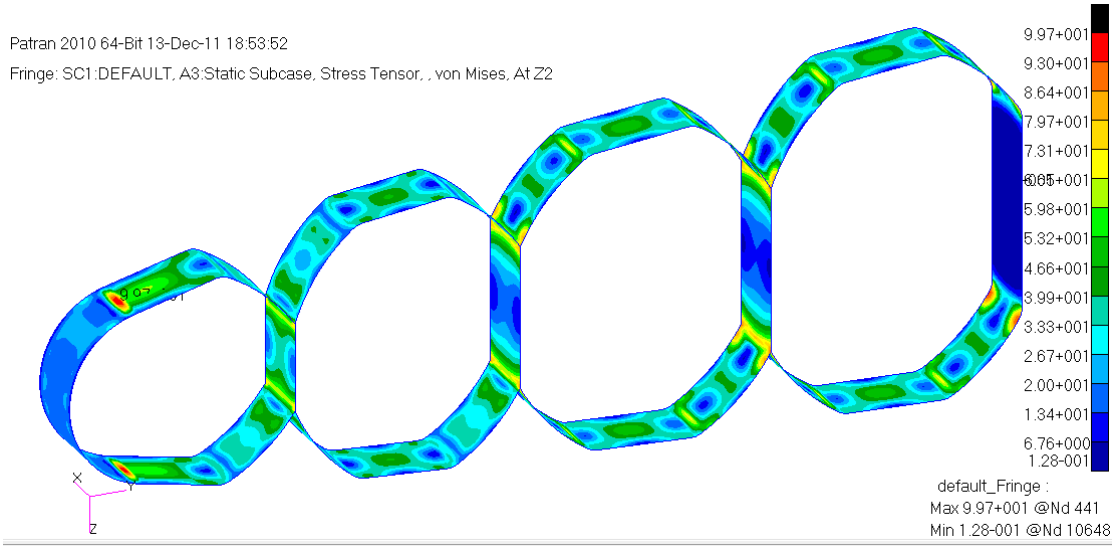

Figure 3.18 Arched braced box model FEA results (1000mm)

From the picture, it is obvious that the stress concentration area is the same as version 1.

Table 3.5 shows the adjusted thickness of every part.

Table 3.5 Skin thickness of arched braced box model components

Part	Braces	skin	bulkhead	Beam shell
Average Thickness	8 mm	24 mm	6 mm	2 mm

The mass estimation can use Patran to calculate, the total mass of version 1 is 8.14×10^2kg.

Comparing to the Y-Brace, the arch shape braced is superior in terms of stress concentration avoiding, as the result the adjusted thickness only 40% of the Y brace. However, the skin thickness in this configuration should be thicken to withstand the bending, the weight penalty from that is not to be neglected. The max tensor happened in the junction where the arch radius changed, it revealed that support structures should be arranged in that section.

Version 3

If uses the whole arched shell, say, the multi-bubble configuration, the result is shown in figure 3.19.

The calculation about radius of the braces and arched bulkheads can check Appendix A.

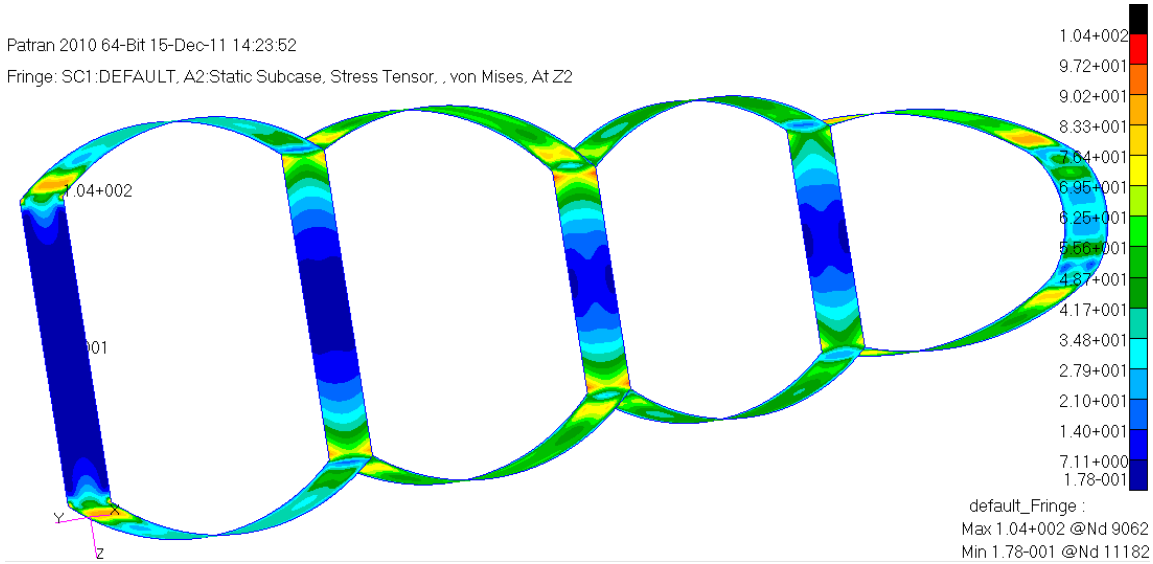

Figure 3.19 Multi-bubble model FEA results (1000mm)

Table 3.6 Skin thickness of multi-bubble model components

Part	**shell**	**bulkhead**	**Beam shell**
Average Thickness	5~7 mm	6 mm	3 mm

The mass estimation can use Patran to calculate, the total mass of version 1 is 3.64×10^2kg.

The stress concentration condition in multi-bubble configuration is much less than the above two types, and the membrane tensor distributes evenly, it means the skin thickness may also evenly in the condition of resisting only the pressure loading.

This configuration also has an outstanding advantage about the weight reduction. The weight is only one third of the Y braced box structure. If take the external skin into account, the weight of multi-bubble is still one second of Y braced box at least.

Another point to notice is that the stress concentration in this structure happens in the junction between beams and skin. Some auxiliary support beams should be arranged in that section to distribute the stress concentration.

3.2.4 Discussion

By comparison, in the author's opinion, the multi-bubble may be a better way than others for definition. So in this thesis, the author focused on the multi-bubble pressurization cabin design.

The method for the multi-bubble design can be divided to two different parts: the inner multi-tube cabin and the outer airfoil. The experience from conventional airliner design can also be used for these two parts.

In this configuration, the bending moment and the torque are mainly carried by the outer skin, and the pressure mainly carried by the inner skin. Two layers of skin seem that it can bring more weight penalty from itself and the auxiliary support components, however, the critical loads in the skin are always the pressure. Outer skin can be very thin to withstand the torque and bending moment as well as maintain the shape of airfoil. All of these issues can use the conventional way to sizing, the only obstacle is the connection between them.

3.3 Final fuselage shape

The whole fuselage section can be separated to the exterior wing and the interior pressurization cabin. The way to design this two pare can also be separated: the outer wing can use the wing design method to estimate the data, and the inner cabin can use the cabin design method. In this thesis, the author would put more focus on the inner pressure cabin design. the model is applied in figure 3.20.

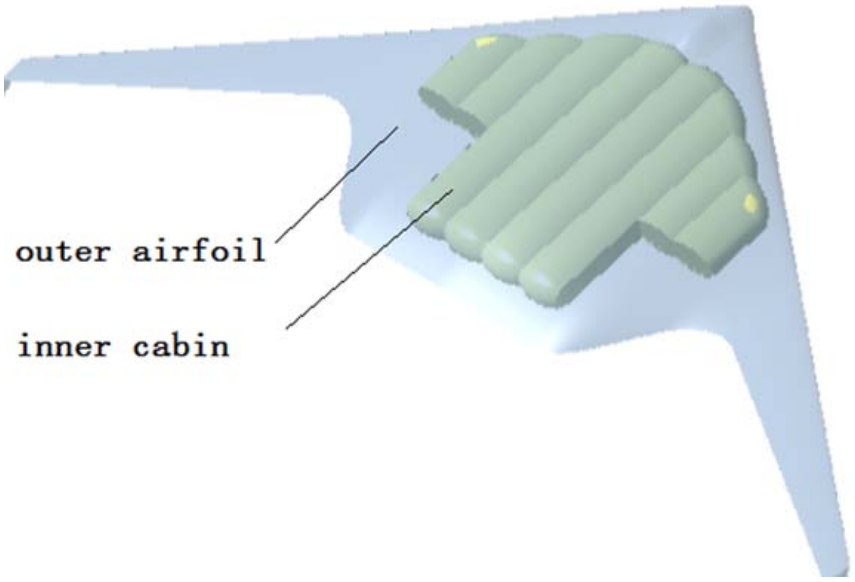

Figure 3.20 Structure layout of the fuselage

3.3.1 External airfoil

The outer fuselage which defined by FW-11 aerodynamic team has many challenges. At first, it should de wide and deep enough to contain a 200 seats cabin, some contradictions generated between aerodynamic performance and the cabin request. To reduce the thickness of the fuselage, the cargo cabins are defined in each side. The length of fuselage is also compromised for the capability of the cabin. It would increase the wet area of inner airfoil to generate more drag.

3.3.2 Internal cabin

The internal cabin initial design was finished by FW-11 structure team. As the author changed the configuration, the model should be updated.

This fuselage can be divided to three parts: pilot cabin in cockpit, passenger cabin and cargo cabin. Pilot cabin could have interference with the nose landing gear, so the floor should be sealed; passenger cabin is the most important part in this thesis, the size and initial design should be defined; cargo cabin can be in conformity to passenger cabin.

3.3.3 Challenges

The main challenge of fuselage is the connection between the external airfoil and internal cabin. In FW-11 model, there is a fuel tank under the floor of passenger cabin which would make the connection more complicated. For initial structure design, the author decided to ignore the other structures between interior and exterior fuselage.

3.4 Landing gear bay

The author took charge of FW-11 landing gear bay design in group design phase. The position of the landing gear has an impact in the fuselage design of a flying wing aircraft. The landing gear position was given by FW-11 CG team, as shown in figure 3.21.

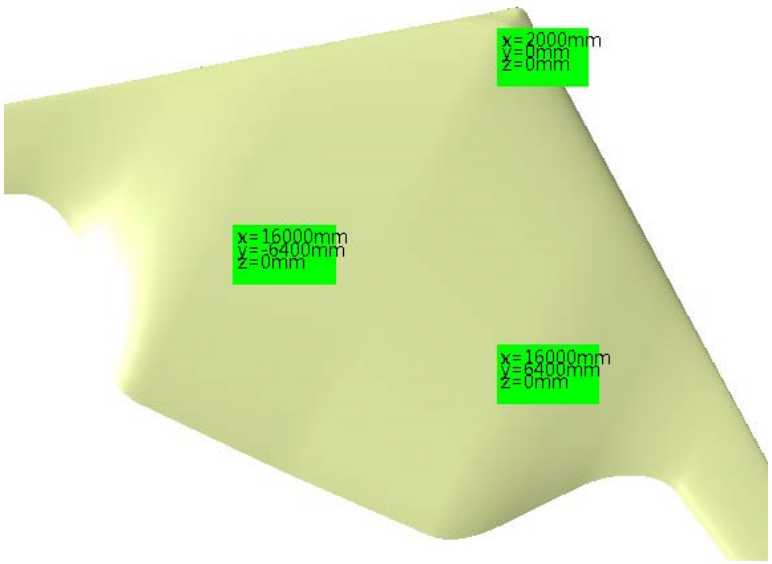

Figure 3.21 Landing gear location

3.4.1 Arrangement

At the beginning, the author found there did not have enough room for landing gear bay between floor and external skin. The conventional approach to deal with it is normally to thicken the fuselage or arrange the fairing. Aerodynamic

team claimed that the thickness of fuselage should not increase any more, but they agreed with auxiliary fairing proposal.

Figure 3.22 shows the fairing arrangement in the first version. The main landing gear and the nose landing gear are both arranged.

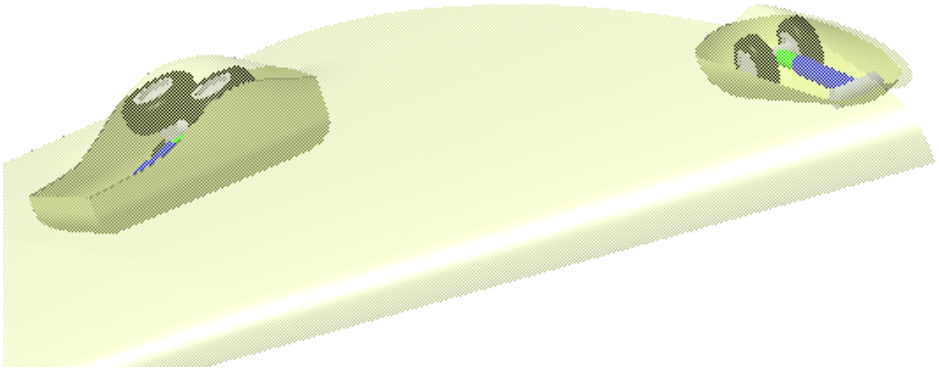

Figure 3.22 Initial landing gear contained condition

Considering the wet area increase of the fairing, and the trouble from manufacturing view point, the main landing gear faring was cancelled, replaced by a independent cabin, the model was updated as shown in figure 3.23, the nose landing gear can be contained by a fairing and the main landing gear can be contained in the independent bay.

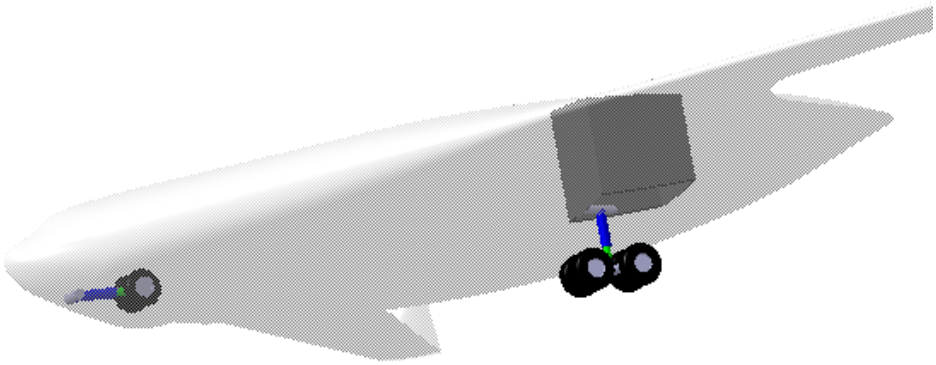

Figure 3.23 Final landing gear contained condition

.

3.4.2 Challenges

There is a fairing in nose landing gear, it can bring more aerodynamic drag.

To avoid it, one way is change the shape of the nose, as shown in figure 3. 24, the other way is the nose landing gear also can be retracts forward, and the floor in pilot cabin can be raised to provide enough room.

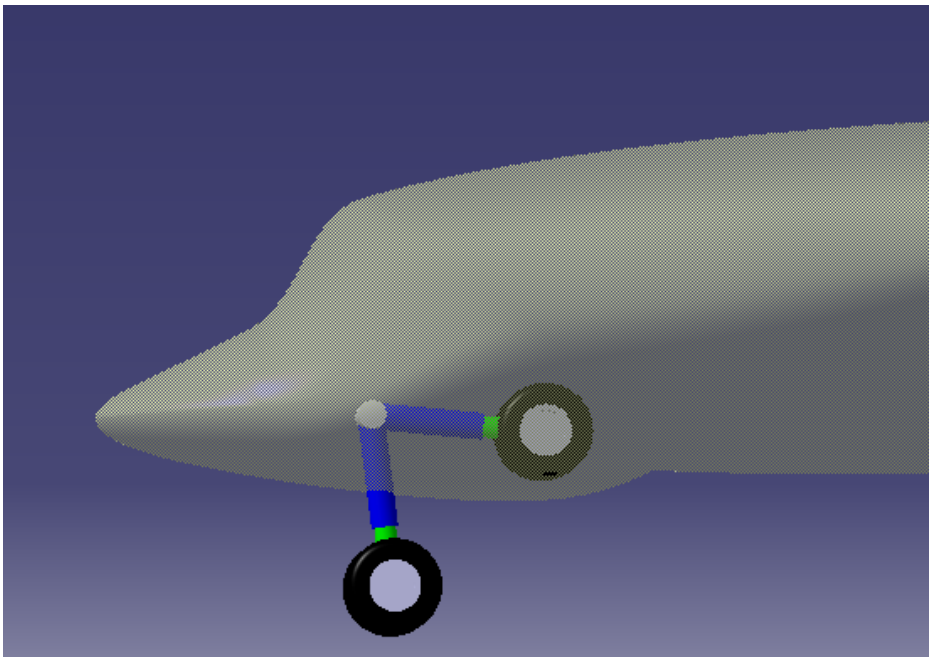

Figure 3.24 Optimized nose landing gear bay

3.5 Pressurization bulkheads

For the whole fuselage, some area need to be sealed for pressurization, it includes the four cylinder shell passenger cabins, four cargo cabins and the pilot cabin in the front of fuselage.

3.5.1 Arrangement

Figure 3.25 shows the pressure bulkheads in the FW-11 model. Two flat bulkheads were used to seal the side wall of pilot cabin, and one for the nose

landing gear bay. The bulkheads at the position of passenger cabin side wall can be defined to flat or arched, it depends on the condition of the main landing gear arrangement. Of course the arched shell is a better choice, however, the worse condition also need to be discussed.

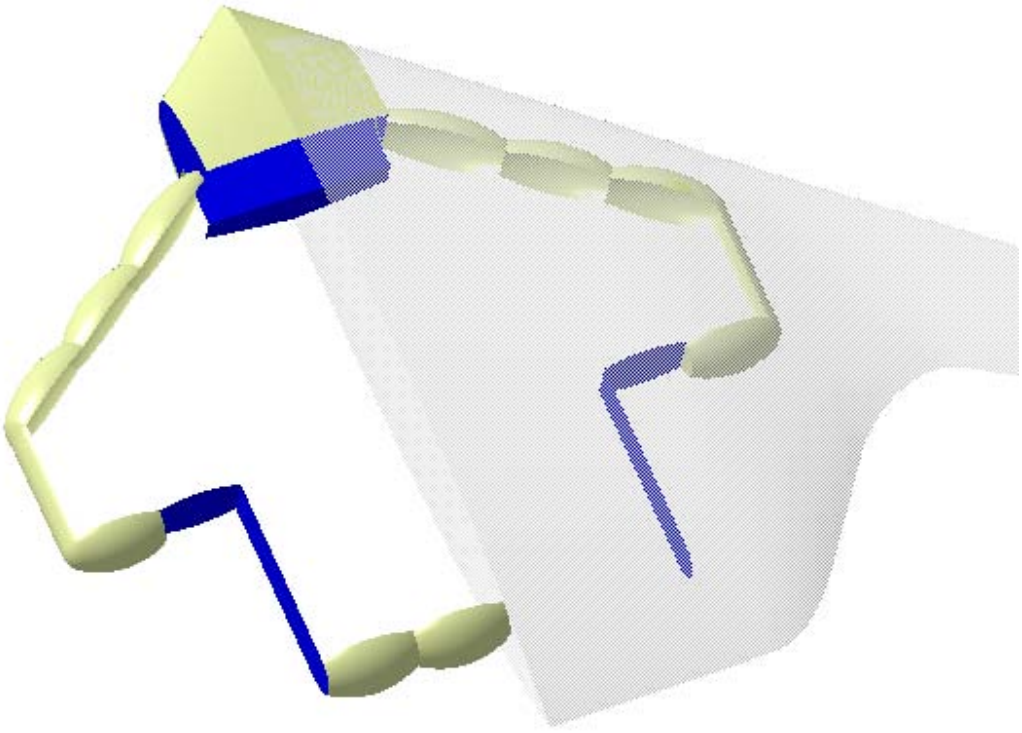

Figure 3.25 The position of pressure bulkheads

In figure 3.25, the yellow shell represent the arched bulkheads or dome shell, the blue represent the flat bulkheads. The bulkheads in front and rear cabins can be designed to a dome shape. Comparing the flat shape, although this hemispherical dome is not easier for manufacturing and assembling, it can provide the lowest membrane tensor under the pressure and reduce the weight by thinning the thickness of bulkheads.

3.6 Inner cabin structure arrangement

The structure layout for FW-11cabin is based on the multi-bubble configuration. The structure should make sure that all the loading paths, thus, there should have the attachments to connect with the main structure components.

3.6.1 Introduction

The initial sizing of the cabin structure is applied on chapter 4. The basic structure arrangement is shown in figure 3.26:

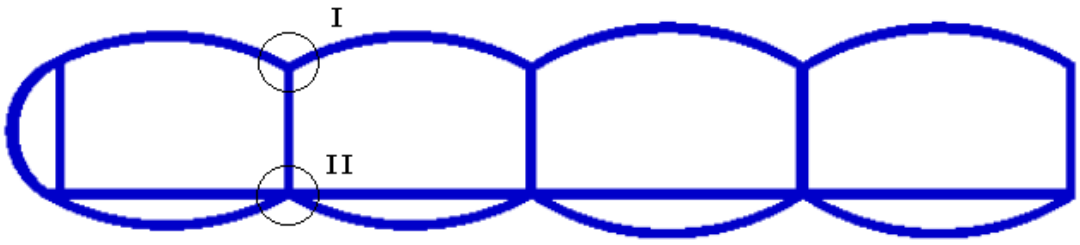

Figure 3.26 Cross-section baseline

3.6.2 Vertical beam structure

Vertical beams are arranged for the reason that there should have a tie in the section where the radius changed. The function of these vertical beams is resists the tension from pressure and the weight load from the structure, passengers and cargo.

The type of these beams can be a thin sheet metal. Considering in the passenger cabin this would make some trouble in manufacturing and assembling, plus the convenient of passengers, it should be replaced by beams.

The cross-section of vertical beams should be considered carefully. Vertical beams can be connected between frames to distribute the point load. If the attended mode is hinge joint, then the beams only resist the tension, a good

choice for the cross-section is the struts. Figure 3.27 shows the typical cross-section and the bearing pattern of two-bar structure.

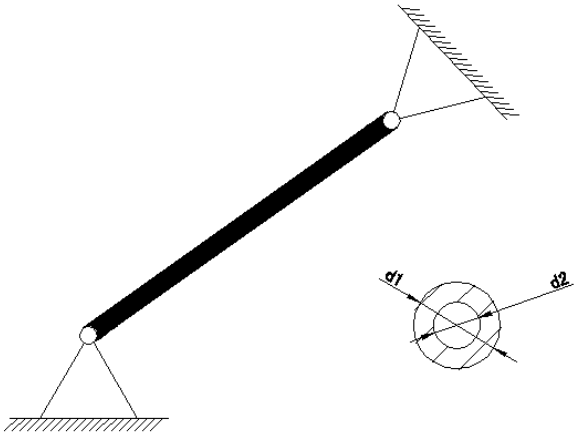

Figure 3.27 Basic type of the struts

3.6.3 Frame arrangement

The author designed two types of structure arrangement for the interior cabin. The main issue between them is the arrangement and shape of frames.

3.6.3.1 Version 1

As shown in figure 3.28, frames are designed to support both inner and outer skin. By such means, the frame can supports both inner pressurization skin and outer airfoil skin.

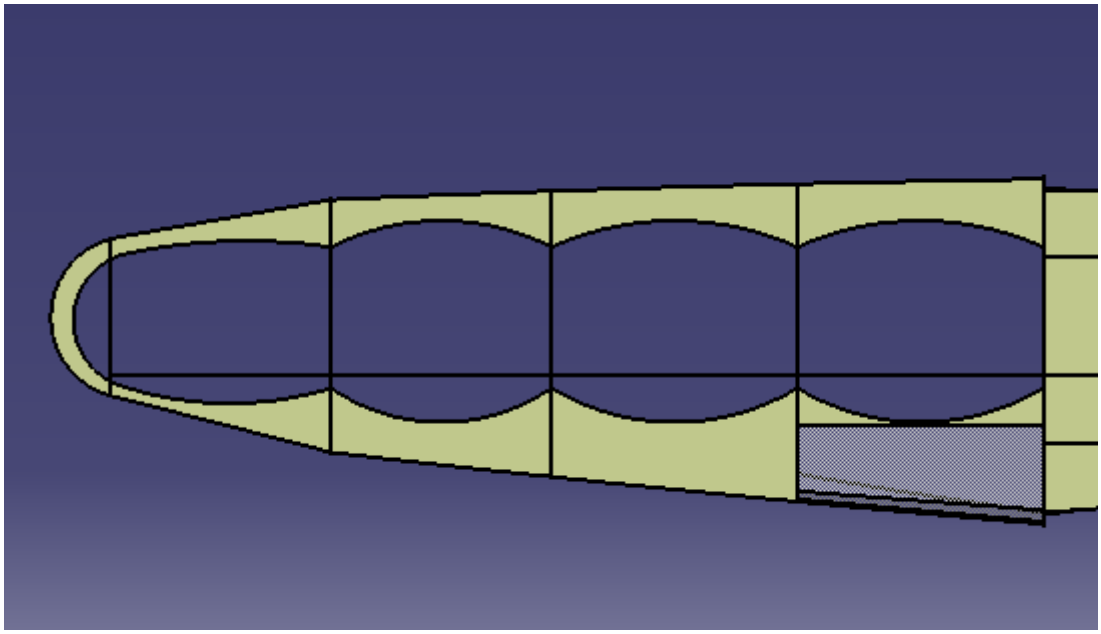

Figure 3.28 The attachment of interior cabin and outer airfoil

One disadvantage of this type of frames is: in some area especially the intersection between bubbles the depth of frames can be oversized.

Although some lightening holes can be arranged to reduce the weight, the weight comparing the conventional airliner under the same capacity may be heavier.

3.6.3.2 Version 2

To avoid the demerits from the over-depth frames, the author considered the other method for the inner cabin design.

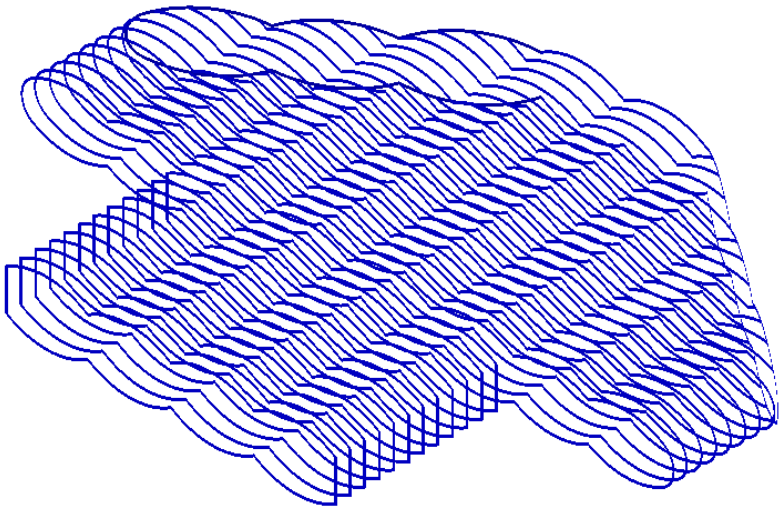

Figure 3.29 Frame baseline

Figure shows the other type of frames in inner cabin. They look like the conventional frames, but the shape changed by the pressure skin. As the inner skin does not need to resist the aerodynamic force, the frame pitch can be longer.

There still have some challenges for this version: the connection between inner cabin and outer airfoil; outer skin reinforcement; shear force distribution from ribs, etc.

3.6.3.3 Discussion

The first principle to design a airliner is the weight reduction. From this aspect, version 1 is not suitable. For version 2, the connection between inner cabin and outer airfoil can be a challenge. Both version 1 and version 2 have their advantages and disadvantages. One solution is discussing the connection with other components, and find out a reasonable arrangement.

3.6.4 Stringer arrangement

The typical shapes of stringer have already introduced by the author in Literature Review. For the different shape, the sphere of application is also different:

- Z section stringer is easy to manufacture but it can lead to torsion instability by the offset of the shear centre
- Top hat section is also easy to manufacture and the structure efficiency is higher. However, according to the enclosed space it made, the inspection process would be difficult.
- J section is difficult to form, but it is suitable to use in the condition of connecting two panels because of the longer flange.
- Y section is difficult to manufacture, but the structure efficiency is the highest. It is also difficult to inspect.

3.6.5 Floor beam arrangement

The author decided to use the typical I shape beam as the floor beam.

Two conditions should be considered in the floor beam initial sizing: the loads in passenger cabin and in cargo cabin. The size of these two beams is different.

For the long distance of fuselage width, it is by no means acceptable to use a single beam in the latitudinal direction in terms of structure rationality and manufacturing.

The floor beams in FW-11 model can be assumed that it is separated to eight freely supported beams in the latitude direction.

The cross-section chosen by the author is I section, and the connection of floor beams can be attached with frames.

3.6.6 Longitudinal support structure arrangement

There has a stress concentration under the pressure in section I as shown in figure 3.30. The connection in joint I have these structure components: skin, frames, stringers and struts, but longitudinal wall beam which resists the stress concentration also need to be arranged.

The stress concentration in joint I has already be discussed in section 3.2.3. Figure shows the exact condition by using FE analysis software.

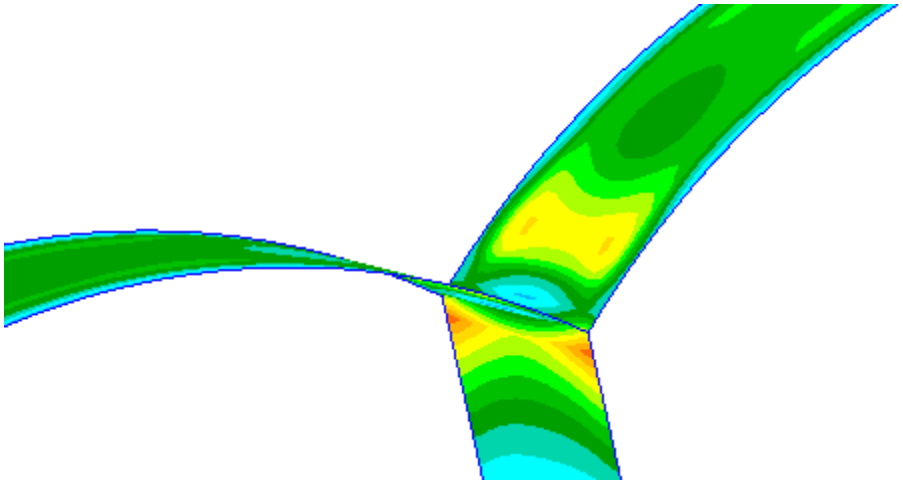

Figure 3.30 Stress concentration at the joint

The author did the first estimated design in joint I, as shown in figure 3.31:

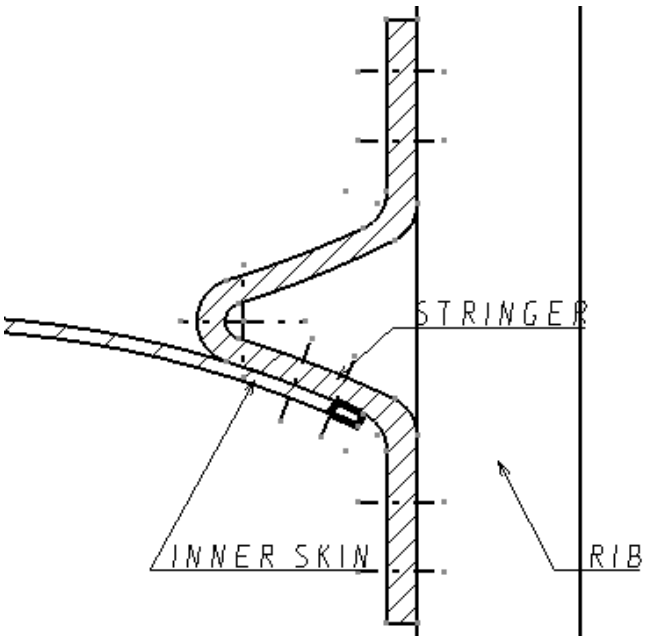

Figure 3.31 One choice for cabin skin attachment

However, this structure is not suitable because the author neglect the tension concentration. The structure in this joint should resists the huge tension and distribute it to frames and vertical struts.

Another type proposed is the reinforced Y beam, as shown in figure 3.32:

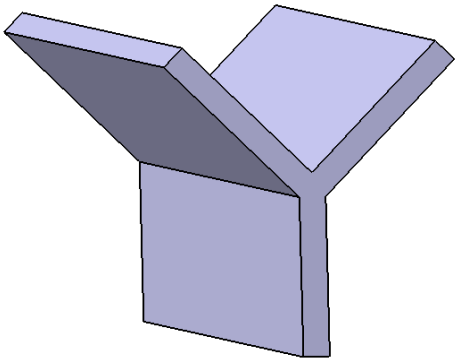

Figure 3.32 The shape of Y beam

3.6.7 Structure connection in joint I and II

The connection in joint I and II should be arranged rational, although it is complex. Some solutions designed by author should be discussed carefully, because they all have merits and defects.

The connection between Y beam, frames and skin in joint I is applied in figure 3.33:

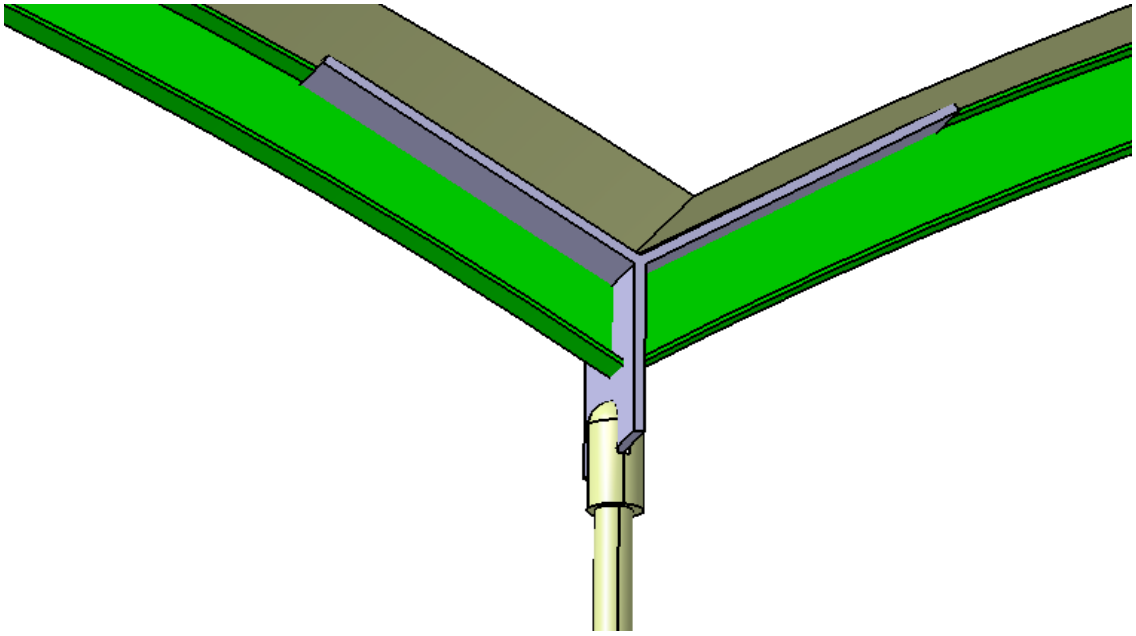

Figure 3.33 A type of arrangement of joint I

Another choice is put frames outside of skin, as shown in figure 3.34. This configuration can avoid the cut-out on frames or Y beams for structure interference.

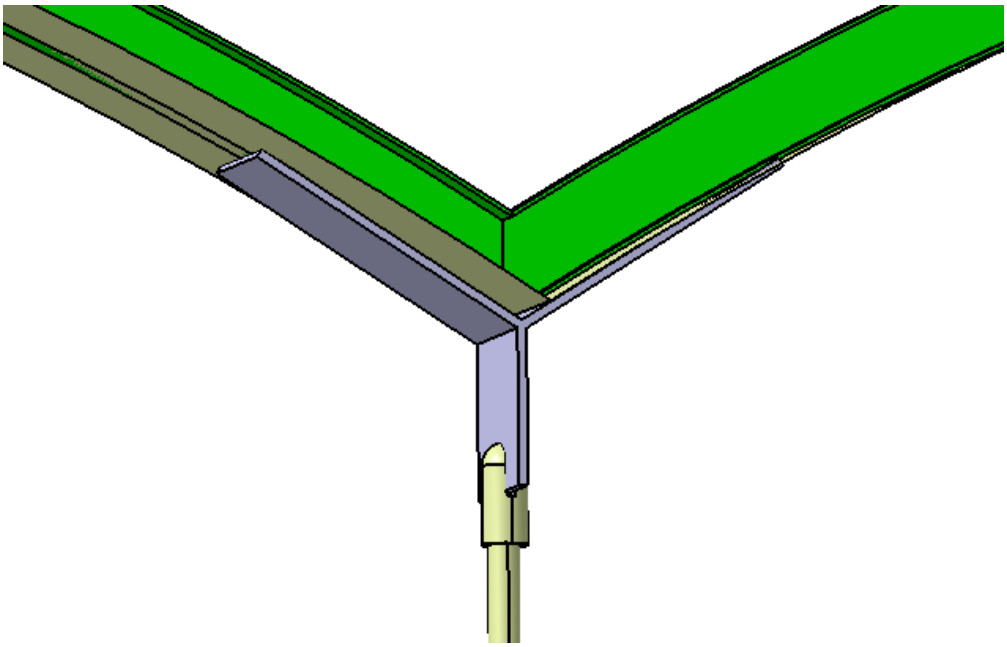

Figure 3.34 Another arrangement at joint I

The connection between Y beam, floor beams, frames and skin in joint II is applied in figure 3.35:

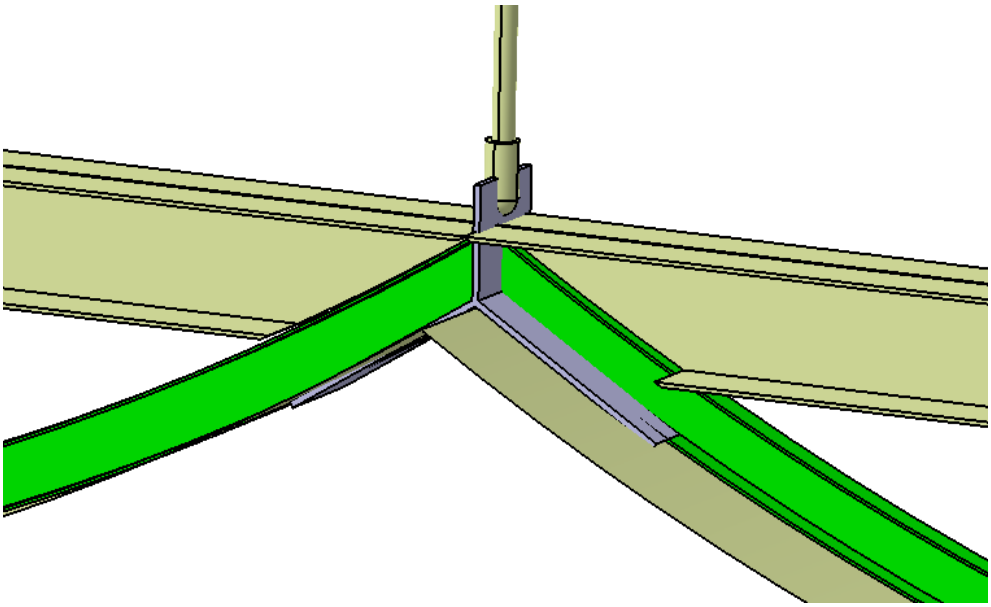

Figure 3.35 A type of arrangement of joint II

Another configuration which arranged frames outside is shown in figure 3.36.

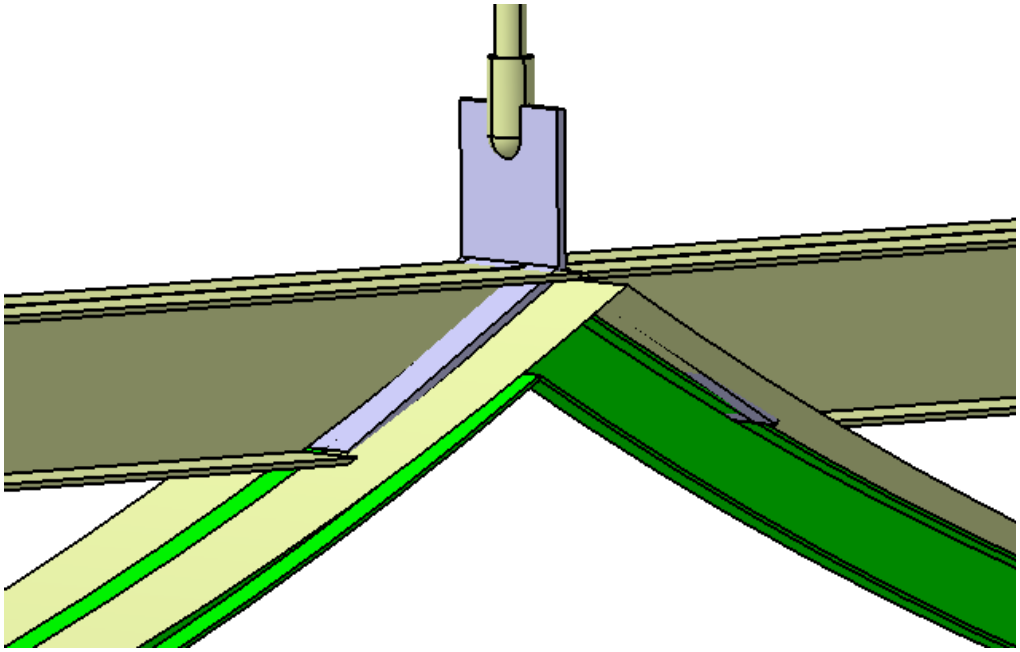

Figure 3.36 Another arrangement at joint II

3.6.8 Cabin configuration

The author has already done all of the main structure components arrangement; the cross-section of cabin is applied in figure 3.37.

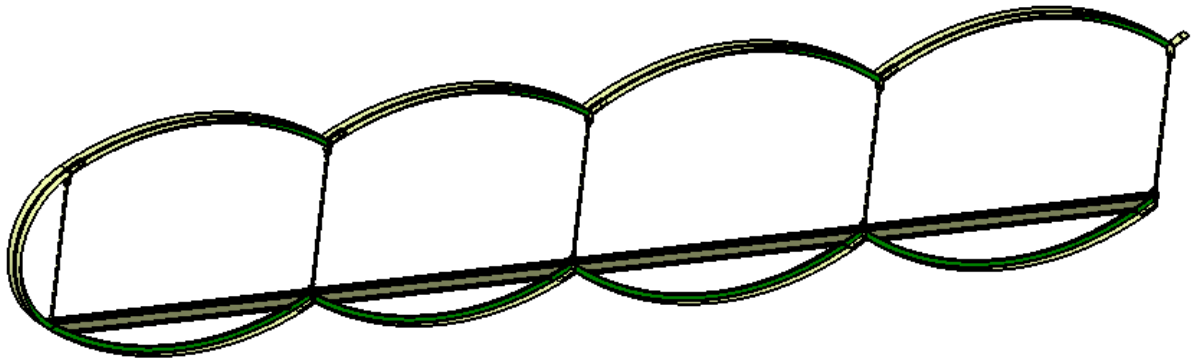

Figure 3.37 Cabin cross-section of FW-11

4 STRUCTURE INITIAL DESIGN

The main purpose for structure initial sizing is to establish a basic fuselage model. These estimated data should be discussed and optimized. For the initial model, the finite element analysis can check whether all the dimension sizes are suitable or not, and change the model more rational.

4.1 Material selection

The usage of aluminium alloys is mature in modern aircraft design. For material selection of each part, borrowing ideas from other successful airliner is more convenient for initial sizing. Because of lacking references about material selection of struts and Y beams, the author assumed that these two kinds of parts should follow the material which used for floor beams.

4.1.1 Skin and pressure bulkhead material selection

Possible aluminium alloys for skin and pressure bulkhead is applied in table 4.1.

Table 4.1 Possible aluminium alloys for skin and pressure bulkhead

Material	2090-T83	2524-T3	2024-T3
Density (kg/$\mathbf{m^3}$)	2590	2768	2770
Young's modulus (GPa)	80.3	71.9	73.3
Shear modulus (GPa)	30		27.9
Tensile yield strength (MPa)	489	310	328
Tensile ultimate strength (MPa)	538	433	454
Compressive Yield strength (MPa)	468	272	279
Poisson's ratio	0.34	0.35	0.33

For the initial design of FW-11 cabin, the material selection is to demonstration the estimation of components. The author would like to select better materials for the definition.

The proper material for skin is 2090-T83.

4.1.2 Frame material selection

Possible aluminium alloys for frame is applied in table 4.2.

Table 4.2 Possible aluminium alloys for frame

Material	**7475-T7351**	**7040-T7451**	**7050-T4**
Density (kg/$\mathbf{m^3}$)	2590	2850	2830
Young's modulus (GPa)	71.7	68	71.8
Shear modulus (GPa)	27	25.2	27.7
Tensile yield strength (MPa)	421	403	400
Tensile ultimate strength (MPa)	496	476	479
Compressive Yield strength (MPa)	380	371	414
Poisson's ratio	0.33	0.33	0.337

The proper material for frames is 7475-T7351

4.1.3 Stringer material selection

Possible aluminium alloys for stringer is applied in table 4.3.

Table 4.3 Possible aluminium alloys for stringer

Material	7349-T6511	7175-T73511	2196-T8511
Density (kg/$\mathbf{m^3}$)	2850	2800	2630
Young's modulus (GPa)	71	71.8	77.6
Shear modulus (GPa)		27.7	
Tensile yield strength (MPa)	625	383	470
Tensile ultimate strength (MPa)	665	457	520
Compressive Yield strength (MPa)	635	429	414
Poisson's ratio		0.337	

The proper material for stringers is 7175-T73511

4.1.4 Floor beam material selection

Possible aluminium alloys for strut is applied in table 4.4.

Table 4.4 Possible aluminium alloys for strut

Material	7475-T7351	7040-T7451	2196-T8511
Density (kg/$\mathbf{m^3}$)	2590	2850	2630
Young's modulus (GPa)	71.7	68	77.6
Shear modulus (GPa)	27	25.2	
Tensile yield strength (MPa)	421	403	470
Tensile ultimate strength (MPa)	496	476	520
Compressive Yield strength (MPa)	380	371	
Poisson's ratio	0.33	0.33	

The proper material for floor beams is 7475-T7351.

4.2 Interior cabin design

The method for FW-11 fuselage design is that the exterior airfoil and interior cabin can be designed separately. When the work is finished, some structure should be developed to connect those two parts.

The interior cabin is similar to the conventional airliner, circular cylinder cabin supported by stringers and frames. However, the other thing should be considered are the connection between interior cabin and exterior airfoil, windows and emergency exit, etc.

4.2.1 Skin structure

For the conventional airliner, the skin structure is always the stiffened shell composed of frames, stringers and skin. In this section, the skin always resists the hoop tensile from the pressure differential and the applied external transverse and torsion; the stringers always resist the axial loads from the bending moment; and frames are always designed to maintain the cross section of the fuselage and shorten the length of the stringers, for heavy frames, it can distribute the concentrated loads.

Apparently, for the multi-bubble cabin design, the guide line of conventional cabin design is a good reference.

4.2.1.1 Skin thickness

The estimating of inner skin in this thesis mainly adopts Dennis Howe’s method applied in 2.4.2.2.From his theory, the three main loading cases which can determine the thickness of skin, they are: pressure, bending moment and torque. And this value should be established firstly, the reason is the other structure should be defined basing on it.

For the semi-monocoque shell, the fuselage skin thickness should be estimated at first. In the FW-11 model, the bending moment and torque shear is not applied; another aspect is that the critical element of skin thickness for the

fuselage is always the pressure loads. For the FW-11 initial design, the author assumed that the maximum skin thickness is t_p.

The thickness definition is restricted by several elements. The relationship between thickness and the weight penalty from itself and support structure can check Appendix A.

Moreover, the radian of the arched skin is also constrained by the condition of enough space. Some compromise should be made for the ideal requirement and the reality. For the FW-11 model, which the author defined multi-bubble and two skin layers configuration, the space seems more precious.

For these reasons, the selection of skin thickness by using the method from Appendix A is 3.3mm for cabin skin, 1mm for side pressure bulkheads. Combined with equation 2-1, the cross-section of FW-11 model is defined in figure 4.1:

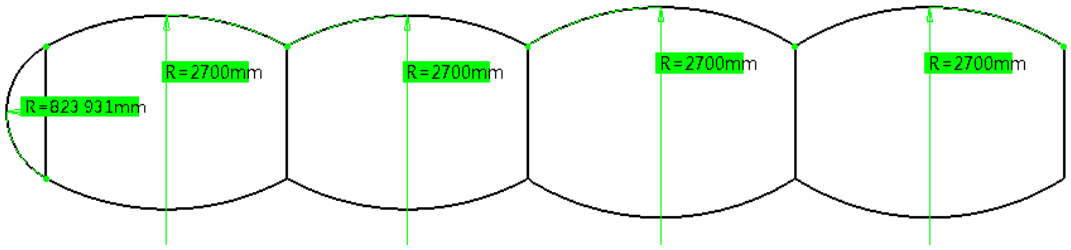

Figure 4.1 Radiuses of cabin pressure skin

4.2.1.2 Stringer initial sizing

The rules for estimating the size of stringers can check 2.4.2.3.

The stringers in interior cabin can also use the conventional method to define. The method to estimate the initial size of stringer section can use the method in 2.4.2.3. The size of stringers for pressurization skin (see figure 4.1) can be estimated as shown in table 4.5:

Table 4.5 Basic dimensions for FW-11 cabin stringers

Skin Radius	Skin thickness	Stringer thickness	Flange width	Stringer height	Stringer pitch
2700	3.27	3.27	52.32	130.80	457.80
823.9	1.00	1.00	16.00	40.00	140.00

The zed-section stringer type is chosen by the author, the size of these two stringers is applied in figure 4.2:

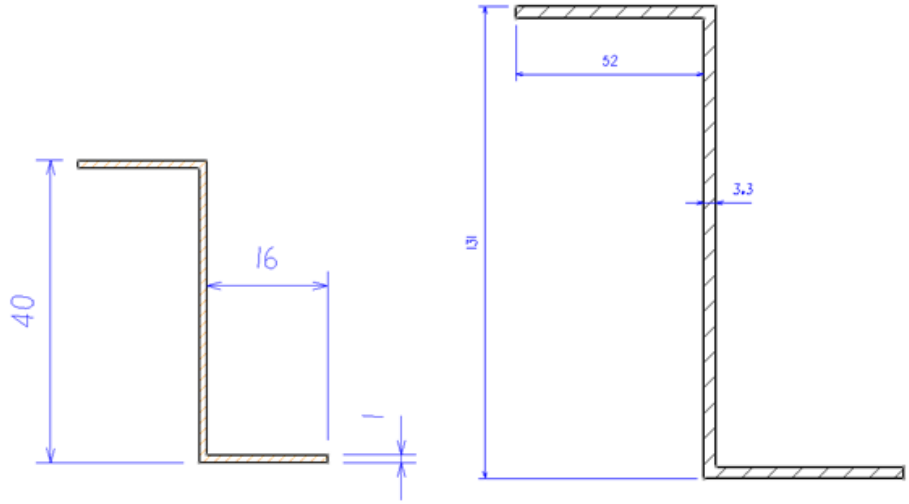

Figure 4.2 Basic dimensions for FW-11 cabin stringers

The arrangement of stringers is shown in figure 4.3:

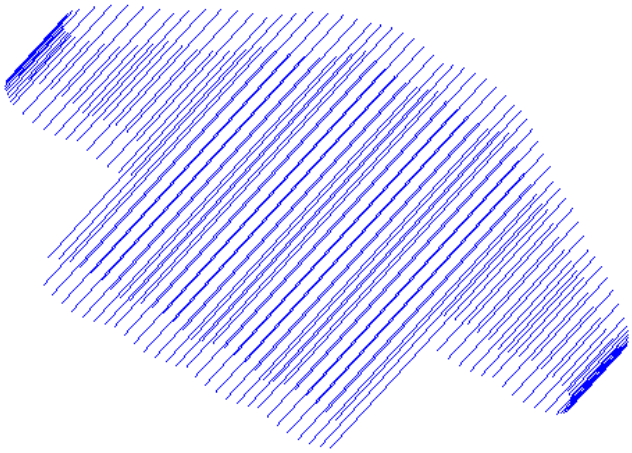

Figure 4.3 Locations of stringers in FW-11 pressure cabin

4.2.1.3 Frame initial sizing

The frame pitch for pressurization skin is normally 0.5 meter in the conventional airliner from suggestion. For the FW-11 multi-bubble fuselage configuration, the pitch is assumed a little wider. In this thesis, the heavily loaded frames should not take into consideration.

The rules for estimating the size of frames can check 2.4.2.4.

By using this method, the value can be calculated. Table 4.6 shows the data of the frame.

Table 4.6 Basic dimensions for FW-11 cabin frames

Skin Radius	Skin thickness	Frame thickness	Frame width	Frame height	Frame pitch
2700.0	3.3	3.3	274.3	685.6	792.0
823.9	1.0	1.0	274.3	685.6	792.0

It is unreasonable for the value such as the frame height which is more than half meter. Being different from the conventional aircraft, the multi-bubble

configuration that has a non-cylindrical fuselage would have a wider width. For FW-11, this value is 22854mm.

To assume that the area of multi-bubble fuselage cross-section equals to the conventional circular cross-section, the equation of the radius can be calculated through the formula is given by:

$$R = \sqrt{\frac{A}{\pi}} \tag{4-1}$$

From FW-11 module, the enclosed area of each symmetrical side is compiled in figure 4.4:

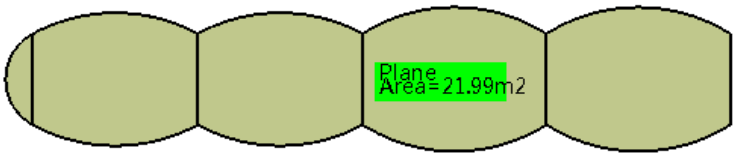

Figure 4.4 The cross-section area of FW-11 interior cabin

The result of the radius is 2650 mm. For avoiding the stress concentration, the thickness of frames should be the same. The dimension sizes of frames are shown in table 4.7 and figure 4.5

Table 4.7 Updated dimensions for FW-11 cabin frames

Skin Radius	Skin thickness	Frame thickness	Frame width	Frame height	Frame pitch
2700.0	3.3	3.3	26.5	66.3	791.0
823.9	3.3	3.3	26.5	66.3	791.0

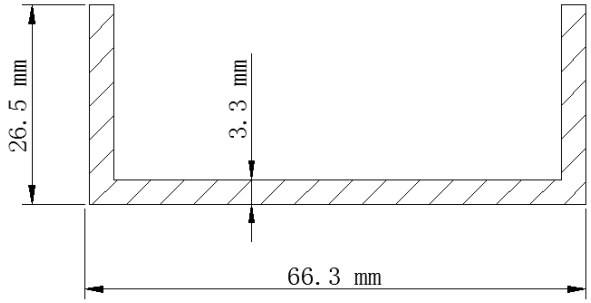

Figure 4.5 Updated dimensions for FW-11 cabin frames

4.2.1.4 Pressurization bulkheads

Dome pressure bulkheads

From M.C. Niu's advise [7], for designing the minimum weight of the dome and minimum amount of interferences stresses at the junction between the dome and the fuselage frame, a 60° sphere cap is the most economic method as shown in figure 4.6:

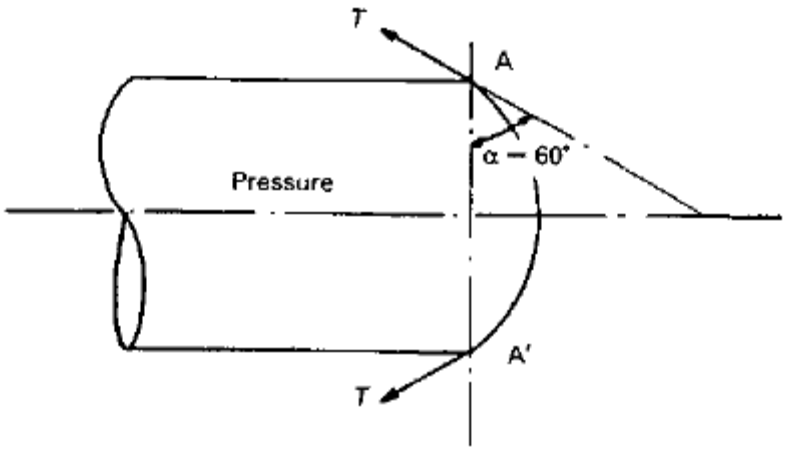

Figure 4.6 60° sphere cap for pressure dome [7]

The method for estimating the size of frames can check 2.4.2.5.

The radius of the hemi-sphere shell in FW-11 Catia model is compiled in figure 4.7:

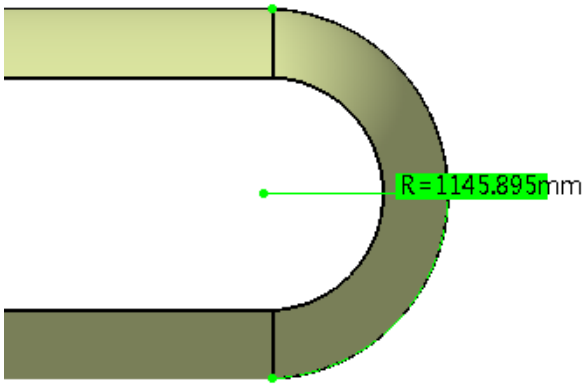

Figure 4.7 Dome radius of FW-11 model

The thickness is:

$$t_p = \frac{\Delta P \cdot R}{2\sigma_p} = \frac{\Delta P \cdot R}{2 \times 100 \times 10^6} = 0.69mm$$

Flat pressure bulkheads

The pressure bulkheads in each side of FW-11 symmetrical fuselage model compiled in figure 4.8:

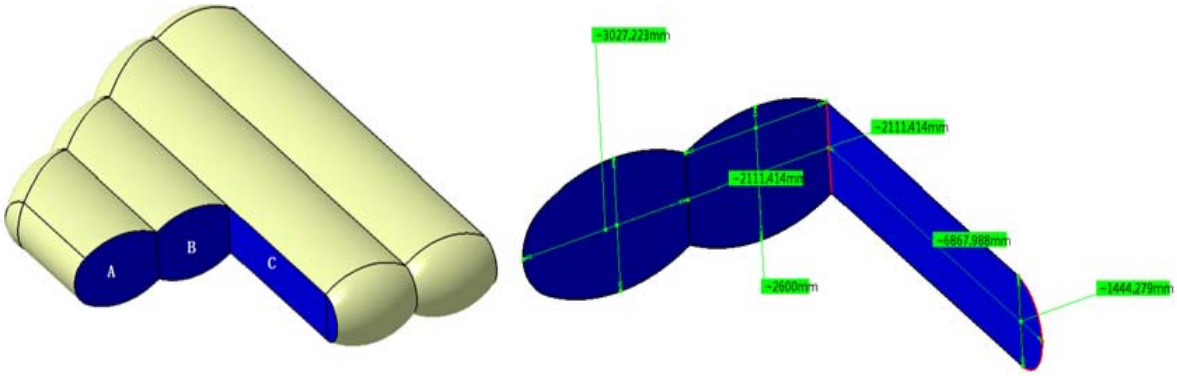

Figure 4.8 Locations and dimensions for flat pressure bulkheads in FW-11 model

In C section, the bulkheads are divided by the frames to eight parts.

The basic dimension for each part is shown in figure 4.9:

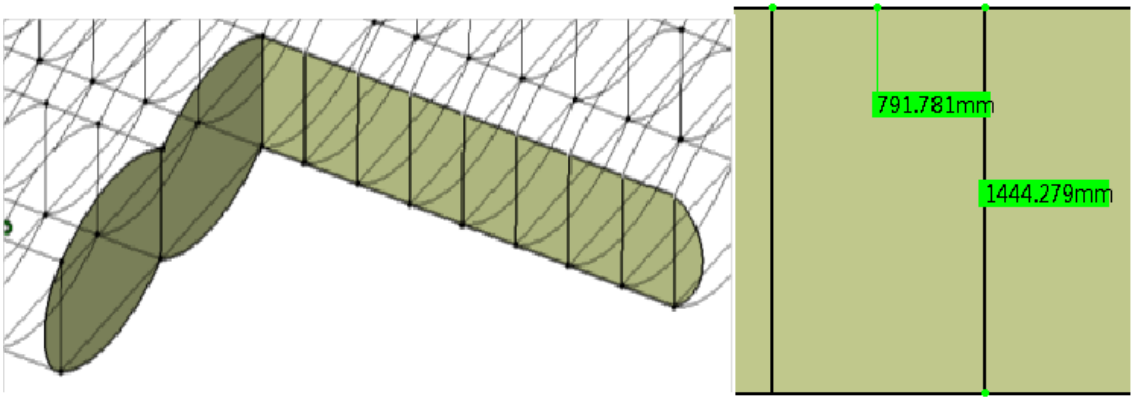

Figure 4.9 Dimensions of bulkheads in section

For FW-11 calculation, in here, the ratio n of the longer to shorter side of support beams is 1444.3/791.2=1.8, the length of shorter side is assumed one tenth of the bulkhead width a which is 79.2 mm, and the skin thickness is restricted to less than 5. In the condition of single row fasteners, the skin thickness t_p is:

$$t_p = \left[\frac{0.71\Delta P a^2\{n^3/(n^3+1.5)\}}{\sigma_a}\right]^{1/2} = 2.1\ mm$$

The shape of support beams has two rows of fasteners, then through the calculation, the skin thickness $t_p$is:

$$t_p = \left[\frac{0.5\Delta P a^2\{n^4/(n^4+0.6)\}}{\sigma_a}\right]^{1/2} = 1.9\ mm$$

The performance by using ESDU 71013 to calculate the maximum deflection and stress is applied in Appendix B.

Section A and B is followed the basic size of section C for convenient.

Conclusion

The thickness of the skin and pressure bulkheads is complied in table 4.8:

Table 4.8 Skin thickness for each parts

Skin status	Thickness (mm)
Skin r=2700	3.30
Skin r=823.93	1.00
domed pressure bulkheads	0.69
flat pressure bulkheads	2.1

4.2.2 Floor beam initial sizing

4.2.2.1 Floor beams in passenger cabin

The equation for shear force , bending moment, bending deflection for the freely supported beam with point load are given by:

$$Q(x) = \frac{Pb}{l} \qquad 0 < x < a \tag{4-2}$$

$$Q(x) = -\frac{Pa}{l} \qquad a < x < l \tag{4-3}$$

$$M(x) = \frac{Pb}{l}x \qquad 0 \le x \le a \tag{4-4}$$

$$M(x) = \frac{Pa}{l}(l - x) \qquad a \le x \le l \tag{4-5}$$

$$f_{max} = -\frac{Pbx}{6lEI}(l^2 - b^2 - x^2) \qquad 0 \le x \le a \tag{4-6}$$

$$f_{max} = -\frac{Pb}{6lEI}[(l^2 - b^2 - x^2)x + \frac{l}{b}(x - a)^{3}] \qquad a \le x \le l \tag{4-7}$$

Where

Q is the shear force

M is the bending moment

f_{max} is the maximum bending deflection

Figure 4.10 shows the basic parameter of l, a, b and P:

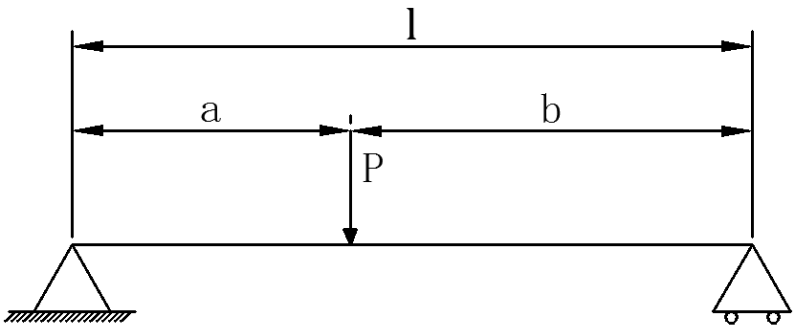

Figure 4.10 Basic parameter of freely support beam

Figure 4.11 shows the seats distance from FW-11 cabin layout team. In this thesis, the seat layout is adopted the all-economic arrangement, as shown in the middle cabin.

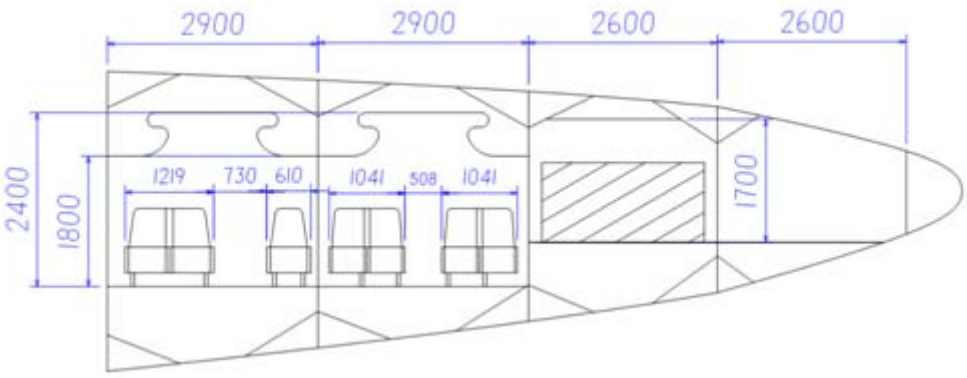

Figure 4.11 Seats arrangement in FW-11 cabin [21]

From CS-25.562, the ATD (anthropomorphic test dummy) is 77kg. The seat is selected KKY-400 manufactured by AVIC Aerospace Life-Support Industries LTD, which is 16.9 kg. The section of beams in aisle should be undertake the weight of ATD, this situation also need to be proposed. The load on floor beams

in passenger cabin can be treated as the point load from seat tracks as shown in figure 4.12:

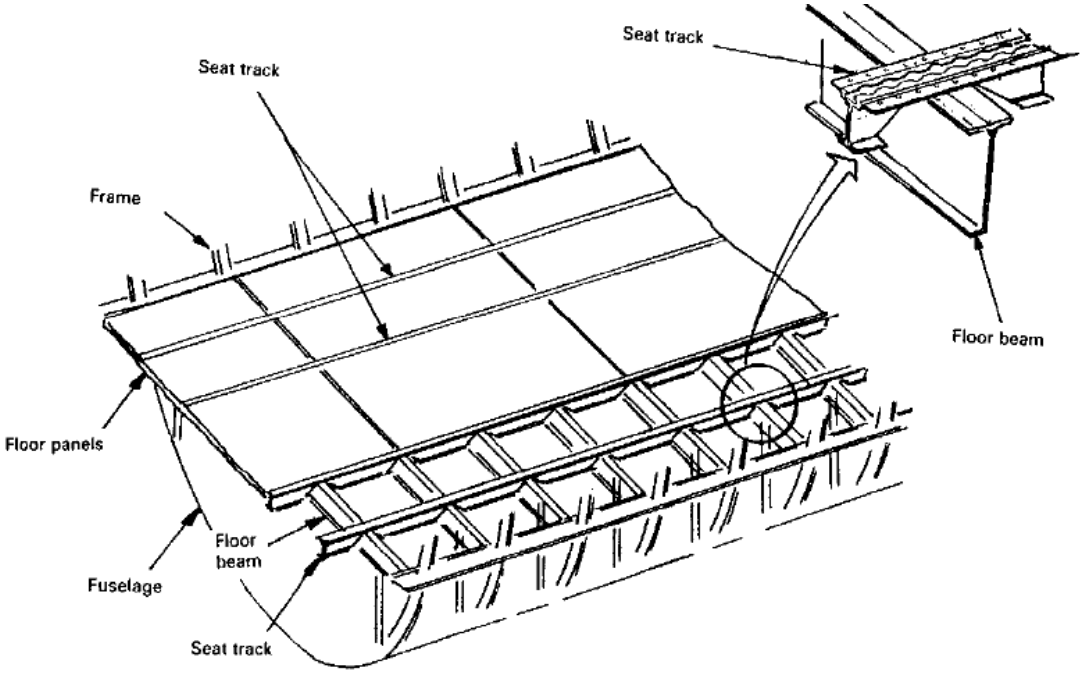

Figure 4.12 Seat tracks in conventional airliner [7]

The force analysis for each beam is applied in figure 4.13:

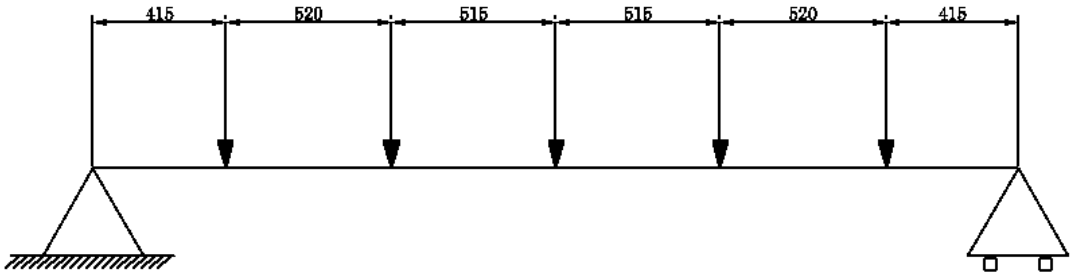

Figure 4.13 Force analysis for each beam in FW-11 passenger cabin

The data for loads on floor beams for each row of passengers is compiled in table 4.9:

Table 4.9 Loads on floor beams of one row passengers

Point	1	2	Aisle	4	5
Distance	415	935	1450	1965	2485
Load	93.9	93.9	77	93.9	93.9

For each point, the loads can be separated to every beam evenly. The cabin layout for FW-11 all economic seat arrangement is shown in figure 4.14:

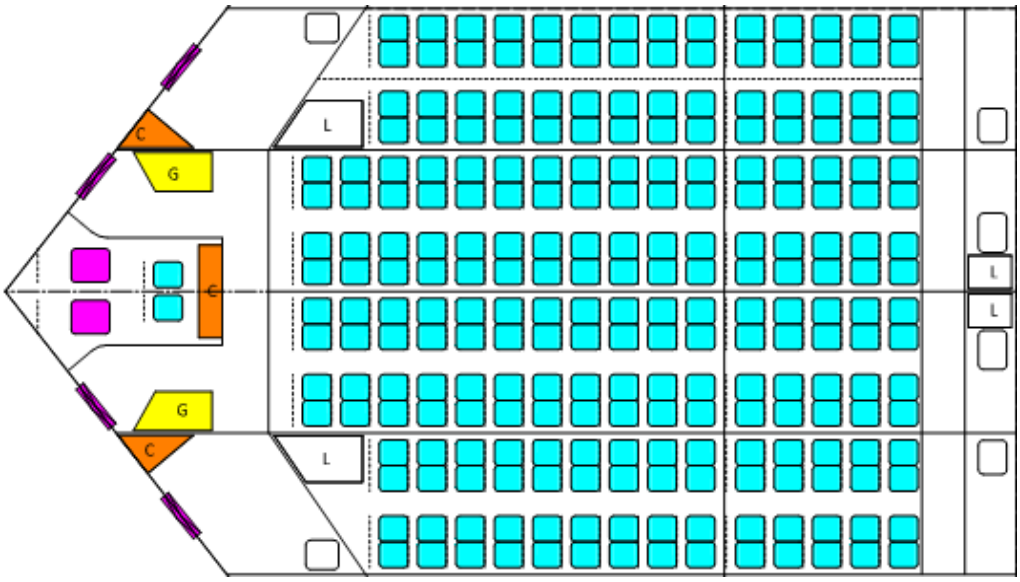

Figure 4.14 FW-11 cabin layout for all economic arrangement [22]

There are 84 floor beams in passengers' cabin, considered the triangle section of front cabin, the number of full-loaded beam is 80, and the numbers of seat rows are 60. From CS-25, the ultimate load is 1.5 times than limit load, the crash load is 6 times in vertical direction.

Thus, the point load for each beam is applied in table 4.10:

Table 4.10 Point loads at each beam in passenger cabin

Point	Seat 1	Seat 2	Aisle	Seat 3	Seat 4
Distance (mm)	415.0	935.0	1450.0	1965.0	2485.0
Limit load (N)	690.2	690.2	566.0	690.2	690.2
Ultimate load (N)	1035.3	1035.3	849.0	1035.3	1035.3
Crash load (N)	4141.2	4141.2	3396	4141.2	4141.2

The shear force at each point is applied in table 4.11and figure 4.15:

Table 4.11 Shear forces at points

Point	Endpoint	Seat 1	Seat 2	Aisle	Seat 3	Seat 4
Distance (mm)	0	415.0	935.0	1450.0	1965.0	2485.0
Limit load (N)	1663.4	973.2	283	-283	-973.2	-1663.4
Ultimate load (N)	2495.1	1459.8	424.5	-424.8	-1459.8	-2495.1
Crash load (N)	9980.4	5839.2	1698	-1698	-5839.2	-9980.4

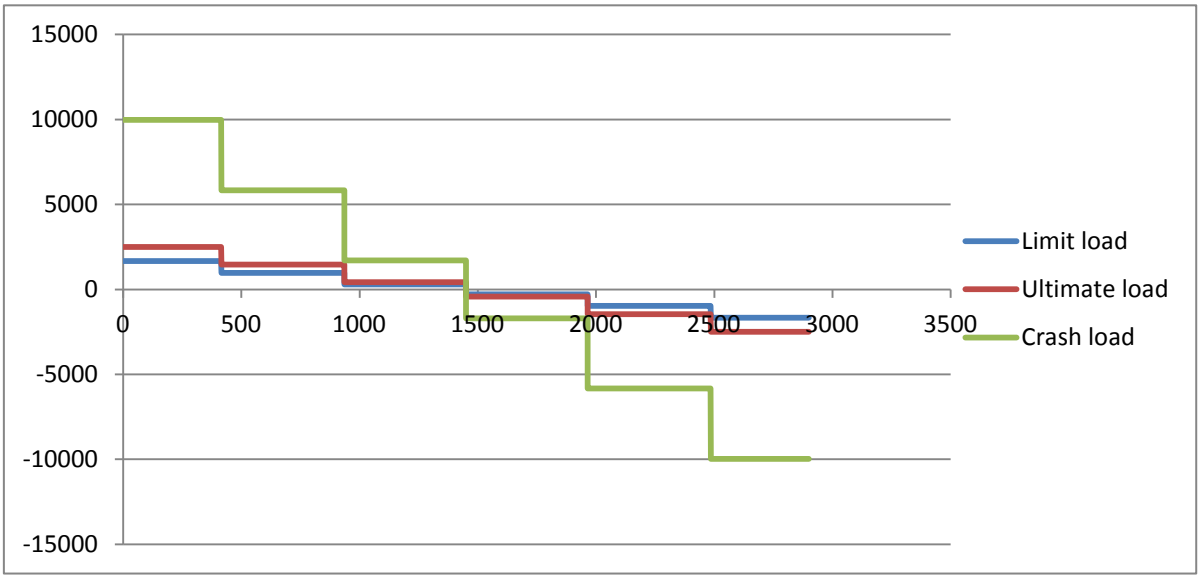

Figure 4.15 Shear forces at points (abscissa: mm, ordinate: N)

The bending moment at each point is applied in table 4.12 and figure 4.16:

Table 4.12 Bending moments at points

Point	Seat 1	Seat 2	Aisle	Seat 3	Seat 4
Distance (mm)	415.0	935.0	1450.0	1965.0	2485.0
Limit load (N*m)	690.3	1196.4	1342.1	1196.4	690.3
Ultimate load (N*m)	1035.5	1794.6	2013.2	1794.6	1035.5
Crash load (N*m)	4141.9	7178.3	8052.7	7178.3	4141.9

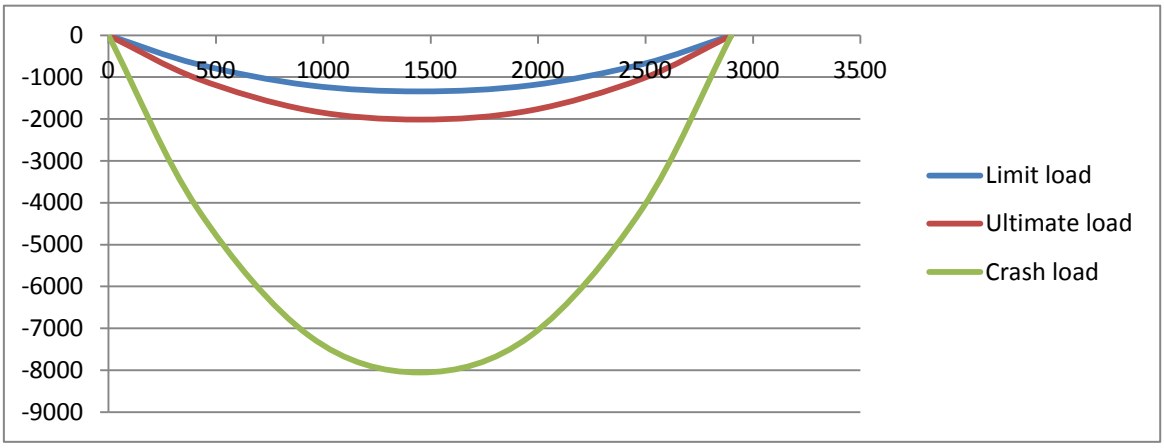

Figure 4.16 Bending moments at points (abscissa: mm, ordinate: N*M)

The bending deflection can use superposition method to calculate. Assuming the beam only support one point load, bending deflection can be calculated by using equation 4-6 and 4-7. The bending deflection at each point is applied in table 4.13:

Table 4.13 Bending deflections at points

Point	Seat 1 (m)	Seat 2 (m)	Aisle (m)	Seat 3 (m)	Seat 4 (m)
Distance	0.415	0.935	1.450	1.965	2.485
Limit load	$1.18 \times 10^{-9}/\mathrm{I}$	$3.73 \times 10^{-9}/\mathrm{I}$	$4.01 \times 10^{-9}/\mathrm{I}$	$3.73 \times 10^{-9}/\mathrm{I}$	$1.18 \times 10^{-9}/\mathrm{I}$
Ultimate load	$1.77 \times 10^{-9}/\mathrm{I}$	$5.60 \times 10^{-9}/\mathrm{I}$	$6.02 \times 10^{-9}/\mathrm{I}$	$5.60 \times 10^{-9}/\mathrm{I}$	$1.77 \times 10^{-9}/\mathrm{I}$
Crash load	$7.06 \times 10^{-9}/\mathrm{I}$	$2.24 \times 10^{-8}/\mathrm{I}$	$2.41 \times 10^{-8}/\mathrm{I}$	$2.24 \times 10^{-8}/\mathrm{I}$	$7.06 \times 10^{-9}/\mathrm{I}$

Where

I is cross sectional moment of inertia.

The maximum bending deflection is the sum of the deflection at each point applied in table 4.14.

Table 4.14 Sum bending deflections at points

Condition	Max deflection (m)
Limit load	$8.92 \times 10^{-9}/\mathrm{I}$
Ultimate load	$1.34 \times 10^{-8}/\mathrm{I}$
Crash load	$5.35 \times 10^{-8}/\mathrm{I}$

If decided to use the bending deflections as the design constraint instead of the requirement from CS25.305 [18] for considering the fuel tank arranged beneath pressured cabins, the author decided to use the common principle which always be used for civil structure. From that, the deflection from live load is less than $\frac{\mathrm{L}}{360}$, and the true load should be less than $\frac{\mathrm{L}}{240}$ in the ultimate condition [23]. Considering to avoid when the airplane under the crash load, the author decided to reduce the allowable deflection under the ultimate load. According to this,the allowable bending deflection under ultimate load is defined by:

$$\Delta \leq \frac{\mathrm{L}}{480} \quad \textbf{(4-8)}$$

Where

Δ is the bending deflection.

L is the length of the beam.

Restrained by this condition, the max deflection in ultimate load condition should be lower than this value. The allowable inertia moment is given by:

$$\frac{\mathrm{L}}{480} = 6\mathrm{mm}$$

$$1.34 \times 10^{-8}/\mathrm{I} \leq 0.006$$

$$\mathrm{I} \geq 1.34 \times 10^{-8}/0.006 = 2.23 \times 10^{-6}\mathrm{m}^4$$

Before established the shape of the beam, the relevant estimation about the size of cross-section should be done first. The author decided to assume the cross section of floor beam is rectangular, and according to the exact data to establish the basic dimension size of other type of beam. The equation of cross sectional moment of inertia is given by:

$$\mathrm{I} = \frac{\mathrm{bh}^3}{12} \quad \textbf{(4-9)}$$

Where

b is the thickness of the cross section

h is the height of the cross section

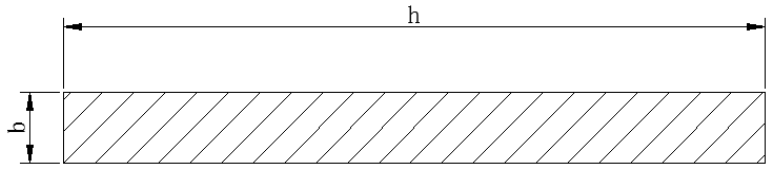

Figure 4.17 Dimensions of rectangular beam

in the initial design phase, the values of aircraft should be estimated at first. Assuming the width h is 5mm, in the ultimate load condition,

$$I = \frac{bh^3}{12} = 2.23 \times 10^{-6} m^4$$

$$h = \sqrt[3]{12I/b} = 175mm$$

This value can use to estimate the size of I section beam.

If the cross section of floor beams is I-section, as shown in figure 4.18:

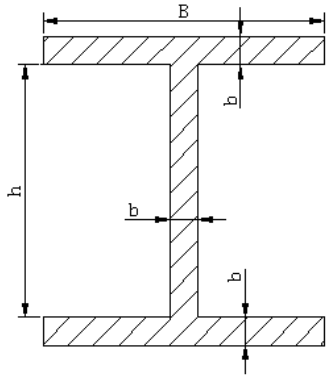

Figure 4.18 Dimensions of I beam

The equation of I-section inertia moment is given by:

$$I = \frac{bh^3}{12} + \frac{Bb^3}{6} + 2bB(\frac{h+b}{2})^2 \quad \textbf{(4-10)}$$

The dimension of floor beam is estimated by the author as shown in table 4.15:

Table 4.15 Estimate parameters of I beam in passenger cabin

parameter	Value (mm)
b	4
B	120
h	120

The inertia moment of this type of I-section beam is:

$$I = \frac{bh^3}{12} + \frac{Bb^3}{6} + 2bB(\frac{h+b}{2})^2 = 4.27 \times 10^{-6} > 2.23 \times 10^{-6} m^4$$

The stress on the beam should be checked for safety. When the floor beams is in the bending condition, the upper section of the beam resists the compression, and the lower resists the tension.

The result shows this type of beam is enough for the FW-11 floor beam.

The equation of beam stress is given by:

$$\sigma = \frac{M(h + 2b)}{2I} \quad \textbf{(4-11)}$$

The stress under the different load is applied in table 4.16:

Table 4.16 Stresses on floor beam in passenger cabin

σ	Value (MPa/m^2)
Limit load	20.1
Ultimate load	30.2
Crash load	120.8

The requirement factors for the beam are applied in table 4.17:

Table 4.17 Stress checking on floor beam in passenger cabin

σ	Tension RF	Compression RF
Limit load	21.0	21.0
Ultimate load	16.4	12.6
Crash load	4.1	3.2

Therefore, the passenger floor beam of this dimension is suitable for FW-11.

4.2.2.2 Floor beams in cargo cabin

The containers in cargo cabin were designed by FW-11 cabin layout team. The main data is:

- Non-standard container dimension: 88 in(width)×125 in(length)×43 in(height)
- Standard pallets with limited height: 88 in(width)×125 in(length)×42 in(height)
- Number of containers (pallets): 6

The weight of containers is 9590kg. For each container, the weight is 1598kg.

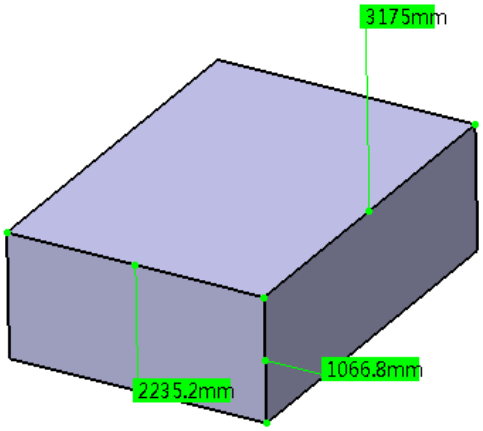

Figure 4.19 Dimensions of FW-11 container

The pitch of floor beams is 791mm. In the worst condition, one container was undertaken by three floor beams. The load for every beam is given by:

Table 4.18 Loads at each beam in cargo cabin

Condition	load(N)
Limit load	5223.4
Ultimate load	7835.1
Crash load	31340.4

The linear uniform load is given by:

Table 4.19 Linear uniform load at each beam in cargo cabin

Condition	Uniform load (N/m)
Limit load	2336.9
Ultimate load	3505.3
Crash load	14021.3

The worst condition of the container position is the container in the middle of the cabin, the bending moment and bending deflection is the maximum value, as shown in figure 4.20:

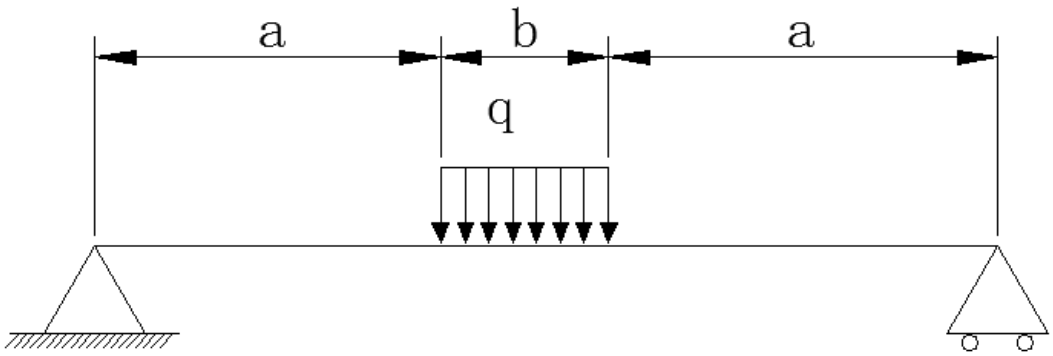

Figure 4.20 Basic parameter of freely support beam under uniform load

The equation of shear force, bending moment and bending deflection for the freely supported beam with uniform load is given by:

$$Q(x) = \frac{qb}{2} \qquad 0 < x < a \tag{4-12}$$

$$Q(x) = \frac{qb}{2} - (x-a)q \qquad a < x < a+b \tag{4-13}$$

$$Q(x) = -\frac{qb}{2} \qquad a+b < x < l \tag{4-14}$$

$$M(x) = \frac{qb}{2}x \qquad 0 \le x \le a \tag{4-15}$$

$$M(x) = \frac{qb}{2}x - \frac{q(x-a)^2}{2} \quad a \le x \le a+b \tag{4-16}$$

$$M(x) = \frac{qb}{2}x - qb\left(x - a - \frac{b}{2}\right) \quad a+b \le x \le 2a+b \tag{4-17}$$

The maximum bending deformation occurs in the section where the uniform load is applied. So the equation is given by:

$$f_{max} = -\frac{\left(2qbx(x^2 - 3(2a+b)^2) + qbx\left(b^2 + 12\left(a + \frac{b}{2}\right)^2\right) - q(x-a)^4\right)}{24EI}$$

$$a \le x \le a+b \tag{4-18}$$

For the FW-11 cargo floor beams, the load is shown in figure 4.21:

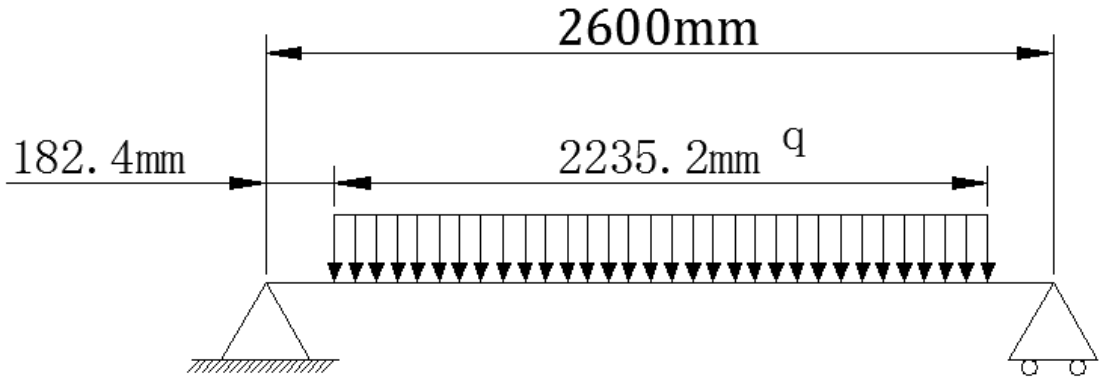

Figure 4.21 Force analysis for each beam in FW-11 cargo cabin

The maximum shear force is in the terminals; the maximum bending moment and bending deflection are happened in the middle of the beam. Table 4.20 shows the values of above in the condition of limit load, ultimate load and crash load.

Table 4.20 Shear forces, bending moment and deflection in different condition

Condition	Max shear (N)	Max bending moment (N.m)	Max deflection (m)
Limit load	2611.7	1863.0	$4.9 \times 10^{-8}/\mathrm{I}$
Ultimate load	3917.6	2903.7	$7.4 \times 10^{-8}/\mathrm{I}$
Crash load	15670.2	11614.8	$2.9 \times 10^{-7}/\mathrm{I}$

The allowable bending deflection under ultimate load is given by

$$\frac{\mathrm{L}}{480} = 5.4\mathrm{mm}$$

Restrained by this condition, the max deflection in ultimate load condition should be lower than this value. The allowable inertia moment is given by:

$$7.4 \times 10^{-8}/\mathrm{I} \leq 0.005$$

$$\mathrm{I} \geq 7.4 \times 10^{-8}/0.005 = 1.36 \times 10^{-5}\mathrm{m}^4$$

First, assuming the cross-section of floor beam is rectangular, the inertia moment of cross section is given by:

$$\mathrm{I} = \frac{\mathrm{bh}^3}{12} = 1.36 \times 10^{-5}\mathrm{m}^4$$

$$\mathrm{h} = \sqrt[3]{12\mathrm{I}/\mathrm{b}} = 320\mathrm{mm}$$

The basic size of rectangular floor beam is 320×5 mm. This value can use to estimate the size of I section beam.

If the cross section of floor beams is I-section, the dimension of floor beam is estimated by the author as shown in table 4.21:

Table 4.21 Basic dimensions of floor beam in cargo cabin

parameter	Value (mm)
b	5
B	140
h	180

The inertia moment of this type of I-section beam is:

$$I = \frac{bh^3}{12} + \frac{Bb^3}{6} + 2bB(\frac{h+b}{2})^2 = 1.44 \times 10^{-5} > 1.36 \times 10^{-5} m^4$$

The stress under different load at cargo floor beam is applied in table 4.22:

Table 4.22 The stress in different condition at cargo floor beam

σ	Value (MPa/m^2)
Limit load	9.7
Ultimate load	15.1
Crash load	60.4

The requirement factors for the beam are applied in table 4.23:

Table 4.23 Stress checking on floor beam in cargo cabin

σ	Tension RF	Compression RF
Limit load	43.4	39.2
Ultimate load	32.9	25.2
Crash load	8.2	6.3

Discuss

From CS25.305, the sizing for floor beams is oversized, and the RF under ultimate load is far more than 2. In the author's opinion, these oversized floor beams must undertake the crash load without failure for fail-safe design to avoid the troubles caused by the fuel tank arrangement beneath the cabin (see figure 3.28). Therefore, if insisting to use the unchanged FW-11 model, a strong support structure even a fair wall should be considered. From this point, these oversized floor beams is suitable.

4.2.3 Strut initial sizing

The struts in pressure cabin are only support tension from the pressure, payload from passengers , cargo, structure and system.

The area of crown shell in FW-11 cabin is 255.17m^2, as shown in figure 4.22:

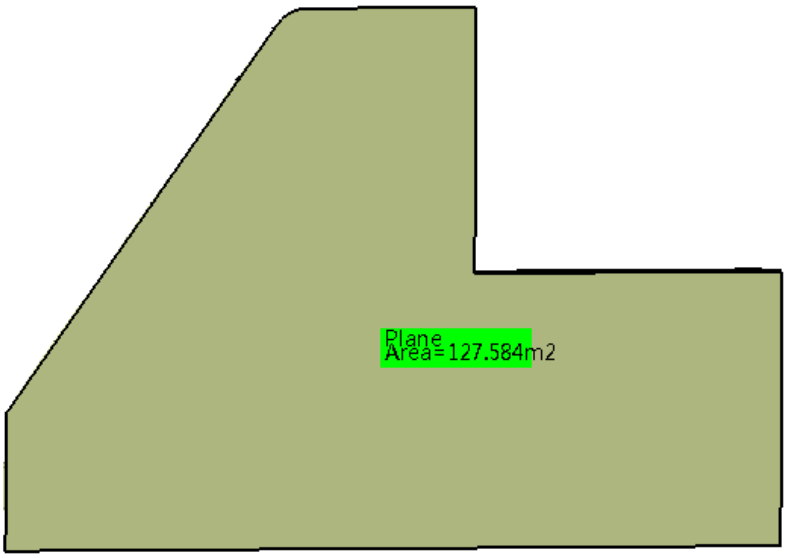

Figure 4.22 Project area of half interior cabin

The lower surface of cabin pressure skin is as same area as the upper crown. The tension caused by pressure is given by:

$$\mathrm{P}_1 = \frac{\mathrm{A}\Delta\mathrm{P}}{\mathrm{N}} \qquad \textbf{(4-19)}$$

Where

P_1 is the tension on every strut caused by differential pressure

A is the projected area of upper crown

ΔP is the working pressure load

N is the number of struts. From Fw-11 model, the number is 107.

Table 4.24 shows the value of P_1 in different condition.

Table 4.24 Tension from pressure under different condition

Condition	ΔP (Pa)	P_1 (N)
Limit load	60481.0	144231.9
Ultimate load	120962.0	288463.8

The payload from FW-11 CG team is 28686 kg. Assuming this load is resisted by the struts evenly, in different condition, the load P_2 on each strut is applied in table 4.25:

Table 4.25 Tension from payload under different condition

Condition	Load (kg)	P_2 (N)
Limit load	28686.0	2627.3
Ultimate load	43029.0	3941.0
Crash load	172116.0	15763.9

The weight of cabin structure and system has no exact value. In the initial design, assuming the weight is one third of the O.E.W. the weight of O.E.W is 75044kg. Then the load P_3 on each strut is applied in table4.26:

Table 4.26 Tension from structure weight under different condition

Condition	Load (kg)	P_3(N)
Limit load	24764.5	2268.2
Ultimate load	37146.8	3402.2
Crash load	148587.1	13608.9

The total loads on each strut are applied in table 4.27:

Table 4.27 Total tension under different condition

Condition	Load (N)
Limit load	149127.4
Ultimate load	295807.0
Crash load	317836.6

The yield tensile strength σ for Al 7475-T7351 is 421 Pa. The author decided that there is no plastic yield under the ultimate load condition. The strut cross-section is given by:

$$A \geq \frac{P}{\sigma} = \frac{317836.8}{421 \times 10^6} = 7.5 \times 10^{-4} m^2$$

Assuming $d_2 = 10.0$ mm, then

$$d_1 \geq \sqrt{\frac{7.5 \times 10^{-4}}{\pi} + 0.01^2} = 18.4 \text{ mm}$$

The final strut cross section size chosen by the author is shown in figure 4.23:

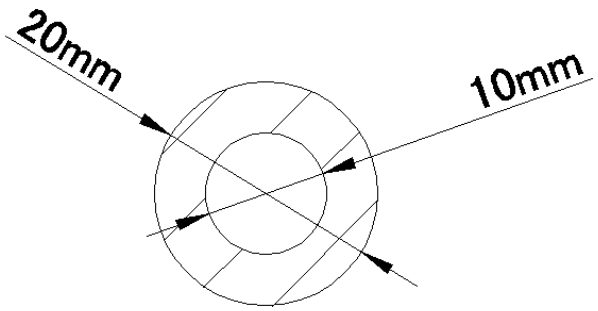

Figure 4.23 Dimensions of strut cross-section

4.2.4 Y beam initial sizing

The main forces Y beams taken are shown in figure 4.24:

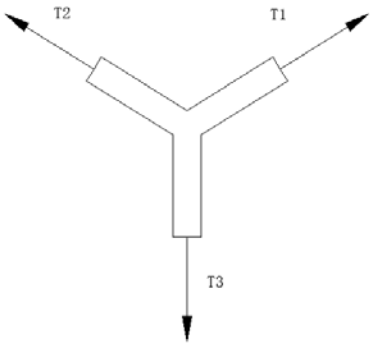

Figure 4.24 Force analysis for Y beam in FW-11 cabin

Where

T1 and T2 is the hoop tension from pressured skin and frames.

T3 is the tension from the struts.

The principle of Y beam sizing is lack of data. In the initial design phase, the size of the Y beam should resist the tension from skin, frames and struts, and distribute the point load concentration.

Figure 4.25 shows the assuming dimension sizes of Y beam for FW-11 interior cabin. The angle is decided by the joint of skin.

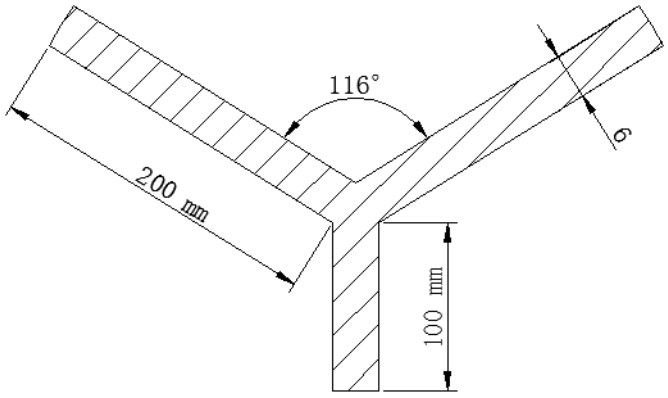

Figure 4.25 Dimensions of Y beam cross-section

5 STRUCTURAL MODEL AND FINITE ELEMENT ANALYSIS

5.1 Structure model

According the data from Chapter 4, the model of FW-11 interior cabin can be defied.

Figure 5.1 shows the CAD model for the FW-11 interior cabin. Frames, stringers, floor and other beams are represent by the lines for FE analysis. Considering the initial design phase, and to simplify the model, the pressured pilot cabin did not be defined by the author. A dome is arranged for keep pressure in that junction.

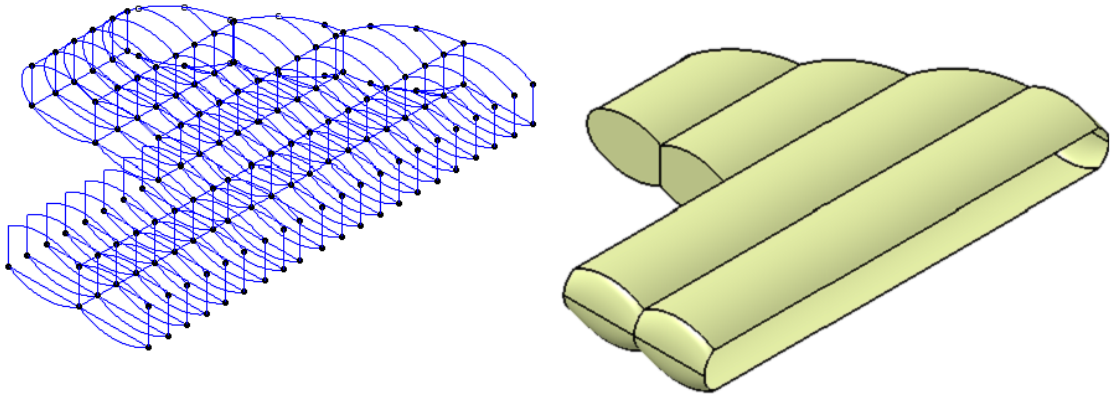

Figure 5.1 CATIA model for FEA

To simplify the model, the flat bulkheads and the pressure domes is defined to the skin which has the equivalent thickness.

5.2 Finite Element Analysis

5.2.1 Model import

The software to do FEA is Patran&Nastran. This analysis is very critical for the whole research, it directly proves the feasibility of this configuration. The data was imported from CATIA model the author did before as shown in figure 5.2, the model units is 1000mm.

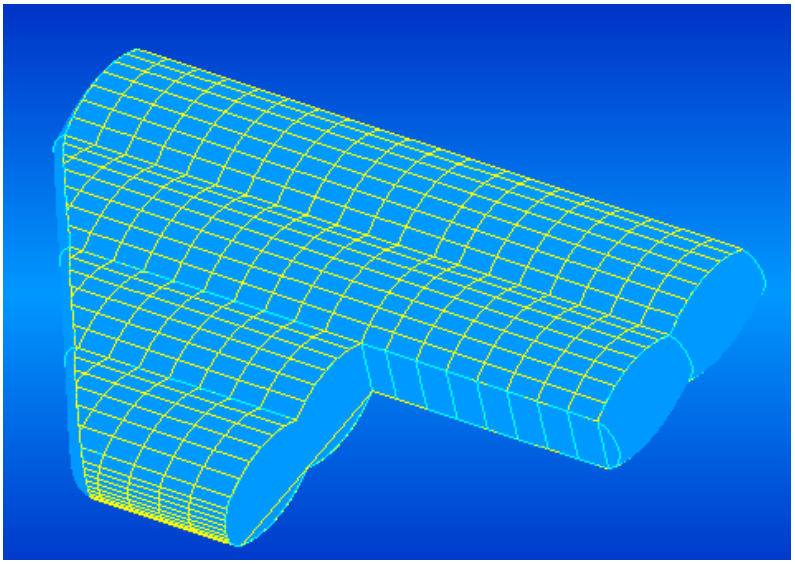

Figure 5.2 Imported model

5.2.2 Mesh

Considering the huge model, too small mesh can cause unnecessary time consuming and analysis error. So the mesh in all components should be defined carefully: for some important area like skin, the mesh should be small enough to distinguish the stress concentration; some components like bulkheads, beams can be a little larger for saving the time.

Figure 5.3 shows the finished mesh arrangement for the whole model

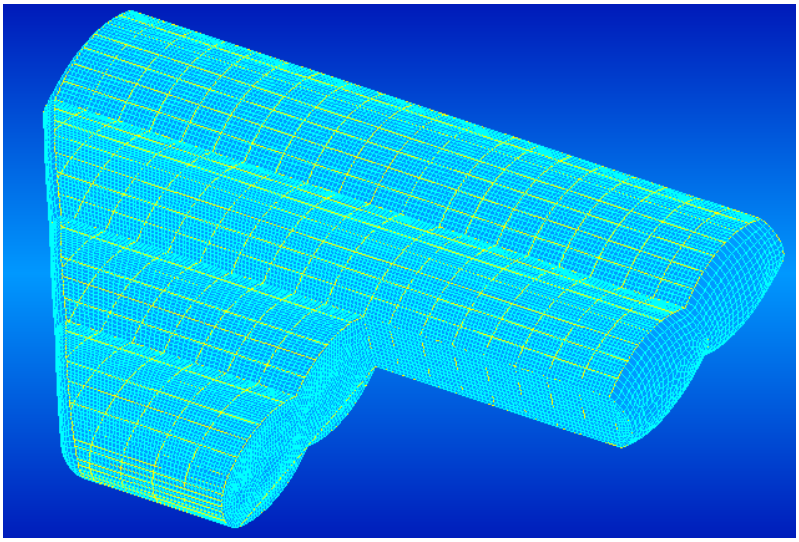

Figure 5.3 Meshes on model

Table 5.1 shows the type and length of mesh in parts.

Table 5.1 Meshing prpperties

part	Kind	Length	part	Kind	Length
Skin r=2700	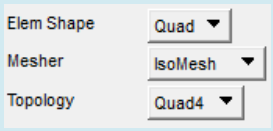	50	Flat bulkheads	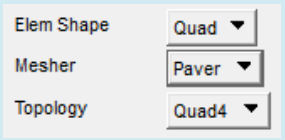	50
Skin r=824	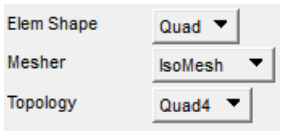	50	Pressure domes	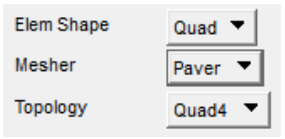	100
Frames	Bar2	75	Y beams	Bar2	75
Stringers	Bar2	75	Floor beams	Bar2	75
Struts	Bar2	100			

5.2.3 Properties of parts

The materials the model used please check Chapter 4.1.

Table 5.2 shows the properties for beam definition.

Table 5.2 Initial dimensions of part

part	type	dimension	part	type	dimension
Skin r=2700	Thin	Thickness 3.3	Flat bulkheads	Thin	Thickness 10
Skin r=824	Thin	Thickness 1	Pressure domes	Thin	Thickness 6
Frames	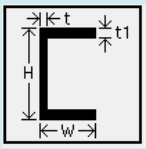	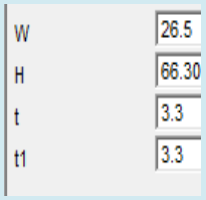	Struts	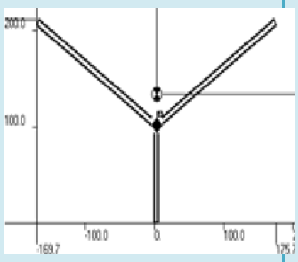	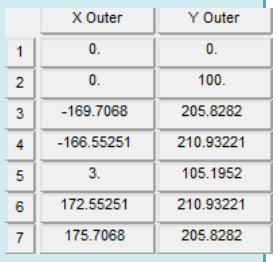
Stringers for 2700 skin	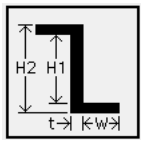	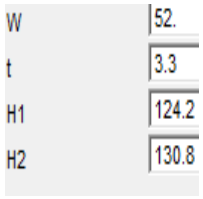	Stringers for 2700 skin	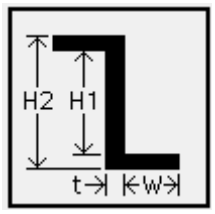	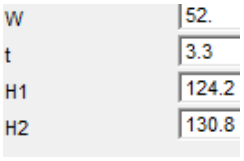
Passenger cabin floor beams	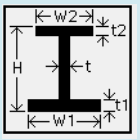	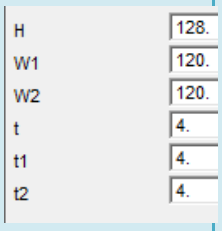	Passenger cabin floor beams	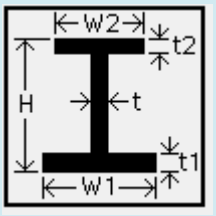	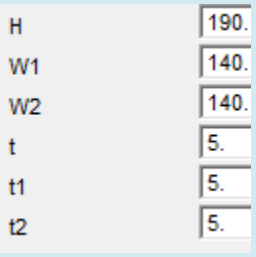
Y beams	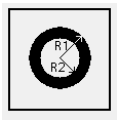	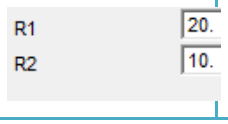			

5.2.4 Boundary conditions

The surface edges are constrained in all directions and rotations as shown in figure 5.4. this joint is the connection between two half cabin.

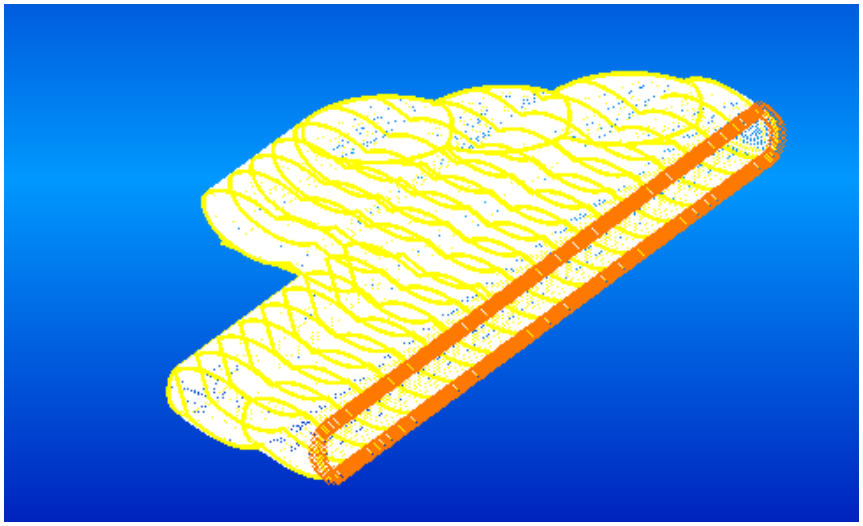

Figure 5.4 Bondary condition

5.2.5 Loads

5.2.5.1 Pressure loads

The pressure loads took into account is the uniform pressure. All the loads are on the interior surface of cabins. Figure 5.5 shows the loads on the interior surface in the multi- bubble shape.

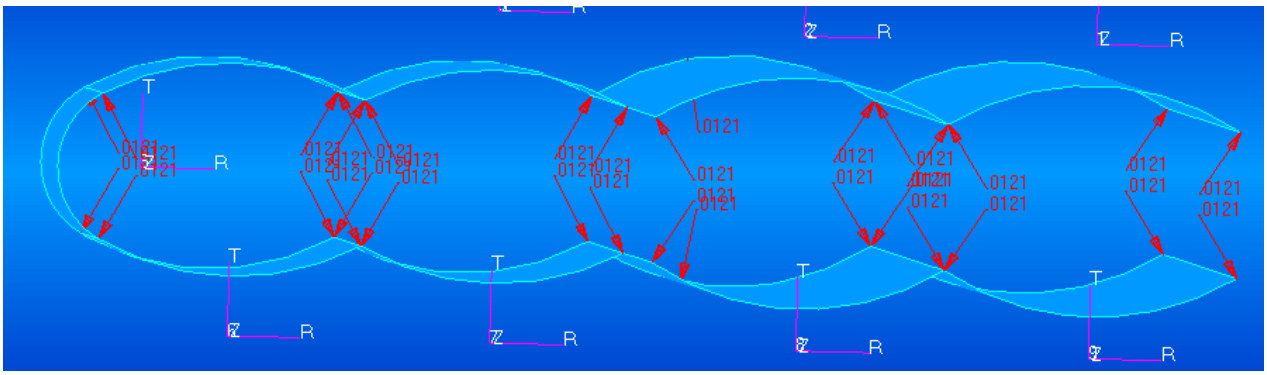

Figure 5.5 Pressure loads on panels

5.2.5.2 Floor loads

The loads on floor beams were translated to uniform loads by the author. Table 5.3 shows the uniform loads on beams.

Table 5.3 Uniform loads on floor beams

Condition	Cargo cabin		Passenger cabin	
	load(N)	Uniform loads(N/m)	load(N)	Uniform loads(N/m)
Limit load	5223.4	2009.0	3326.8	1147.2
Ultimate load	7835.1	3013.5	4990.6	1720.9
Crash load	31340.4	12054.0	19960.8	5883.1

Figure 5.6 shows the loads condition on model.

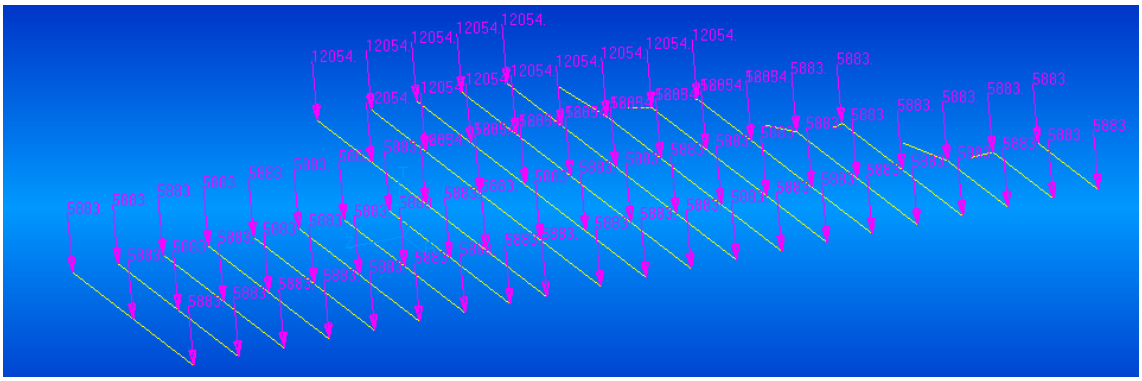

Figure 5.6 Floor beam uniform loads

5.2.6 Results

Figure 5.7 shows the FEA results for the whole fuselage under the ultimate load.

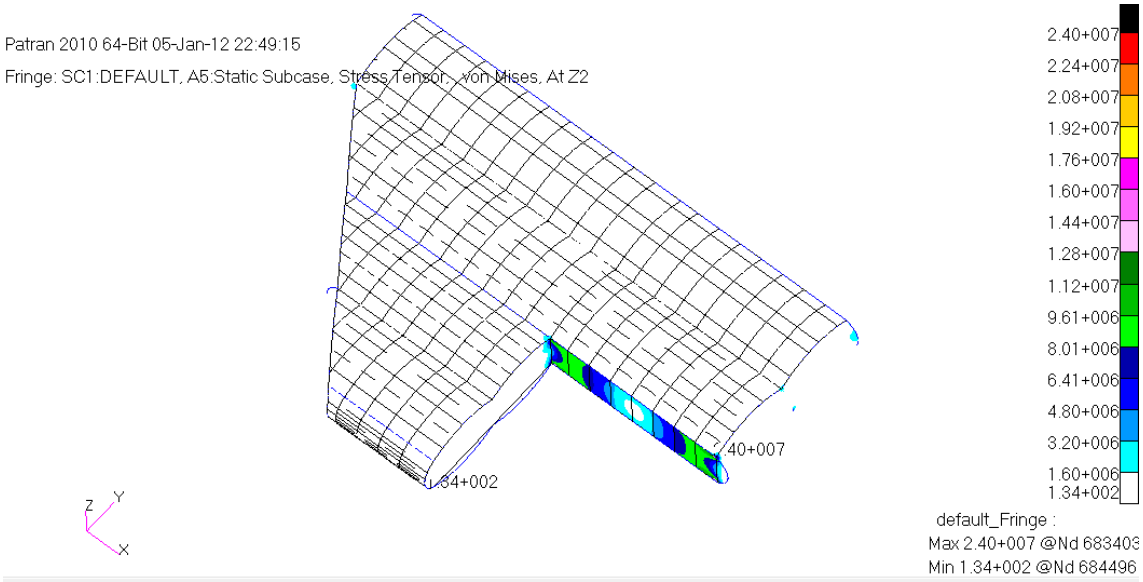

Figure 5.7 Primary result of FEA (1000mm)

The stress concentration mainly occurs at the bulkheads where the equivalent thickness defined 10mm, and the junctions of the pressure dome.

The aim of the author is to define the basic structural parts rather than design every parts of the fuselage perfectly. Further design of this fuselage would be the main job of the next AVIC team. So the author only researched the section of the fuselage.

The design and analysis of flat bulkheads please check Appendix B.

5.2.6.1 Ultimate pressure load condition

For checking the skin thickness whether enough or not, the author chose the ultimate pressure load case at first.

Figure 5.8 and 5.9 show the stress concentration and deformation in sensitive area. As expected, stress concentrations mainly occur in the area where the arch changed, the solution for it is adding the skin thickness or tighten the pitch of the stringers. According to these sectional stress concentrations, latter would be a better way.

Figure 5.9 also shows the outset struts resist more stress than others.

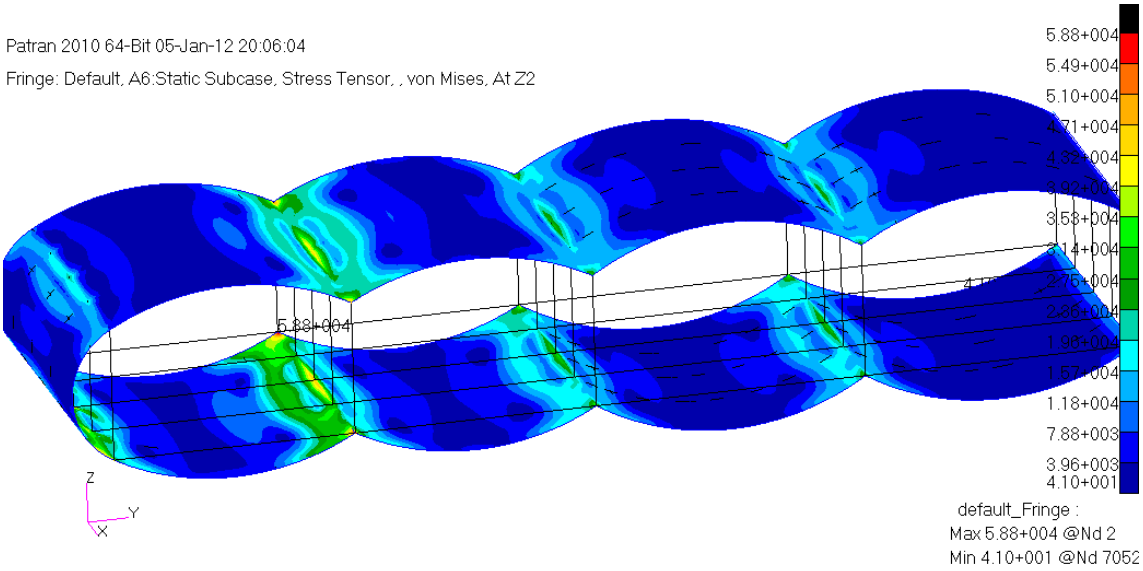

Figure 5.8 Tension under ultimate pressure (1000mm)

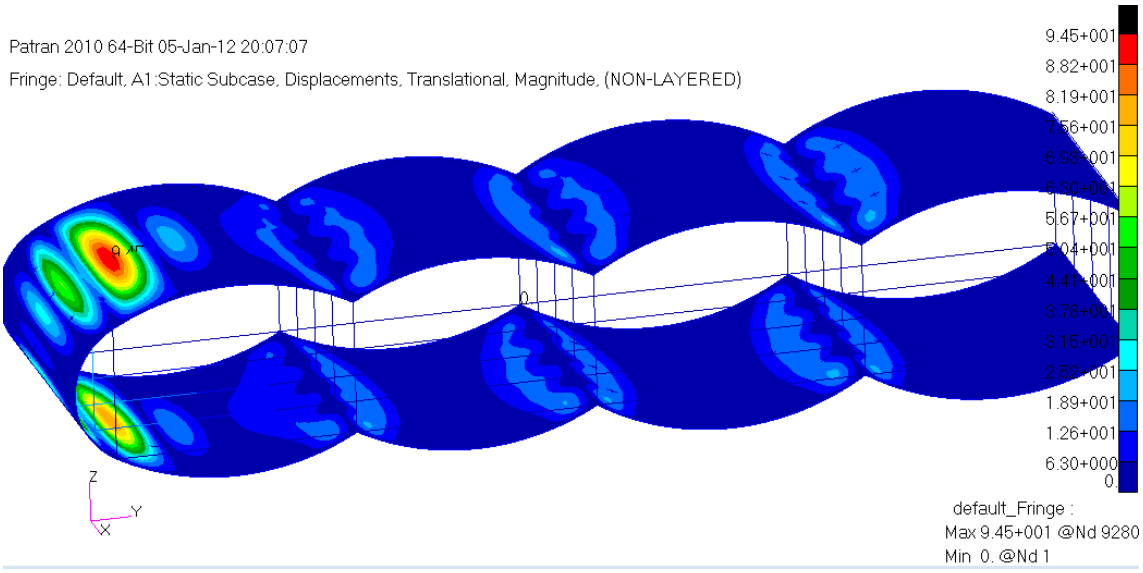

Figure 5.9 Deformation under ultimate pressure (1000mm)

5.2.6.2 Ultimate pressure and payload condition

Figure 5.10 and 5.11 shows the stress concentration and the deformation of the cabin structure. Comparing with the ultimate pressurization condition, more stress in the junction because of the floor load. One thing should be noticed that the stress at passenger cabin skin is lower than cargo.

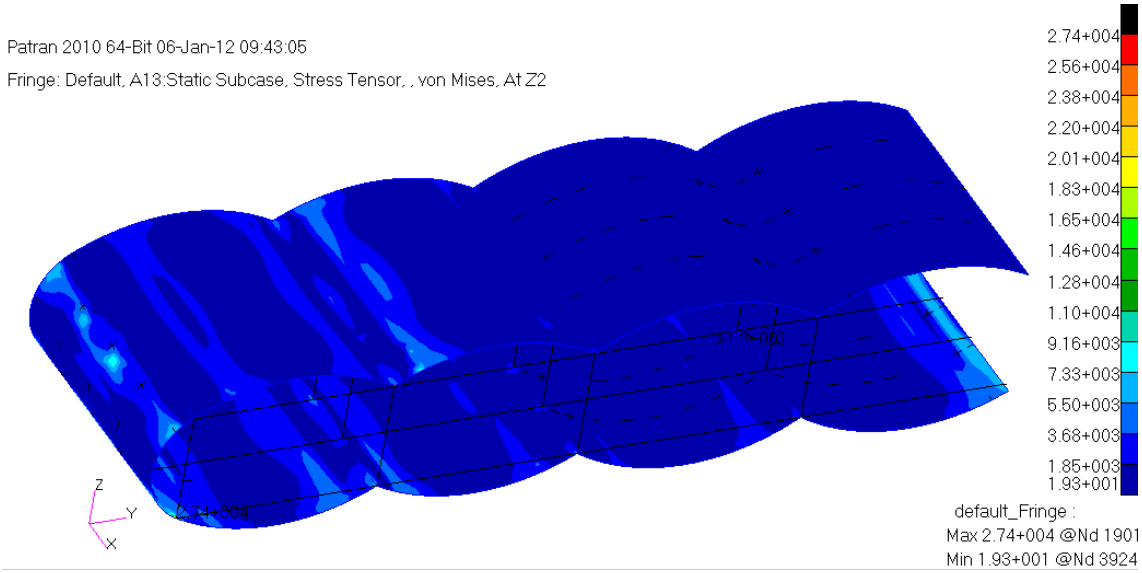

Figure 5.10 Tension under ultimate pressure & payload (1000mm)

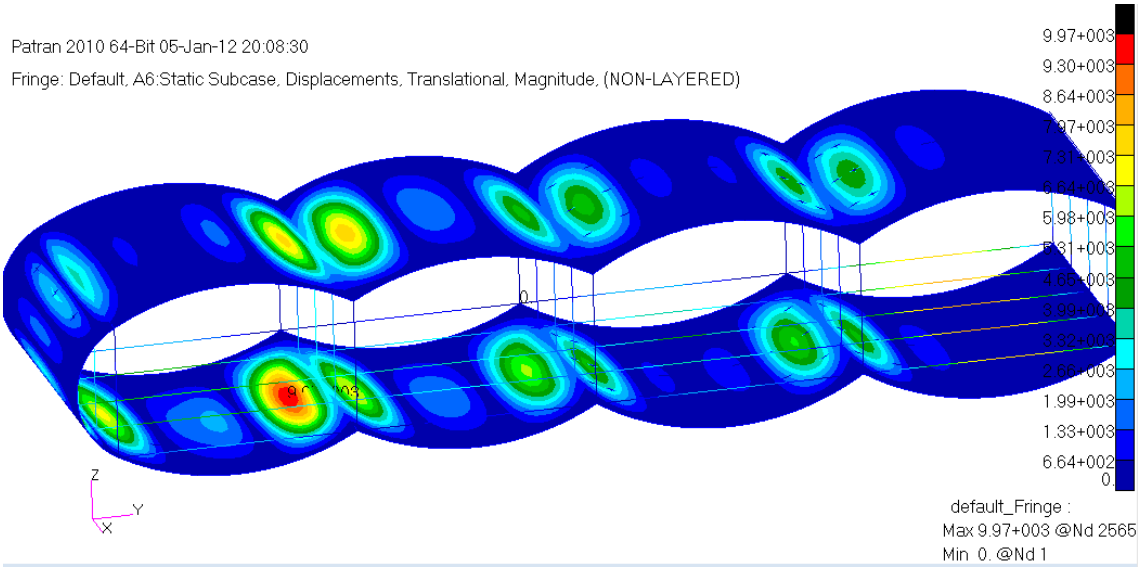

Figure 5.11 Deformation under ultimate pressure & payload (1000mm)

5.2.6.3 Discussion

The initial size of skin defined by using Danis Howe's method is sufficient in the section where the stress is equivalent. However, it is much suitable for the conventional skin sizing. The junction as shown in results generated great stress concentration, even the author use Y beams to distribute them as much as possible.

Struts were expected resist tension equivalently, but the results show that they should be reinforced at the cargo cabin where the payload is much higher than passenger cabin.

The solution author want to use is thicken the thickness of skin, and modify the structural beams especially Y beams.

Table 5.4 shows the adjusted dimensions of the structure.

Table 5.4 Adjusted dimensions of parts

part	**Initial (mm)**	**Adjusted (mm)**	**part**	**Initial (mm)**	**Adjusted (mm)**
Skin section 1	1	2.5	Skin section2	3.3	5
Skin section 3	3.3	5.5	Skin section4	3.3	5
Skin section**4**	3.3	4.5	Y beams	Thickness 6	Thickness 10
Stringers pitch at passenger cabin	458.7	400.6	Stringers pitch at cargo cabin	458.7	356.8
Frames	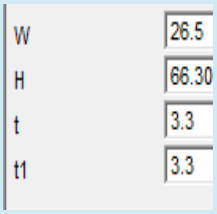	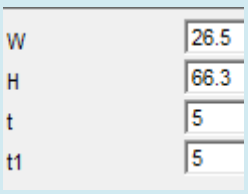	Struts	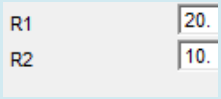	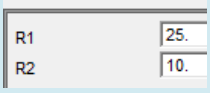

Figure 5.12shows the results by using the updated data.

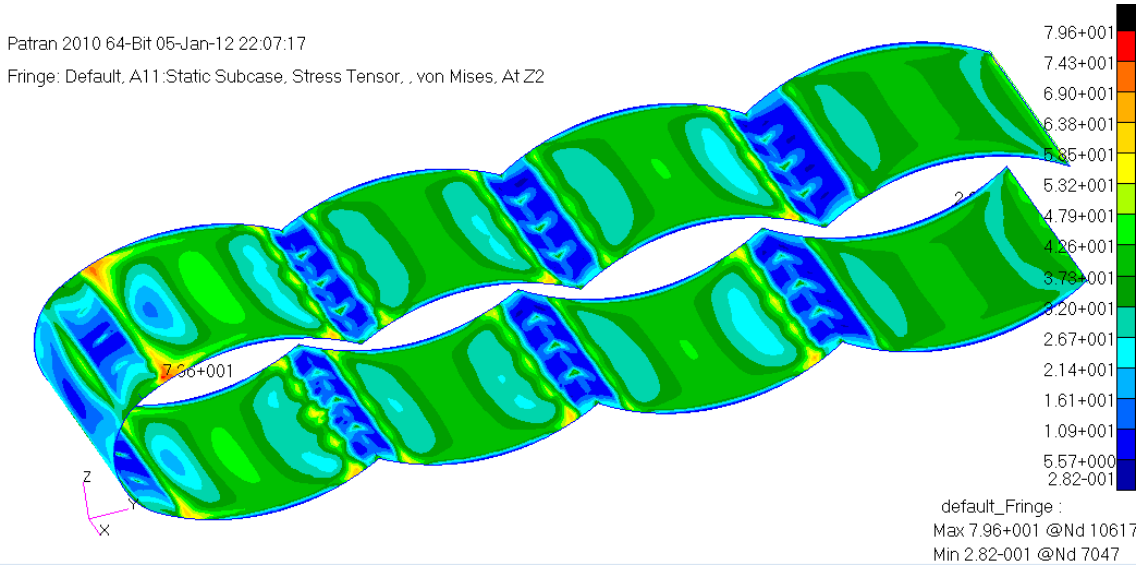

Figure 5.12 FEA results by using adjusted data (1000mm)

The author underestimated the initial dimensions for being lack of references and experience of this unconventional multi-bubble fuselage. Y beams and frames play an important part in distributing the stress concentration, so they should be designed carefully and arranged at the sensitive area.

6 CONCLUSION AND FUTURE WORK

6.1 Conclusion

The research of the author did in this thesis is an in-depth study based on the FW-11 GDP program. The main job the author did for fuselage structure in GDP about conceptual design is multi-bubble propose, which was not adopted by the GDP FW-11 structure. This continues research may further explain the advantages and disadvantages for this configuration give an advice for next AVIC team for their Initial design and provide the basic data for them.

The main conclusions reached are:

- Multi-bubble configuration can avoid stress concentration than others for the flying-wing fuselage design, and also can reduce the structure weight. Table 6.1 shows the weight reduction data from 3.2.3.2. Theoretically, the outer skin weight is much less than the pressurized inner skin, so the weight reduction is remarkable.

Table 6.1 Weight comparison for three configurations

Y-Braced Box	1160kg
Arched braced box	814kg
Multi-bubble	364kg+outer skin weight

- The room inside the inner wing of flying-wing airliner should be arranged efficiently to reduce the thickness.
- The weight penalty of multi-bubble is mainly from two layers of skin and the longitudinal support beams.
- The method for initial design of conventional fuselage is suitable for flying-wing multi-bubble design except the stress concentration sensitive areas.
- Compromise should be made between the perfect dimensions and more effective arrangement for interior cabin.

- Heavily support frames should be considered for the multi-bubble fuselage design.
- Narrowly arranged stringers and thicker skin can be used to reinforce the stress concentration area.

6.2 Future work

Further work for the multi-bubble structure design is mainly:

- Keep researching on the whole fuselage FEA result and reduce the stress concentration by arranging heavily support structures.
- The cross-section of this multi-bubble configuration can be optimized to increase the depth for capability and avoid stress concentration.
- Structural optimizing should be considered to reduce unnecessary dimensions for weight reduction.
- The attachment in the structure joint should be arranged to attach those parts.
- The attachment between interior cabin and outer airfoil should also be discussed and research.
- The structure impacted by the bending moment and torsion need to be considered.
- Cabin layout need to be optimized to distributed the load.
- The cockpit cabin should be designed.

REFERENCES

[1]. Sung Hwan Cho, Cees Bil and Javid Bayandor, *Structural Design and Analysis of a BWB Military Cargo Transport Fuselage*, AIAA 2008-165

[2]. http://www.nasm.si.edu/collections/artifact.cfm?id=A19600302000

[3]. Tapper, O. (1973). *Armstrong-Whitworth Aircraft since 1913*. London: Putnam

[4]. Gunston, Bill, *Northrop's Flying Wings*. *Wings of Fame*. Volume 2. London: Aerospace Publishing, 1996. ISBN 1-874023-69-7. ISSN 1361-2034. pp. 24–37.

[5]. E.T. Wooldridge. *The Northrop bombers*. http://www.century-of-flight.net/Aviation%20history/flying%20wings/Northrop%20bombers.htm

[6]. Tom Gurbach, *Future Air Transport Technologies*, Boeing Phantom Works, 2010.

[7]. Niu.M.C., *Airframe Structural Design*, Hong Kong Conmilit Press Ltd. 1999.

[8]. Howe, D. (2004), *Aircraft Loading and Structural Layout,* Professional Engineering Publishing.

[9]. Ronald T. Kawai, Douglas M. Friedman and Leonel Serrano,*Blended Wing Body (BWB) Boundary Layer Ingestion (BLI) Inlet Configuration and System Studies,* Huntington Beach, California. 2006.

[10]. V. Mukhopadhyay, *Blended-Wing-Body (BWB) Fuselage Structural Design for Weight Reduction,* AIAA 2005-2349, 2005

[11]. Niu.M.C., *Composite Airframe Structures*, Hong Kong Conmilit Press Ltd.1999

[12]. http://kketua.blogspot.com/2011/07/carbon-fiber-reinforced-polymer-cfrp.html

[13]. BOTELHO, Edson Cocchieri; SILVA, Rogério Almeida; PARDINI, Luiz Cláudio and REZENDE, Mirabel Cerqueira. *A review on the development and properties of continuous fiber/epoxy/aluminum hybrid composites for aircraft structures. Mat. Res.* [online]. 2006, vol.9, n.3, pp. 247-256. ISSN 1516-1439.

[14]. http://www.boeing.com/newairplane/787/design_highlights/#/VisionaryDesign/Composites/AdvancedCompositeUse

[15]. http://www.boeing.com/newairplane/787/design_highlights/#/VisionaryDesign/Composites/OnePieceBarrel

[16]. George Marsh, Airbus takes on Boeing with composite A350 XWB, 05 January 2008http://www.airbus.com/galleries/photo-gallery/

[17]. NASA-TM-X-74335, *US standard atmosphere*,1976

[18]. European Aviation Safety Agency (2007), *Certification Specifications for Large Aeroplanes CS-25*.

[19]. MSC Software, *MSC. Nastran 2004 Design Sensitivity and Optimization User's Guide,* 2004

[20]. Federal Aviation Administration, *Metallic Materials Properties Development and Standardization (MMPDS*), October 2006

[21]. AVIC FW-11 GDP group, *Specification for AVIC 4th GDP,* AVIC FW-11 GDP group, Cranfield University, 2011

[22]. Rui Pires, *Practical FEA Applied to the AVD MSc GDP, Tutorial 3,* Cranfield University.

[23]. T. Bartlett Quimby, *A Beginner's Guide to the Steel Construction Manual,* http://www.bgstructuralengineering.com/BGSCM/Contents.htm

[24]. Rui Pires, *Practical FEA Applied to the AVD MSc GDP, Tutorial 7,* Cranfield University.

[25]. ESDU 72012, *Information on the use of Data Items on the buckling of plates and compression panels manufactured from isotropic materials*.

[26]. http://www.pw.utc.com/products/commercial/pw4000-94.asp

[27]. http://www.i-a-e.com/products/overview.shtml

[28]. Ronald T. Kawai, Douglas M. Friedman and Leonel Serrano,*Blended Wing Body (BWB) Boundary Layer Ingestion (BLI) Inlet Configuration and System Studies,* Huntington Beach, California. 2006.

[29]. Liebeck, R. H., *Design of Subsonic Airfoils for High Lift*, AIAA 2002-0002, January 2002.

[30]. Reuther J, Jameson A., *Aerodynamic shape optimization of wing and wing-body configuration using control theory*, AIAA-95-0123, 1995.

[31]. Tjoetjoek Eko Pambagjo, Kazuhiro Nakahashi, Kisa Matsushima, *FLYING WING CONCEPT FOR MEDIUM SIZE AIRPLANE,* Tohoku University, Japan, 2002.

[32]. Richard M. Wood and Steven X.S. Bauer. *Flying wings / flying fuselage.* AIAA-2001-0311, 2001.

[33]. R.H. Liebeck, M.A. Page and B.K. Rawdon. *Blended wing body subsonic commercial transport.* AIAA 98-0438, 1998.

[34]. H. Smith. *College of aeronautics blended wing body development programme.* Proceeding of CAS 2000, 2000.

[35]. Liebeck, R. H. *Configuration Control Document CCD-3: Blended Wing Body,* Final report Under Contract NAS1-20275 NASA Langley Research Center, Oct. 1, 1997.

[36]. Sykiotis, G., Buse, A., et al. *Aeolos: An Ultra Heavy Lift Aircraft*, 2002/2003 AIAA Undergraduate Team Aircraft Design.

[37]. Liebeck, R. H., *Design of the Blended Wing Body Subsonic Transport*, Journal of Aircraft, Vol. 41, No.1, Jan-Feb, 2004

[38]. Potsdam, M. A., Page, M. A., and Liebeck, R. H., *Blended Wing Body Analysis and Design*, AIAA Technical Papers.

[39]. Boni, L., Fanteria, D.,*Development of Analytical Methods for Fuselage Design: Validation by Means of Finite Element Analysis*, Dipartimento di Ingegneria Aerospaziale, Universita di Pisa, Pisa, Italy, 2004.

[40]. Angles Hervas, *Box-wing aircraft structural fuselage design*. Cranfield University, 2011.

[41]. Sundeep Luckshan Arandara, *Preliminary Design of Fuselage Sections Metallic*, CRANFIELD UNIVERSITY, 2011

APPENDICES

Appendix A Skin shell define method

A.1 Introduction and methodology

This method based on the theory for estimating skin thickness under pressure from Denis Howe. The equation is given by Equation (2-1).

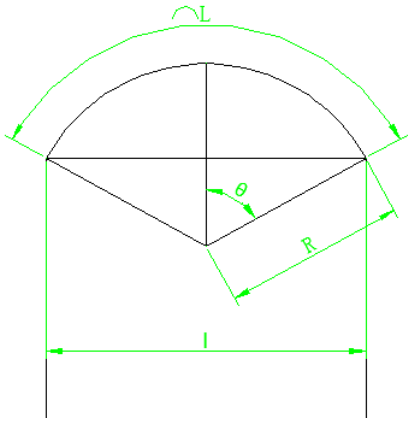

Figure A.1 Dimensions at cabin cross-section

Figure A.1 shows the relationship between the angle θ and the radius r in a cross-section of multi-bubble. The equation is given by:

$$\sin\theta = \frac{l}{2R} \tag{A-1}$$

Then the arc length is given by:

$$\mathrm{L} = 2\frac{57.3\pi\mathrm{R}}{180}\sin^{-1}\frac{l}{2r} = \frac{57.3\pi\mathrm{R}}{90}\sin^{-1}\frac{l}{2R}$$

From Equation (2-1),

$$R = \frac{\sigma_p \cdot t_p}{\Delta P}$$

Then

$$\mathrm{L} = \frac{57.3\pi\mathrm{R}}{90}\sin^{-1}\frac{l}{2R} = \frac{57.3\pi\sigma_p t_p}{90\Delta P}\sin^{-1}\frac{\Delta P l}{2\sigma_p t_p} \tag{A-2}$$

Assuming the density of a material is ρ, and then the weight of the length h skin is given by:

$$W_{skin} = h \times L\rho t_p = \frac{57.3\pi\sigma_p \rho h {t_p}^2}{90\Delta P} \sin^{-1}\frac{\Delta P l}{2\sigma_p t_p} \quad \textbf{(A-3)}$$

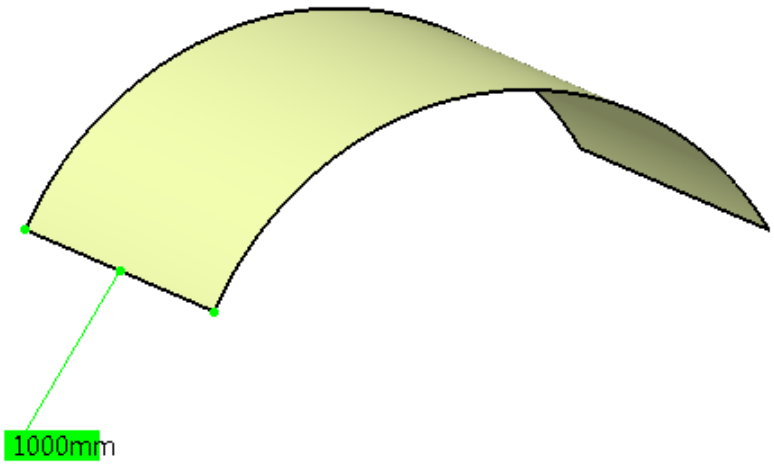

Figure A. 2 The value of h for demonstration

For the fuselage initial design, the main principle is weight reduction. Using the method of Equation (A-2) and Equation (A-3) can find a rational value of t_p, which considers not only the weight of skin, but also the proper arch length for the weight reduction of the skin shell structure.

Form the estimation of stringers by using Denis Howe's method, the stringer shape is shown in figure A.3:

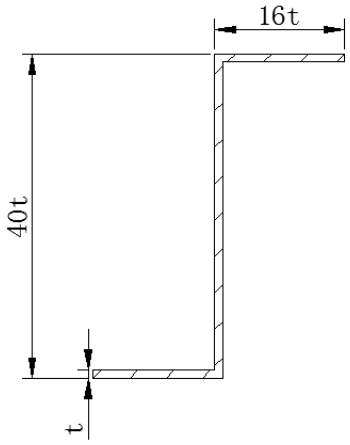

Figure A.3 Sringer size by using Denis Howe's method

According to that, the stringer weight for h length is given by:

$$\mathrm{W_{stringer}} = 70\mathrm{h}\rho {t_p}^2 \quad \textbf{(A-4)}$$

The pitch of stringers is 3.5 times of stringer height, which means 140t, for a arc skin which length is L, the number of stringers is $\mathrm{L}/140\mathrm{t}$. The stringers weight on this h length arch skin is given by:

$$\mathrm{W_{stringer}} = \frac{\mathrm{h}\rho_2 {t_p}^2}{2} * \frac{57.3\pi\sigma_p t_p}{90\Delta P}\sin^{-1}\frac{\Delta P l}{2\sigma_p t_p} = \frac{57.3\pi\sigma_p \mathrm{h}\rho_2 {t_p}^3}{180\Delta P}\sin^{-1}\frac{\Delta P l}{2\sigma_p t_p} \quad \textbf{(A-5)}$$

Then, the total weight of the arch skin is given by:

$$\mathrm{W} = \mathrm{W_{skin}} + \mathrm{W_{stringer}} \quad \textbf{(A-6)}$$

$$= \frac{57.3\pi\sigma_p\rho_1 \mathrm{h} {t_p}^2}{90\Delta P}\sin^{-1}\frac{\Delta P l}{2\sigma_p t_p} + \frac{57.3\pi\sigma_p\rho_2 \mathrm{h} {t_p}^3}{180\Delta P}\sin^{-1}\frac{\Delta P l}{2\sigma_p t_p}$$

A.2 Instance 1

Instance 1

The length of **l** is 2900mm, σ_p=100MN/m^2, ΔP=120962Pa, h=1000mm, then the Equation (A-2) and Equation (A-3) is given by:

$$L = \frac{57.3\times100\times10^6\pi t_p}{90\times120926}\sin^{-1}\frac{120962\times2900}{2\times100\times10^6 t_p} = 1653.2t_p\sin^{-1}\frac{1.8}{t_p} \quad (t_p \geq 1.8)$$

$$W_{skin} = \frac{57.3\pi\sigma_p\rho_1 h{t_p}^2}{90\Delta P}\sin^{-1}\frac{\Delta P l}{2\sigma_p t_p} = 1653200\rho_1{t_p}^2\sin^{-1}\frac{1.8}{t_p} \quad (t_p \geq 1.8)$$

$$W_{stringer} = \frac{h\rho_2{t_p}^2 L}{2} = 826600\rho_2{t_p}^3\sin^{-1}\frac{1.8}{t_p} \quad (t_p \geq 1.8)$$

$$W = 1653200\rho_1{t_p}^2\sin^{-1}\frac{1.8}{t_p} + 826600\rho_2{t_p}^3\sin^{-1}\frac{1.8}{t_p}$$

$$= 826600{t_p}^2(2\rho_1 + \rho_2 t_p)\sin^{-1}\frac{1.8}{t_p}$$

Assuming $\rho_1 = \rho_2 = 2.58\times10^{-6} kg/\text{mm}^3$,

$$W = 826600\left(2\rho_1 + \rho_2 t_p\right)\sin^{-1}\frac{1.8}{t_p} = 2.13{t_p}^2(2 + t_p)\sin^{-1}\frac{1.8}{t_p}$$

The relationship between t_p (mm) and L (mm) is shown in figure A.4:

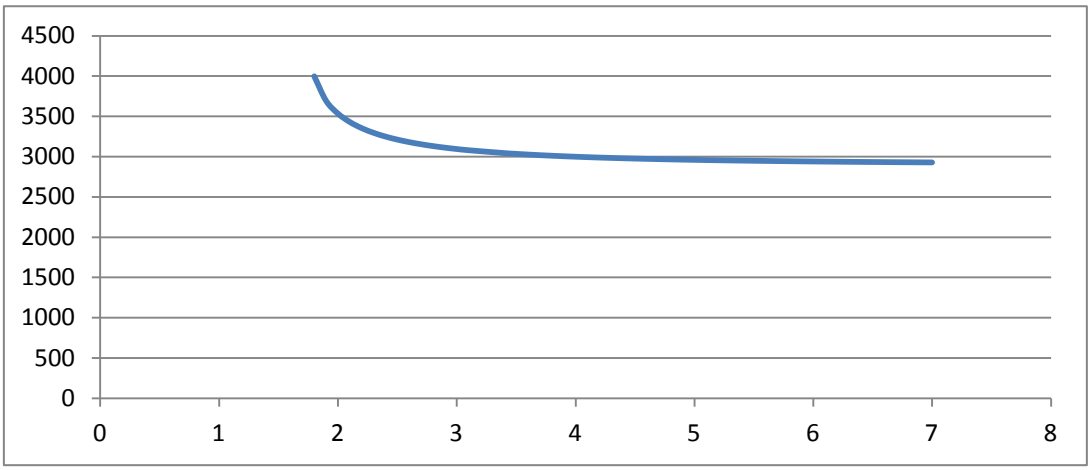

Figure A.4 The graph of t_p (abscissa,mm) and L (ordinate,mm) for 2900 distance

The relationship between t_p (mm) and W (kg) is shown in figure A.5:

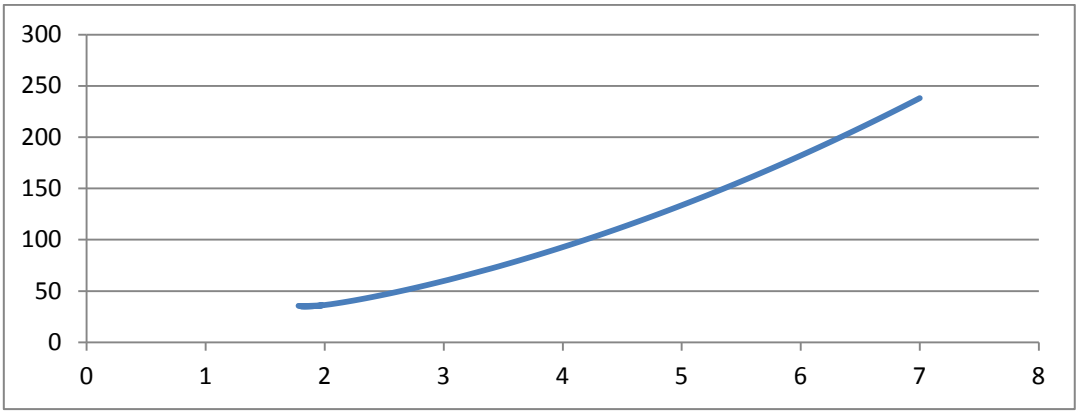

Figure A.5 The graph of t_p (abscissa,mm) and W (ordinate,kg) for 2900 distance

The relationship between t_p (mm) and R (mm) is shown in figure A.6:

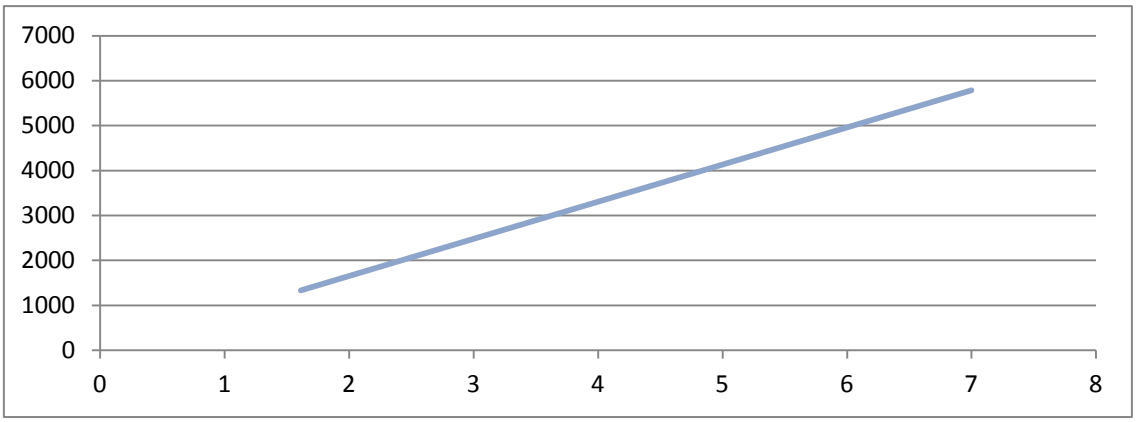

Figure A.6 The graph of t_p (abscissa,mm) and R (ordinate,mm) for 2900 distance

The proper thickness of t_p may between 2.5mm and 3.3mm.

A.3 Instance 2

The length of *l* is 2600mm, σ_p=100MN/m^2, ΔP=120962Pa, h=1000mm, then the Equation (A-2) and Equation (A-3) is given by:

$$\mathrm{L} = \frac{57.3\times100\times10^6\pi t_p}{90\times120926}\sin^{-1}\frac{120962\times2600}{2\times100\times10^6 t_p} = 1653.2t_p\sin^{-1}\frac{1.6}{t_p} \quad (t_p \geq 1.6)$$

$$\mathrm{W_{skin}} = \frac{57.3\pi\sigma_p\rho_1 h{t_p}^2}{90\Delta P}\sin^{-1}\frac{\Delta P l}{2\sigma_p t_p} = 1653200\rho_1{t_p}^2\sin^{-1}\frac{1.6}{t_p} \quad (t_p \geq 1.6)$$

$$\mathrm{W_{stringer}} = \frac{h\rho_2{t_p}^2 L}{2} = 826600\rho_2{t_p}^3\sin^{-1}\frac{1.6}{t_p} \quad (t_p \geq 1.6)$$

$$W = 1653200\rho_1 {t_p}^2 \sin^{-1}\frac{1.6}{t_p} + 826600\rho_2 {t_p}^3 \sin^{-1}\frac{1.6}{t_p}$$

$$= 826600{t_p}^2(2\rho_1 + \rho_2 t_p)\sin^{-1}\frac{1.6}{t_p}$$

Assuming $\rho_1 = \rho_2 = 2.58 \times 10^{-6} kg/\text{mm}^3$,

$$W = 826600\left(2\rho_1 + \rho_2 t_p\right)\sin^{-1}\frac{1.6}{t_p} = 2.13{t_p}^2(2 + t_p)\sin^{-1}\frac{1.6}{t_p}$$

The relationship between t_p and L is shown in figure A.7:

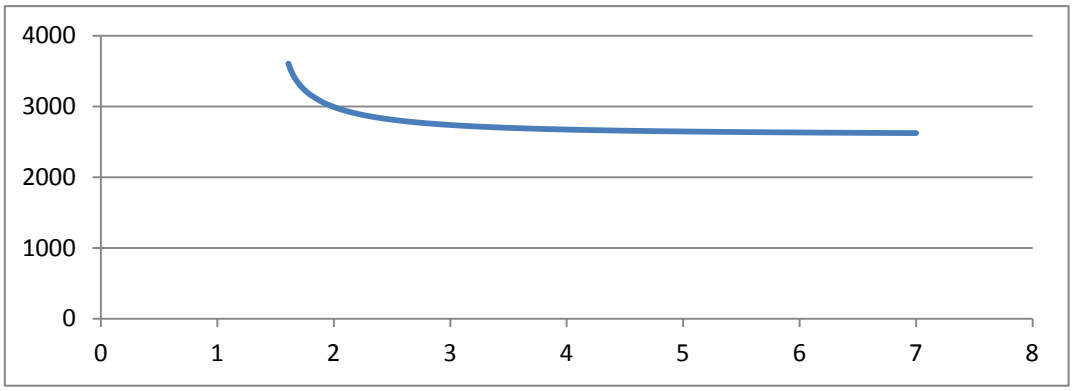

Figure A.7 The graph of t_p (abscissa,mm) and L (ordinate,mm) for 2600 distance

The relationship between t_p and W is shown in figure A.8:

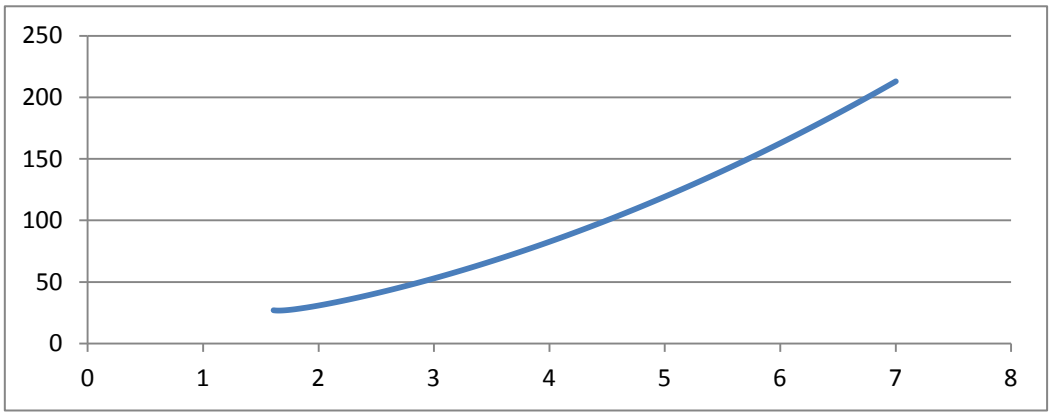

Figure A.8 The graph of t_p (abscissa,mm) and W (ordinate,kg) for 2600 distance

The relationship between t_p (mm) and R (mm) is shown in figure A.9:

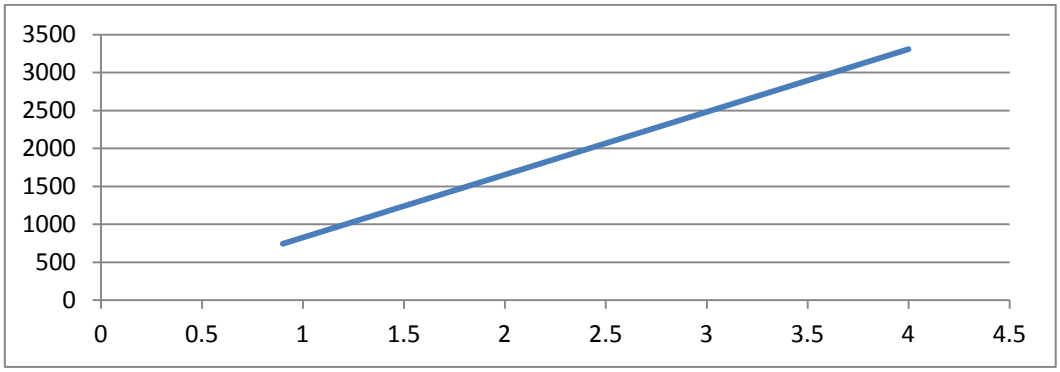

Figure A.9 The graph of t_p (abscissa,mm) and w (ordinate,mm) for 2600 distance

The proper thickness of t_p may between 2 mm and 3 mm.

A.4 Instance 3

The length of L is 1180mm, σ_p=100MN/m^2, ΔP=120962Pa, h=1000mm, then the Equation (A-2) and Equation (A-3) is given by:

$$\mathrm{L} = \frac{57.3\times100\times10^6\pi t_p}{90\times120926}\sin^{-1}\frac{120962\times1180}{2\times100\times10^6 t_p} = 1653.2t_p\sin^{-1}\frac{0.72}{t_p} \quad (t_p \geq 0.72)$$

$$\mathrm{W_{skin}} = \frac{57.3\pi\sigma_p\rho_1 h{t_p}^2}{90\Delta P}\sin^{-1}\frac{\Delta P l}{2\sigma_p t_p} = 1653200\rho_1{t_p}^2\sin^{-1}\frac{0.72}{t_p} \quad (t_p \geq 0.72)$$

$$\mathrm{W_{stringer}} = \frac{h\rho_2{t_p}^2 L}{2} = 826600\rho_2{t_p}^3\sin^{-1}\frac{0.72}{t_p} \quad (t_p \geq 0.72)$$

$$\mathrm{W} = 1653200\rho_1{t_p}^2\sin^{-1}\frac{0.72}{t_p} + 826600\rho_2{t_p}^3\sin^{-1}\frac{0.72}{t_p}$$

$$= 826600{t_p}^2(2\rho_1 + \rho_2 t_p)\sin^{-1}\frac{0.72}{t_p}$$

Assuming $\rho_1 = \rho_2 = 2.58\times10^{-6}kg/\mathrm{mm}^3$,

$$\mathrm{W} = 826600\left(2\rho_1 + \rho_2 t_p\right)\sin^{-1}\frac{1.6}{t_p} = 2.13{t_p}^2(2 + t_p)\sin^{-1}\frac{0.72}{t_p}$$

The relationship between t_p and L is shown in figure A.10:

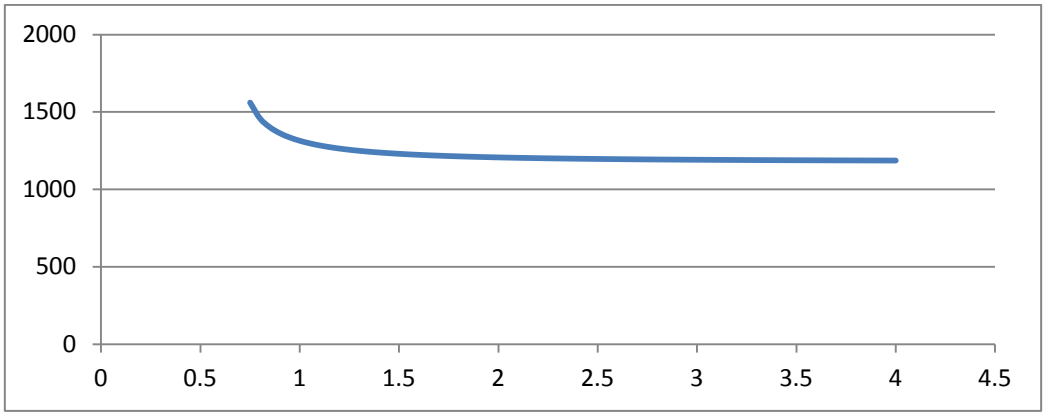

Figure A.10 The graph of t_p (abscissa,mm) and L (ordinate,mm) for 1180 distance

The relationship between t_p and W is shown in figure A.11:

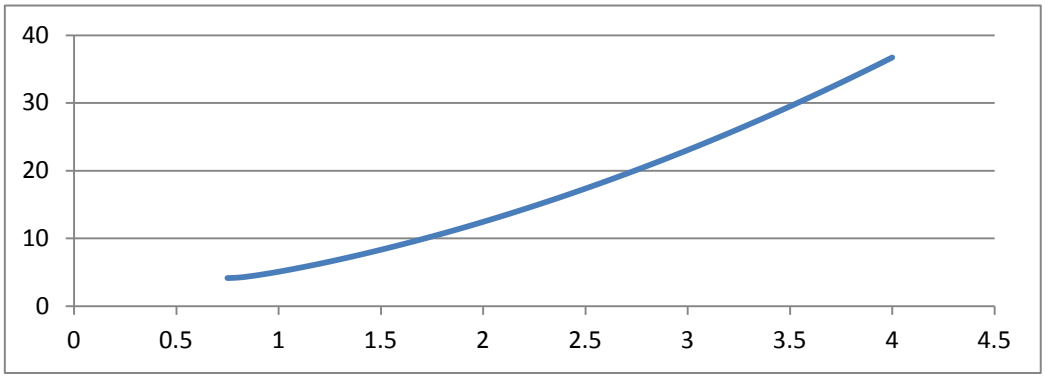

Figure A.11 The graph of t_p (abscissa,mm) and W (ordinate,kg) for 1180 distance

The relationship between t_p (mm) and R (mm) is shown in figure A.12:

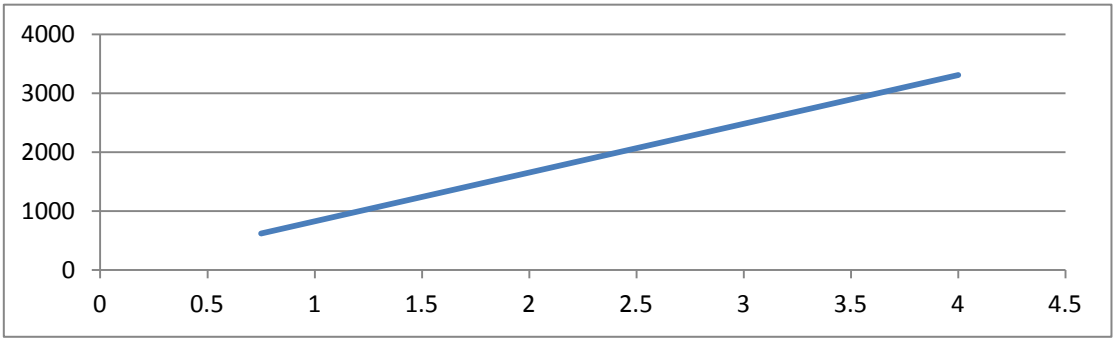

Figure A.12 The graph of t_p (abscissa,mm) and R (ordinate,mm) for 1180 distance

The proper thickness of t_p may between 0.8 mm and 1.2 mm.

Discuss

The skin shell radium is depends on the balance between the space situation and the weight penalty. It means although the excellent condition is that the whole arch shell would be a semicircle, the troubles are also exist from manufacturing and structure interference. In this phase, the author decided to select the balanced data between the weight and the arch length, as shown in table A-1:

Table A.1 skin radius and thickness selection

position	Skin Radius(mm)	Skin thickness(mm)
Passenger cabin	2700.0	3.3
Cargo cabin	2700.0	3.3
Side shell	823.9	1.0

Appendix B Pressure bulkheads performance by using ESDU 71013 [25]

The condition of the bulkheads in C section shows below:

- The length and width of this flat rectangular plate is a= 144.4 mm, b= 79.2 mm, the skin thickness t = 2.1 mm in the two rows of fasteners condition.
- The edges of this plate are free to rotate but fixed against movement in the plane of the plate. The uniform pressure load is 120962Pa.
- The Young's modulus of the material which was decided to use Aluminium 2090-T83 E is 80.3 GPa, the Poisson ratio v is 0.34.

Using table B.1 can find proper figures to obtain the deflection and particular stresses from the different boundary condition.

The result is figure B.2, figure B.3 and figure B.4 may proper.

To calculate the relative data shows below:

$$r = \frac{(\mathbf{1} - \mathbf{v^2})}{\mathbf{0.91}} = \frac{(\mathbf{1} - \mathbf{0.34^2})}{\mathbf{0.91}} = 0.98$$

$$\frac{b}{t}(r\frac{p}{E})^{1/4} = \frac{79.2}{2.1} \times (0.98 \times \frac{120962}{80.3 \times 10^9})^{1/4} = 1.29$$

$$\frac{a}{b} = \frac{144.4}{79.2} = 1.82$$

From figure B.2 in Appendix B, for $\frac{b}{t}(r\frac{p}{E})^{1/4} = 1.29$, the deflection $\frac{\delta}{t} < 0.5$. is too small for the large deflection theory.

From figure B.3, $\frac{f_{c2}}{p}(\frac{t}{b})^2 < 0.1$ is also too small to use.

Figure B.4 is proper for this condition although the value from it will be overestimated for the true value.

According to figure B.3,

$$\frac{\delta}{t}(\frac{E}{rp})(\frac{t}{b})^4 = 0.103$$

also,

$$\frac{f_{C2}}{p}(\frac{t}{b})^2 = 0.58$$

and

$$\frac{f_{E2}}{p}(\frac{t}{b})^2 = 0$$

Now,

$$r\frac{p}{E}(\frac{b}{t})^4 = 0.98 \times \frac{120962}{80.3 \times 10^9} \times (\frac{79.2}{2.1})^4 = 2.99$$

and

$$p(\frac{b}{t})^2 = 171\text{MPa}$$

There for,

$$\delta = 0.103 \times 2.99 \times 2.1 = 0.65\,\text{mm}$$

also,

$$f_{C2} = 99\text{MPa}$$

$$f_{E2} = 0$$

f_{C2} is bending stress according the linear theory from figure B.3, the small middle surface stress f_{c2} also need to be considered.

According to figure B.2, when $\frac{b}{t}(r\frac{p}{E})^{1/4} = 1.29$,

$$\frac{f_{c2}}{p}(\frac{t}{b})^2 = 0.06$$

Hence,

$$f_{c2} = 10.3\text{MPa}$$

The corresponding bending stress is:

$$f_{C2} - f_{c2} = 89\text{MPa}$$

Also,

$$f_{E2} = f_{e2} \approx f_{c2} = 5.14\,\text{MPa}$$

a	length of plate
b	width of plate
E	Young's modulus
f_C	maximum total stress at centre
f_c	stress at middle surface corresponding to f_C
f_D	maximum total stress on diagonals
f_d	stress at middle surface corresponding to f_D
f_E	total stress at mid-point of long edge
f_e	stress at middle surface corresponding to f_E
p	normal pressure on plate
r	ratio $(1-\nu^2)/0.91$ (when $\nu = 0.3$, $r = 1$)
t	plate thickness
δ	maximum deflection of plate
ν	Poisson's ratio

Figure B. 1 Parameters for flat panel calculation

Table B. 1 Figure selection under different condition [25]

Applicability	*Type of edge restraint*		*Number of figure*	*Deflection* δ	*Stress f (denoted by its suffixes)*											
					Total						*Middle surface*					
	Rotation	*In-plane translation*			*C*1	*C*2	*D*1	*D*2	*E*1	*E*2	*c*1	*c*2	*d*1	*d*2	*e*1	*e*2
Small and large deflections	Free	Free	1 5 6	x	<	x	<	x	x	0	<	x	<	x	x	0
	Fixed	Free	2 7 8	x	<	x	<	<	<	x	<	x	<	<	<	0
	Free	Fixed	3 9	x	<	x	<	<	<	x	<	x	<	<	<	x
	Fixed	Fixed	4 10 11	x	<	x	<	<	<	x	<	x	<	<	<	x
Small deflections only ($\delta/t<0.5$)	Free	Free to Fixed	12	x	<	x	<	<	<	0	0	0	0	0	0	0
	Fixed	Free to Fixed	12	x	<	x	<	<	<	x	0	0	0	0	0	0

Number 3 of figure is Figure B.2, Number 9 of figure is Figure B.3, and Number 12 of figure is Figure B.4.

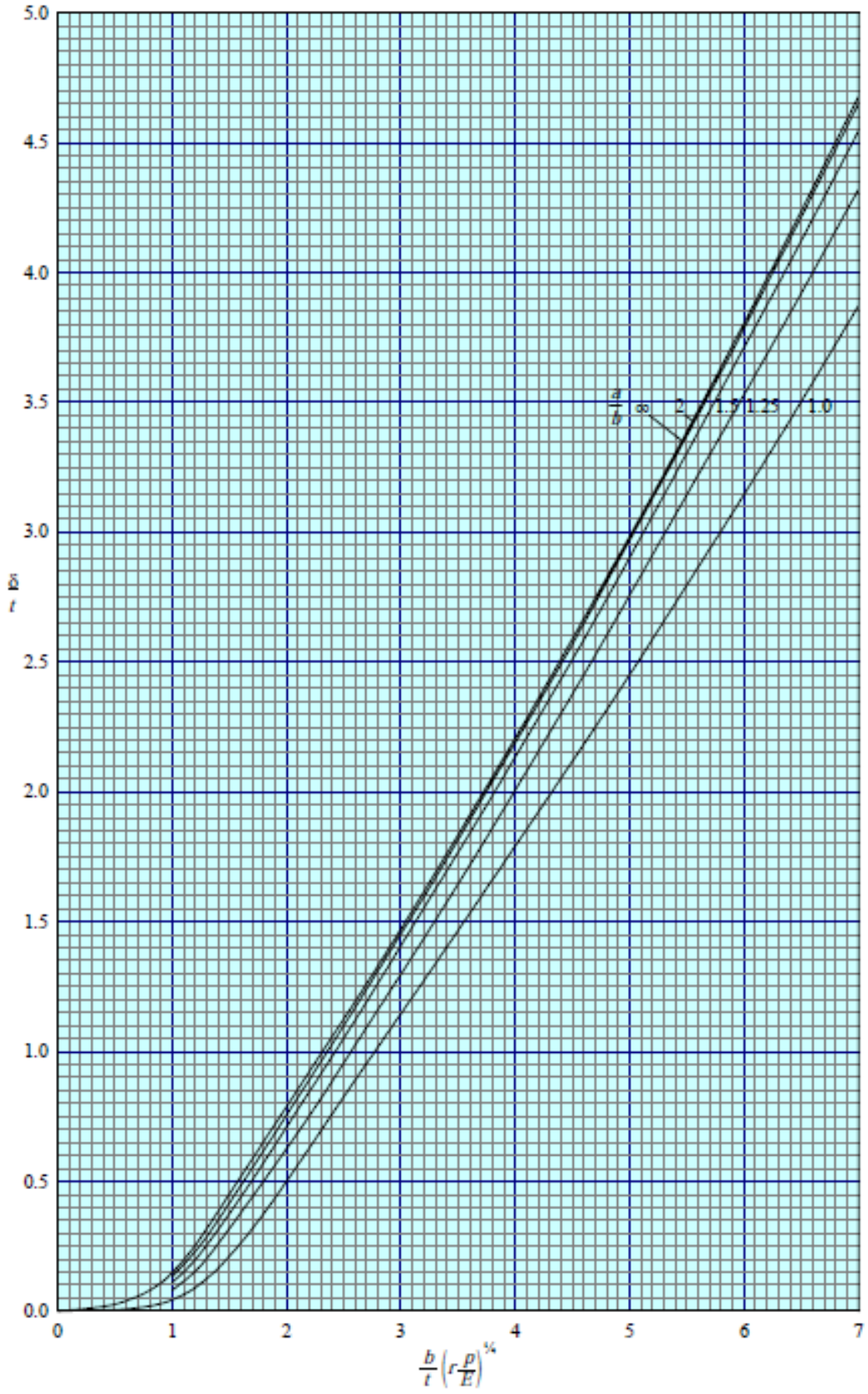

Figure B.2 Edges fixed in translation and free in rotation [25]

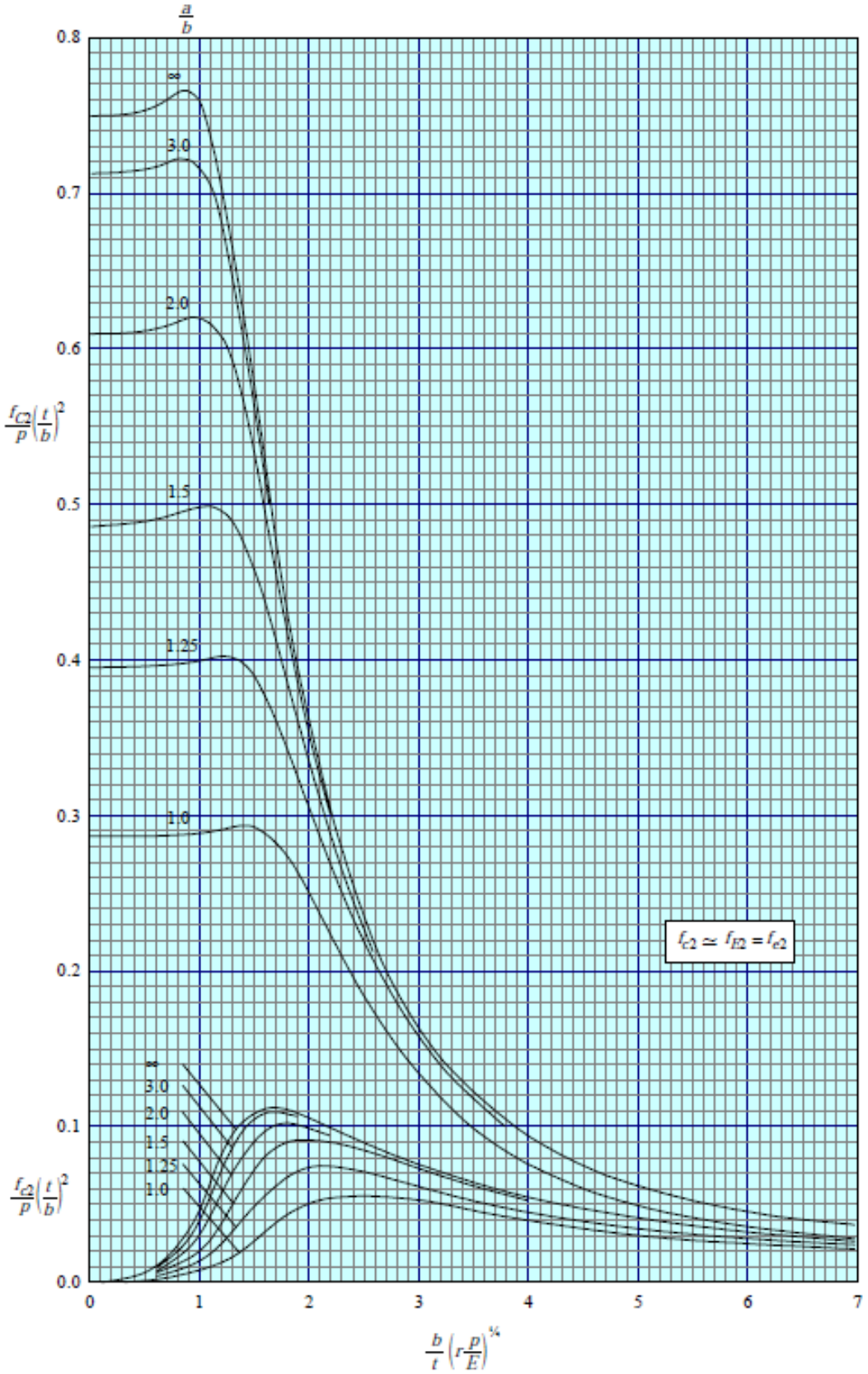

Figure B.3 Edges fixed in translation and free in rotation [25]

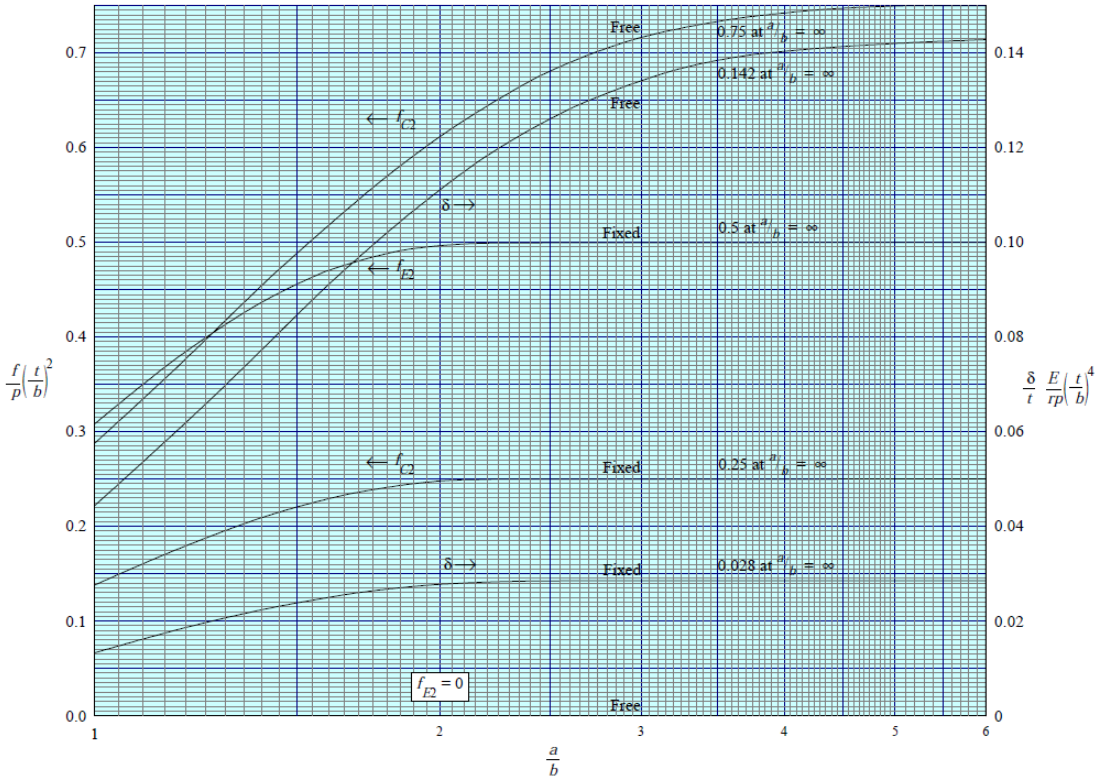

Figure B.4 Edges restrained in rotation as shown (translational restraint has negligible effect in the small deflection range) [25]

Appendix C APPENDIX C GDP contribution in other subject

C.1 Phase I(i) Engine Manufacturers

The main task in this phase lies below: (from Professor H. Smith)

Comprehensive surveys of manufacturers that produce civil transport engines in the thrust category appreciate to 150-250 passengers airliners. The review should include, amongst other data, the following:

What engines do they produce and how do they fit into their 'family' structures? Have the engines been produced in collaboration with other companies and what was/is the work share? How many units have been sold and what is the market share? What is the history of these engines, when launched, updates/stretches etc? Planned replacements? How are projects funded? What engine concept and technologies where used manufacture processes, materials, systems, avionics etc? What has been/could be updated? What future concepts are being considered?

The decision of this phase was established to focus on the trunk-liners which contained 4 aircrafts, 5 manufacturers and 5 engine families.

The author mainly responded for the two famous engine manufacturers, Pratt & Whitney and IAE, and chose two typical engines, PW4062 and V2500.

The features of PW4000-94 family are [26]:

- Based on the JT9D series engines.
- The first model in Pratt & Whitney's high-thrust family for large aircraft.
- Robust fan blades.
- Full-authority Digital Electronic Control (FADEC).
- Advanced super alloy turbine materials and cooling.

Program Milestones
December 1982 - Program launch
April 1984 - First engine run
August 1985 - First flight
July 1986 - FAA engine certification
June 1987 - Revenue service
September 1991- 180-minute ETOPS approval for A300/310
July 1993-180 - minute ETOPS approval for 767
August 1999 - 2,000th engine delivered
November 2002- FAR 33 Certification HPC Ring Case
February 2003 - 60 million hours of operation

Figure C.1 The milestone of PW4000-94 family [26]

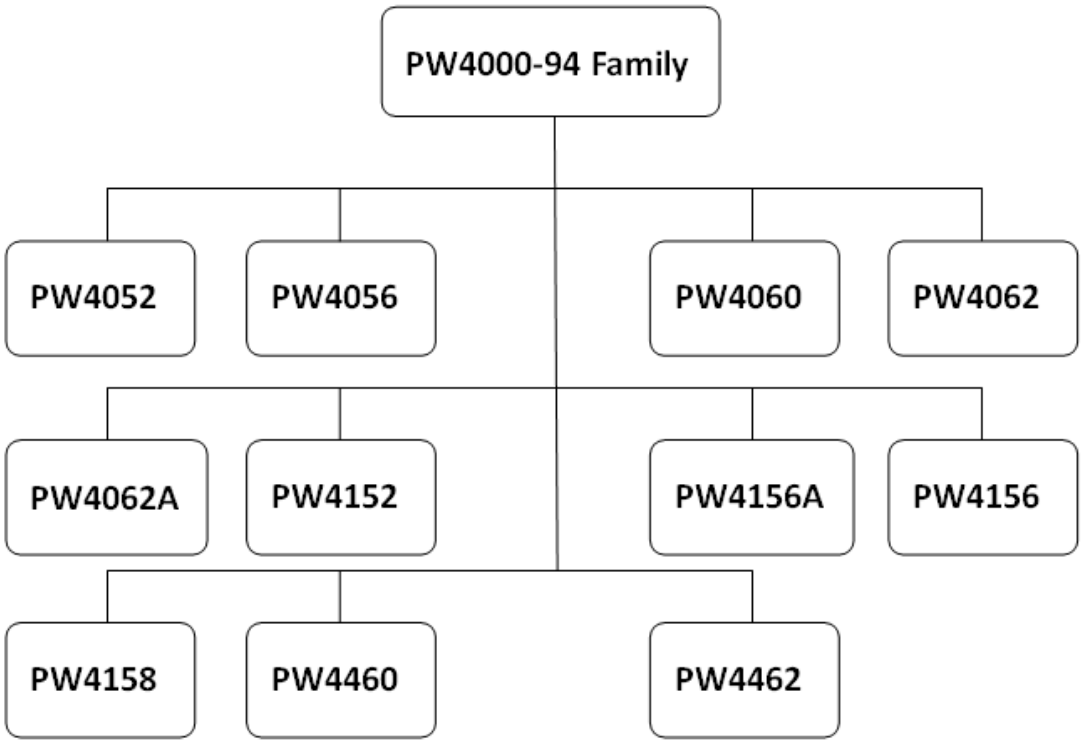

Figure C.2 PW 4000-94 Family Tree [26]

The features of V2500 family as shown in figure 3.3.

- The latest in 3D aerodynamics in the High Pressure Compressor to improve handling and efficiency with reduced core temperatures
- The latest in materials and cooling technology in the High Pressure Turbine resulting in an increase in efficiency and component lives
- Adjustments in the Low Pressure Turbine

Figure C.3 The features of V2500 family [27]

This type of engine was designed by IAE and partners, they are: Pratt & Whitney, Rolls-Royce, Japanese Aero Engine Corporation and MTU Aero Engines.

Table C.1 The milestone of V2500family [27]

Program Milestones					
Jan	1984	Program launch	Jul	1997	V2524 entered service
Nov	1985	First engine to test	Jan	1999	V2500-A1 Phoenix EIS
May	1988	First flight	Sep	2002	2000th engine delivered
Jun	1988	V2500-A1 type certificate	Dec	2004	2500th engine delivered
May	1989	V2500-A1 revenue service	Jun	2005	V2500Select launched
Jan	1992	120-minute ETOPS	May	2006	180-min ETOPS
Nov	1992	V2500 A5/D5 type certificate	Dec	2008	SelectOne™ Entered Service
Apr	1995	V2533-A5 launched on A320-200	Dec	2008	IAE celebrated 25th anniversary
Jun	1995	V2524-A5 launched on A319	Aug	2009	4000th engine delivered

Table C.2 V2500 family members [27]

Type	Thrust (kN)	Bypass ratio	Production start year	Aircraft type
V2500-A1	111	5.4:1	1989	A320
V2522-A5	97.68	4.9:1	1992	A319
V2524-A5	106.75	4.9:1	1996	A319
V2525-D5	111	4.8:1	1995	MD90
V2527-A5	117.88	4.8:1	1993	A320
V2528-D5	124	4.7:1	1995	MD90
V2530-A5	139.67	4.6:1	1994	A321
V2533-A5	146.80	4.5:1	1996	A321

C.2 Phase I(iii) Family issues

In this phase, the author should find out the questions lies below: (from Professor H. Smith)

Does the proposed requirement involve the design of a family of aircraft or just a single design point?

By doing some research, the author found that the family of Airbus A320 is very typical. They both use the same airfoil, the difference between them is just stretch/shorten the length of fuselage by add/delete frames behind and after the wing to achieve the different capacity.

Table C. 2 Airbus A320 family

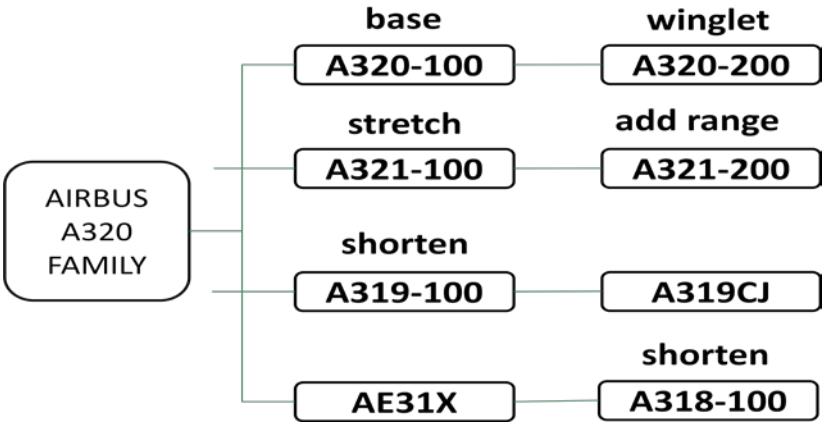

Definitely, by using this way, the whole numbers of the family can share the same pilot course and maintenance equipments, the cost and the time consuming for design and manufacturing also can be reduced.

For flying wing airliner, there are separate passenger cabins. The way to develop the family is not only stretch or shorten the fuselage, but it also can add more cabins for passengers, cargo and fuel tanks.

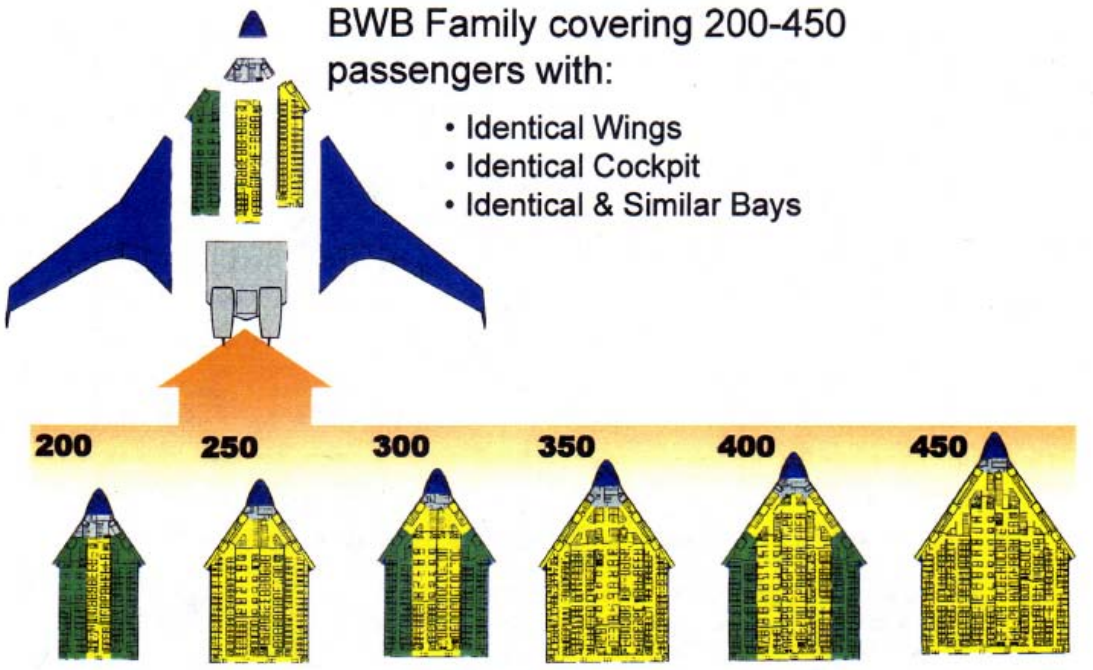

Figure C.4 the family issue concept for flying wing airliner [28]